Induction heating simulation of out of autoclave production techniques

Design of method to simulate induction heating system of out of autoclave mould to scale to full scale production

F.A. van Duin

TU Delft

Induction heating simulation of out of autoclave production techniques

Design of method to simulate induction heating system of out of autoclave mould to scale to full scale production

by

F.A. van Duin

to obtain the degree of Master of Science
at the Delft University of Technology,
to be defended publicly on Tuesday August 6, 2019 at 10:00 AM.

Student number: 4416333
Project duration: Oktober 1, 2018 – July 30, 2019
Thesis committee:

Assoc. Prof. Dr. ir. R. Groves,	TU Delft, supervisor, chairholder
Asst. Prof. Dr. ir. O.K. Bergsma,	TU Delft, Comittee member
Assoc. Prof. Dr. ir. I. Fernandez Villegas,	TU Delft, Comittee member
Ir. S. van den Berg,	Fokker Aerostructures, company supervisor

This thesis is a public version of the confidential version available at Fokker

An electronic version of this thesis is available at http://repository.tudelft.nl/.

TU Delft

Preface

This report was written to obtain a master degree at the faculty of Aerospace Engineering of TU Delft. This thesis had a duration of eleven months including a literature review of two months. The thesis assignment focusses on understanding the fundamentals of induction heating, for the heating of an out of autoclave production technique developed at Fokker Aerostructures. The nine months of research was divided over two locations. The research was started in TU Delft, Aerospace Structures & Materials Laboratory were was focused on retrieving the material properties and gaining sufficient knowledge of the induction heating process. The next steps in the research were based at Fokker Aerostructures, Hoogeveen where the simulations were verified with a small scale setup. During the master thesis, Dr. Roger Groves was my supervisor from TU Delft. Roger let me look into my work from a different perspective when this was needed to solve the problems that I was facing. Thanks for this input when it was needed. Sebastiaan van den Berg, daily supervisor at Fokker Aerostructures helped me with the specific knowledge of the simulations in Abaqus CAE. Furthermore it would like to thank Sebastiaan for the advice when this was needed and encouraged me to find my own answers.

F.A. van Duin
Delft, August 2019

Abstract

This master thesis is part of research at Fokker Aerostructures to an out of autoclave production method for thermoplastic composites. The production will use two heating steps. The first step is an infrared oven to form the material roughly in the correct shape. Secondly, an induction heated press is used to shape the product to the final dimension and to come to the desired material properties. The objective of this thesis is to simulate the induction heating process of this production method to make it possible to simulate the production method before the mould is produced.

A literature review was performed to find the parameters influencing the induction heating process. The main phenomena and basic principles can be found in chapter 2. The contributing material properties and their variance as a function of temperature were estimated based on comparison with similar metals. Electric resistivity was found to be the material property which varies the most in the temperature range of the induction heating setup.

Taking the material properties as a constant value instead of variable as a function of temperature introduces an error on the temperature estimated by a simulation. In chapter 3 the propagation of error was analyzed using an approximate analytical relation found by Jankowski [15]. Found was that electric resistivity not only varies the most over the temperature work range but also has the biggest influence on the estimated temperature in a simulation.

there was found that this specific material property has the biggest influence on the accuracy of the result of the simulation, therefore this material property was measured to define its value as a function of temperature. To make this possible a setup used before at TU Delft was adapted to work in the working range of thermoplastic composites, see section 3.2. The electrical resistivity was measured with a four point measured method found by 'van der Pauw' [7]. The full setup was placed in an oven to measure the electrical resistivity over the range 0 untill 450 $^{\circ}C$.

At this point in research, the electrical resistivity was known as a function of temperature. The commercial software JmatPro was used to calculate the other influencing material properties as a function of temperature based on the chemical composition and some other properties based on the production method of the material. The measured data and the material properties at room temperature from the literature review were used to validate the calculated data of JmatPro.

After the material properties were known as a function of temperature the next step is designing an induction heating setup which can be used to validate the simulation model. Therefore a 20x30x0.8 cm flat metal plate with a meander type coil was used as induction heating setup, see chapter 4. The relatively simple geometry made it possible to validate the simulation with the results from the experiment. The temperature was measured with thermocouples to measure at exact locations and thermal camera to visualize the heating pattern as a function of time.

In the same chapter, the temperature graphs of the experiment and simulation were compared. There was concluded that the thermal properties where estimated correct based on the estimated cooling properties. There was still an error between the temperature lines in the heating phase which was concluded to be the result of the magnetic permeability. The magnetic permeability was found as a non-linear variable but has to be taken into account as a linear variable in Abaqus CAE to work with these high-frequency simulations. Together with the fact that the magnetic permeability retrieved from JMatPro could not be verified with other data as could be done with the temperature dependence material properties. An exact determined material property would increase the accuracy of the simulation. The simulations of done in Abaqus CAE are still valuable as they predict the heating pattern of the correct which was verified with the thermal image measurements and the thermocouple data.

The final chapter combines the findings in the experimental research to the induction heating of the out of autoclave mould. Chapter 5.1 describes what is needed for an accurate model of the induction heating process from start to finish. This starts from an estimated power consumption of the induction heating system to pick a generator size, thereafter how the material properties have to be collected for the model. The procedure which results in an accurate model of a new induction heating design.

Section 5.2 describes the effect of the shape of the coil. The regularly used meander type coil did not appear to be the best option in terms of efficiency and temperature profile for big surface heating. The current in the opposite direction in the coil takes care of less efficient heating performance. As it is not always possible to direct all the current in the same direction when designing an induction heating setup so an option to shield the conflicting areas was mentioned. Two designs were purposed based on the size of the experiment mould. To equally heat this surface a pancake coil was purposed. Realistically future mould designs do not have this flat shape, therefore a second design was purposed were concentrators were used to help equally heat the surface in conflicting areas.

Contents

1

Introduction

1.1. Background

At Fokker Aerostructures an extensive knowledge have been gathered in the production of thermoplastic composite (TP) parts. In the last decades autoclave processing and thermoforming production methods have been researched and successfully put in production. Although thermoforming has been proven cost effective it is limited to dimensions of 1 x 1.5 m and simple geometries [32, p.3]. Autoclave processing is currently the main production technique at Fokker Aerostructures when producing larger parts like skins, spars and integrated structures. This autoclave processing comes with a lot of manual labor when preparing moulds, auxiliary materials have to be used in the process and the move rate is limited due to cycle times in the autoclave.

Therefore Fokker Aerostructures is researching the options of producing TP composites in an Out of Autoclave (OoA) press co-consolidation technique. Project title: "*the technology development plan for Out-of-Autoclave OoA Press co-consolidation of thermoplastic composites for small / mid-size parts for aerospace*". The project has the aim of reducing the production cycle from 4-7 hours to 10-30 minutes by the use of an OoA press instead of an autoclave, see figure 1.1.

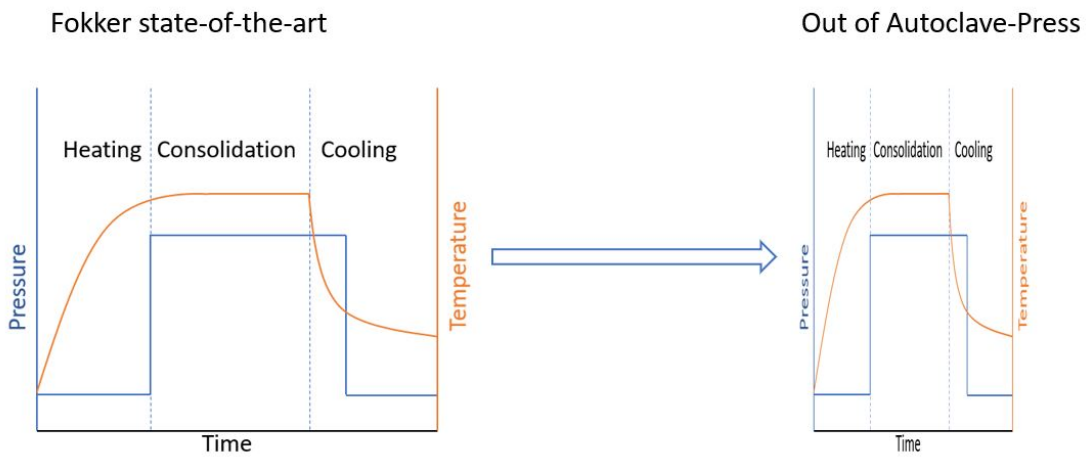

Figure 1.1: Cycle time benchmark autoclave- versus OoA press consolidation, source[33]

This project aims to develop a production cycle where a final product is made in two heating steps. Figure 1.2 describes the manufacturing steps needed for this new production techniques. It starts with an flat ultrasonic cutter to cut TP prepregs in shape and assemble the lay up of the composite part. After that the lay up is heated with an infraread (IR) oven and formed roughly into the final shape, see figure 1.2 B). After thermoforming the co-consolidation step is performed in an press with a heated mouldsurface using induction heating (IH),figure 1.2C. This co-consolidating step is required to achieve

the correct mechanical properties. Keeping this induction heating process as short as possible is key to the success of this manufacturing process.

Figure 1.2: Next generation OoA production process. A): flat ultrasonic Automatic Tape Layer ATL, Automatic Fiber Placement AFP laminator, B): forming of preform in press with IR oven and C): (Co)-consolidation tool in press, induction heating and cooling of tool

From earlier research [11, p.43] was concluded that there was too little fundamental knowledge on the induction heating to successful model this step of the process. Induction heating is based on a multi physics process with non-linear material properties varying as function of temperature this makes it a difficult or even near to impossible process to optimize via trial and error. As the dimension of the mould is a function of the heating performance it is necessary to first develop an reliable simulation model before producing the mould. The scope of this master thesis is to describe the induction heating of the OoA press mould so that is known what is needed to model this step in the production process. Therefore the fundamentals of induction heating will be investigated, an analysis will be made of the material and process parameters and the accuracy will be determined to obtain a useful simulation model. Verification will be done on a small scale experimental IH, similar size to that shown in figure 1.3(approximately 0.5x0.5 [m]). A schematic overview of the production method is given in figure 1.4, where product is placed between two mould surfaces which are heated via an induction coil. A specific pressure (P) in combination with a temperature (T) is needed to achieve the correct material properties of the final product.

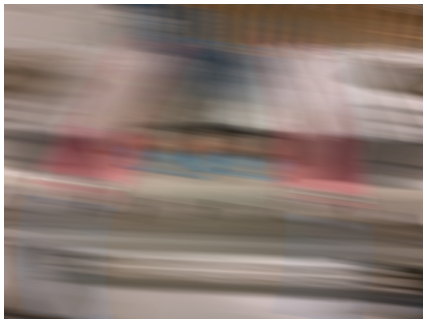

Figure 1.3: Experimental setup at Fokker

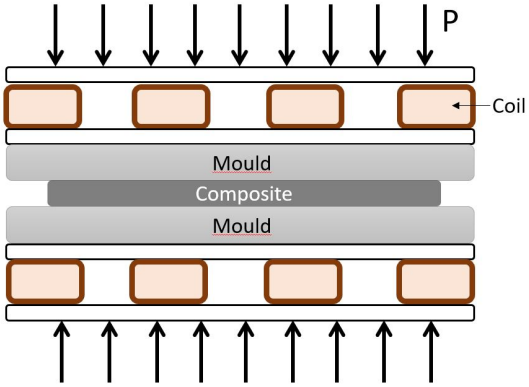

Figure 1.4: Schematical overview

Chapter 2 will summarize the literature review performed before this master thesis[30]. It will also present specific induction heating terminology which will be used in the rest of the report. Chapter 2.5 will conclude the literature review and form the research question of this thesis. Chapter 2.6 will describe the structure of the report.

2

Literature review

2.1. Induction heating

Induction heating is a preferred way of heating due to a number of reasons: speed, efficiency, highly repeatable and being able to heat up material locally[19, p.1]. Induction heating is a method where a workpiece is heated up inducing a current in the material itself which result in joule and eddy current heating. This is unlike many other heating mechanisms where heat is transferred through convection or conduction from a separate heat source instead. A typical induction heating setup is displayed in figure 2.1. It can be divided into a generator, an inductor(or coil) and an conductor (or workpiece). The inductor is made from an electrical conductive material, often copper, and the conductor from an electrically conductive metal, which does not have to be magnetic.

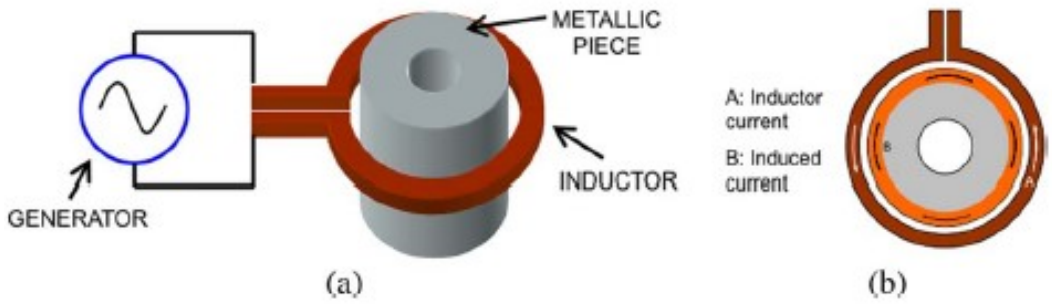

Figure 2.1: Typical arrangement of an induction system, source[17]

In this setup, the generator supplies an Alternating Current (AC) to a coil and the coil generates a magnetic field at the same frequency as the generator. The workpiece near the coil will experience the magnetic field and currents will be induced in the workpiece. This heating is effected by two phenomena: Eddy current loses and magnetic hysteresis. Eddy current heating is the main contributor of the heating while typically magnetic hysteresis contributes only 6% to 8% [21, p.107][1]. Eddy current heating can take place in every conducting material and not only magnetic materials. The coil generates a magnetic field which induces an eddy current in the workpiece, equal in frequency but opposite in direction to the current in the coil. This current will produce heat via the Joule effect (I^2R)[1]. The other effect, hysteresis loss, plays only an effect for ferromagnetic materials[10, p.3]. When a ferromagnetic material is induced with a time varying magnetic field, some of the energy is lost as heat when the polarities of the magnetic field switches as function of the AC signal. The heat is a reaction

[1] It is assumed in many applications that the surface is well above the Curie temperature and so is not magnetic, so magnetic hysteresis has no heating contribution.

of the internal friction between the molecules during the magnetization- demagnetization of the time variant magnetic field. The amount of heat generated due to hysteresis is directly proportional to the area enclosed in the hysteresis loop, see figure 2.2. In the figure the axis are labeled with magnetic flux density (B) and magnetic field intensity (H). This area is a function of the grain size, temperature, frequency, chemical composition and magnetic field intensity. This hysteresis effect plays only a major role at high frequencies ($> 100Hz$)[21, p.34], and mainly at the surface of the workpiece due to the skin effect, see section 2.1.1.

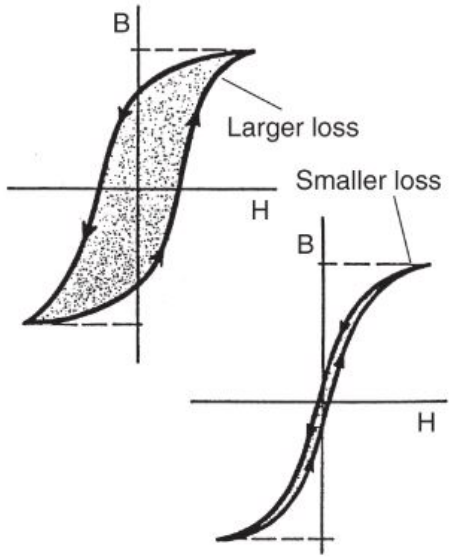

Figure 2.2: Typical hysterisis loop, source [1, p.9]

Induction heating is a multidisciplinary phenomena composed of complex interactions involving electromagnetism, heat transfer, material science, metallurgy and circuit analysis all influencing the performance of an IH system. Still the technology is used in many industries due to its high efficiency, speed and repeatability. The following section will give the necessary information about the electromagnetic effects and the effect of the material properties to give an impression on what is necessary to know before simulating the induction heating of the IH setup at Fokker.

2.1.1. Theory behind induction heating

As mentioned above, IH is a function of current induced in an conductor from an inductor. The performance of this IH process is therefore depending on the uniformity of the field created in the workpiece. As a function of the dimensions and material properties of both the coil (inductor) and workpiece (conductor) this induced current is not equally distributed over the surface of the workpiece resulting in a non-equal heating pattern over the surface of the workpiece. This effect does not have to be a disadvantage and can even be used as and advantage in for example selective hardening processes. These phenomena are a function of electromagnetic effects and material properties of both the coil and workpiece. The most important electromagnetic effects are: skin effect, proximity effect, ring effect, slot effect and end- and edge effects [10, p.3]. These effects will briefly explained in the following chapters.

Skin effect

The skin effect is the result of the non-uniform distribution of AC through the thickness of a conductor. AC makes the current concentrate at the surface of the workpiece [22, p.61]. When taking an cylindrical workpiece (load) as an example, there is no current flow at the center of the workpiece and the current increases in value exponentially in a radial direction, see figure 2.3. This skin effect has as a consequence that at the center there is no direct heating due to eddy current. Due to the skin effect for this example, 86% of the power and 63% of the current concentrates at the surface [1, p.9][22, p.61]. This can be described by the reference depth δ $[m]$ which defines the distance at which the current reduces by a function e. The penetration depth δ is a function of the electrical resistivity ρ, the relative magnetic permeability μ_r and the frequency f. As the material properties change as function of temperature, δ

can change substantially. The current through the thickness of the circular billet in figure 2.3 can be calculated with the following relation:

$$I = I_0 e^{\frac{-\gamma}{\delta}} \tag{2.1}$$

$$\delta = 503\sqrt{\frac{\rho}{\mu_r f}}, [m] \tag{2.2}$$

Where the δ is the penetration depth, γ[m] is the distance from the surface, I_0 [A] the current density at the workpiece surface, μ [NA^{-2}] the relative magnetic permeability of the material, ρ [kgm^3], and f the frequency of the magnetic field [Hz]. Where the penetration dept is the distance where the current decrease exponentially to e^{-1} compared to the surface. And the power density decreases to e^{-2} compared to the value at the surface. With these relations it can be described that at δ the the current density is at 37% of the surface value and the power density at 14% of its surface value. This means that 86% of the power density will concentrate at the skin of the surface of the workpiece [23].

It can be derived from this two equations that the δ is also a function of the frequency f. This property is used in surface hardening of tools to steer the depth the heat is applied during the heating; where preferably only the skin is heated when after rapidly cooled to minimize the change in properties in the rest of the tool.

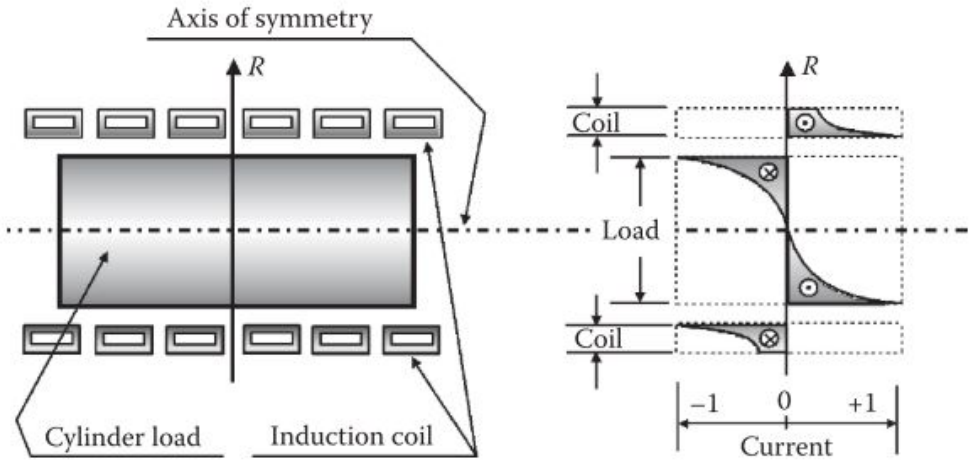

Figure 2.3: Cross-section of distribution of AC current through the radius R in an cylindrical load, source:[22]

Proximity effect

The proximity effect is the effect of multiple conductors in one magnetic field. These conductors will affect the local magnetic field with their own magnetic fields. When two conductors are close, the direction of the magnetic fields can complement each other. The opposite is also true, when the direction of the magnetic field is opposite the magnetic field can decrease in intensity as is visible in figure 2.4. The distance between the two conductors defines the strength of the electromagnetic proximity effect. This proximity effect is an complex factor when designing an IH system and has to be taken into account. Shielding or surrounding metal structures can be beneficial in terms of efficiency of IH system. [22, section 3.1.3]

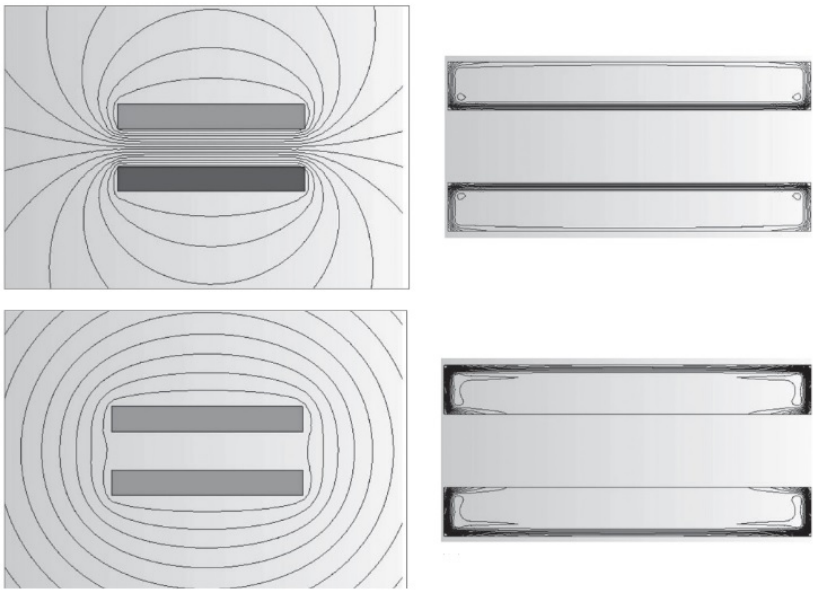

Figure 2.4: Proximity effect and effect of current direction,top; current in opposite direction, bottom; current in same direction, left; magnetic field and right current density. Source[22]

Ring effect

This effect will occur when an coil is bent, the current takes the shortest path through the conductor and will have an higher density at the inside of the coil [22, section 3.1.5.]. The magnetic flux lines will be more concentrated at the inner radius of the coil, which is an result of the shortest distance to the workpiece and the lowest impedance path. Figure 2.5 explains the effect with an sketch. This effect plays a positive role when the workpiece is placed inside the coil, for example in an tool hardening situation. In case of the mould used for the experiment this can deliver improved performance in the bends of the inductor.

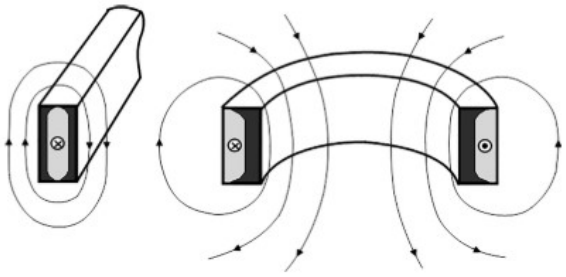

Figure 2.5: ringeffect in induction coil [22]

Slot effect

The slot effect takes place where a coil is placed close to the workpiece and the magnetic field lines are squeezed in between the coil and the workpiece. The closer the coil is positioned to the conductor the denser the magnetic flux in-between the coil and the conductor is. As a result, the magnetic field in the coil will be ‘pushed’ towards the workpiece as shown in figure 2.6. The rest of the current will be distributed at the sides of the coil. This effect is used to heat the workpiece locally and to increase the efficiency of the IH system as it redirects the magnetic fields/ current to the location that is desired.

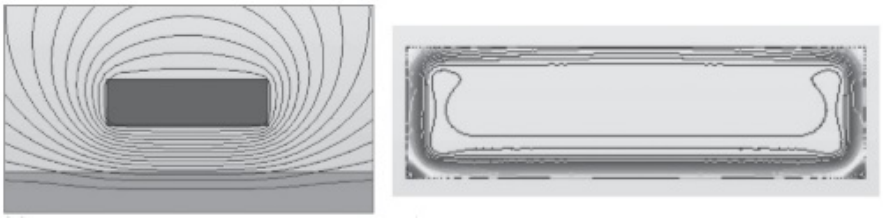

Figure 2.6: slot effect,left: magnetic field lines outside inductor, right: Magnetic field lines inside inductor, source: [22]

End- and edge effect
Field distortions and corresponding distributions of induced currents resulting in varying temperature profiles near edges of the workpiece length are called end- and edge effects. This effect plays an important role when heating a bigger surface in an uniform way [22, section 3.1.7]. Often the edge effect is studied by evaluating the power density distribution across a workpiece in the x or y direction as shown in figure 2.7, P/P_c represent the normalized power density with P_c as the power at the center of the plate. By assuming that the width and length is much longer than its thickness, the part can be divided into three sections; the central part, longitudinal part and the transverse part. When the plate is experiences a uniform magnetic field the sections in the longitudinal and transverse direction experience an field distortion which result in higher temperatures in these areas. The central part of the plate will not experience this field distortions and the heat performance will act as if it is an infinite plate. This effect is often used in assumptions made for simulation and verification. The end- and edge effect are particularly important when the inductor or conductor is moving relative to each other, often the case in automated hardening processes.

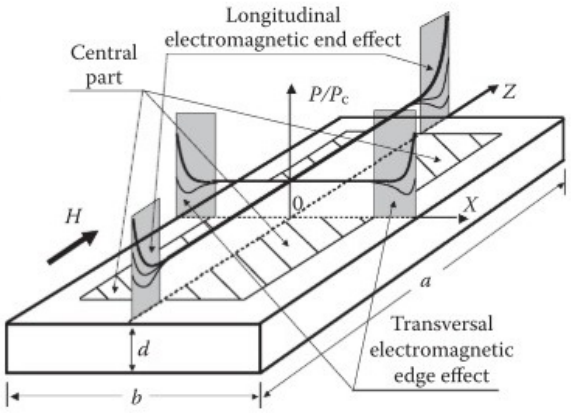

Figure 2.7: Electromagnetic end and edge effect on a slab, source: [22]

2.1.2. Material properties
To be able to heat a material by induction heating the material has to be conductive but not per definition magnetic. The material properties of the workpiece will have an effect on the performance of the heating. The material properties can be divided in electromagnetic properties and thermal properties.

Electromagnetic properties
The electromagnetic properties can be described by a number of parameters. From the literature report it was determined that the electrical resistivity and the magnetic permeability are the most important material properties that influence the electromagnetic properties of metals and also the IH process [30]. For pure materials the electric resistivity can be approximated with by a linear function of the temperature [22, section: 3.1.1.1],[21]:

$$\rho(T) = \rho_0[1 + \alpha(T - T_0)] \tag{2.3}$$

Where $\rho(T)$ is the electric resistivity as a function of temperature T, T_0 is the ambient temperature and ρ_0 is the electric resistivity at ambient temperature. The α is the temperature coefficient of electrical resistivity $[^\circ C^{-1}]$ which is linear for pure metals but will become nonlinear for changes in lattice,

material/phase transformations and other materials than pure metals for example: carbon steels, alloyed steels and graphite [22]. The electrical resistivity is important for modeling of IH because it has an effect on most important parameters of the IH system including the following parameters: depth and heat generation, temperature distribution, heating efficiency, coil impedance. To give an example, for most metals ρ can increase by 300% compared to its initial value, when comparing a room temperature to 450 °C range.

Magnetic permeability
The relative magnetic permeability μ_r describes how the material conducts magnetic flux compared to vacuum or air. μ_r is a non-dimensional parameter and for a non magnetic material μ_r has value 1. Often relative magnetic permeability is used in short as magnetic permeability. Also the product of the magnetic permeability and the constant permeability of free space μ_0. $\mu = \mu_r\mu_0$ is equal to the ratio between the magnetic flux density (B) and magnetic field intensity (H):

$$\frac{B}{H} = \mu = \mu_r\mu_0 \tag{2.4}$$

For ferromagnetic metals the magnetic permeability is defined by a complex function of: structure, chemical composition, prior treatment, grain size, frequency of the IH, intensity of magnetic field and temperature. The magnetic permeability has a non-linear relation with magnetic field and temperature. Special attention has to be met for the Curie point which stands for the temperature were a ferromagnetic metal loses its magnetic properties, at this point $\mu_r = 1$ and no hysteresis heating is present. In case the material has to be heated to a higher temperature than the Curie point, the frequency and/or current through the coil has to be adopted to this change in material property. The magnetic permeability has influence on the electrical phenomena like: skin effect, electromagnetic edge and end effect, but also proximity and ring effects[18].

Thermal properties materials
Thermal conductivity k, describes the rate heat travels through a conductive material. The higher the value of k the faster the material increase in temperature. The value of k is dependent on the temperature and for most materials it is described by a non-linear relationship. Depending on the purpose a high value of thermal conductivity can be a benefit. For heating purposes an high value of k has the benefit of creating an uniform heating pattern [22, chapter 3.2.1.1]. The Wiedermann-Franz law describes an relationship between the thermal conductivity and electrical conductivity.

$$\frac{\kappa}{\sigma} = LT \tag{2.5}$$

The ratio equals a constant (L) multiplied by temperature (T). L is the Lorenz number. Literature notes that there are some violations for this relation. The ratio can be used as an estimation for initial design.

Heat capacity C, is the amount of heat a material can absorb per unit mole before it increases by a certain temperature step. The heat capacity is highly related to the specific heat c, which is the heat capacity per unit mass instead per unit mole which is a more workable number in experiments. The specific heat is highly dependent on the following but not limited to: chemical composition, residual elements, grain size, plastic deformation and prior heat treatment [18].

Although not important on first sight, the **density** is also important to describe the IH process. The density of the materials can also vary, although this is over a much lower range than the specific heat and thermal conductivity (which can differ by 50 % in value for a temperature range from room temperature till 450 °C) it is still noticeable lower by higher temperatures (about 10% in the same range).

2.1.3. Expected variance material parameters

The material properties are varying as a function of temperature. In literature often simulations are performed with values found at room temperature; often because data is not available as a function of temperature. To perform an accurate simulation it is necessary to know the variation in material properties. To illustrate this the data available from another ferromagnetic metal, steel, is found and is listed in table 2.1. All the important data over the temperature range room temperature until 450 °C are given. The variance in value is given as % and indicated with higher or lower with >,< respectively.

From this data it can be seen that the electric resistivity is changing more than the other parameters and is presumably most useful to know accurately. Based on the variance of input parameters, the effect on the simulation will be analyzed in chapter 3.1 with the use of the Maxwell equation.

Electromagnetic properties	**Symbol**	**Unit**	**Expected deviation**
Electric resistivity	ρ	$[\Omega \cdot m]$	300% >
Magnetic permeability	μ	$[\frac{J}{A^(2)\cdot m}]$	100% >
Thermal properties			
Specific heat	c	$[\frac{J}{kgK}]$	50%>
Thermal conductivity	k	$[\frac{W}{mK}]$	50%<
Density	ρ	$[\frac{kg}{m^3}]$	10%<
Cooling properties			
Convection	α	$[\frac{W}{m^2}]$	-
Radiation	C_s	$[\frac{W}{m^2}]$	-

Table 2.1: Material characteristics for induction heating for standard steel, source [30]

2.2. Process parameters

2.2.1. Temperature

The temperature is often measured during experimental research on induction heating. This is done with the use of thermocouples (often type-K) or thermal cameras. Thermocouples are relative inexpensive which makes them often used even in combination with an thermal camera for verification. [16, p.3588] used an thermographic camera to verify the heat build up during the IH process. Here was chosen for a camera to see the heat spread over a surface in time, which is not possible with a number of thermocouples. A similar situation was used at [13, p.165] where K-type thermocouples where used as a verification. Often the thermal cameras are useful when optimizing an heating profile because the temperature change over a large surface in time can be measured and analyzed.

2.2.2. Magnetic field

When using IH in highly demanding situation like welding where the duration is short and the heating rate will be high it is necessary to know the IH process in great detail. As the temperature is a result of the magnetic field it is useful to know the magnetic field lines around the coil. Another benefit described by [8] is that the magnetic field can describe the differences in process parameters, or the wear and tear of the generator – inductor combination.
The magnetic field measurement sensor described in this project measures frequency and components (amplitude) of the magnetic field at 16 channels. Which can be used to measure the magnetic components B_x, B_y, B_z at 5 locations. At the moment the sensors are used at a manufacturing site at Fokker to measure the induction welding tool to verify the induction tool for production.

2.2.3. Frequency

With the magnetic field measurement sensor could also the frequency be measured. Another way of measuring the frequency is with the use of an LCR[2] meter what is used in [4, p.86],[5, p.1284] to measure the frequency dependency of a Litz wire depending on a variable load. This process was used for optimization of the generator inductor combination and calculate and verify impedance with analytical model.

[2]A LCR meter is a general purpose measurement devise to measure inductance (L),capacitance(C) and resistance (R) and can also be used to measure frequency.

2.2.4. Current, Voltage

The current, voltage and frequency are important parameters when operating an induction heating process. Often the current and voltage are set and measured on the generator itself. When a custom IH system is designed it is important to know the current through the coil to calculate the efficiency and for optimizing the IH process. In [15, p.2778] an current clamp was placed between the coil and the generator. In this research the current, voltage, phase angle, impedance and frequency were measured during the experiment.

2.3. Modeling

As already mentioned IH is an multi physical phenomenon where electromagnetic properties, heat transfer, metallurgical phenomena and circuit analyses are interacting at the same time. This makes it a highly nonlinear process which is costly or even an impossible process to optimize via trial and error. Computer simulation makes it possible to retrieve process details which would otherwise not be available. Computer simulation also plays a major role when a system has to be optimized. The learning curve can be shorted to make it possible to retrieve the effectiveness of changing certain parameters. Computer simulations are based on the governing equations. In the case of IH these are relations that describe the electromagnetic field that is formed by the induction coil and form the description of the thermal processes. The thermal processes can be distinguished in three components; heat conduction, convection and radiation which are relatively easy to describe by a time variant Fourier equation [23, p.109].

$$c\gamma\frac{\delta T}{\delta t} + \nabla\cdot(-k\nabla T) = Q \tag{2.6}$$

Where γ $[kg/m^3]$ is the density of the metal, c $[J/kgK]$is the specific heat, Q is the local flux density $[W\cdot m^{-2}]$, κ is the material conductivity $[W\cdot m^{-1}\cdot K^{-1}]$ and δT is the temperature gradient $[K\cdot m^{-1}]$.

The electromagnetic fields are described using the Maxwell equations that consist of four equations derived from the laws of Ampere, Faraday and Gauss. Depending on the geometric situation and the required accuracy certain simplifications can be made to make the equations simpler. The following equations are Maxwell's equation in differential form.[23, p.104]

$$\nabla\times H = J + \frac{\delta D}{\delta t} \quad (from \quad Ampere's \quad law) \tag{2.7}$$

$$\nabla\times E = -\frac{\delta B}{\delta t} \quad (from \quad Faraday's \quad law) \tag{2.8}$$

$$\nabla\cdot B = 0 \quad (From \quad Gauss' \quad law) \tag{2.9}$$

$$\nabla\cdot D = 0 \quad (from \quad Gauss' \quad law) \tag{2.10}$$

Where H is the magnetic field intensity, J is conduction current density, D is electric displacement field, E the electric field intensity and B is magnetic flux density. Calculating the magnetic fields can be done by solving the Maxwell equations, per different situation rewriting the relations to simplify and neglect certain components. How this is done is not discussed in this literature review. Analytic solutions can only be found in case of certain geometries and when the process is highly simplified for example in [15] used in section 3.1 for graphite cylinders. In other cases the use of an computer is needed to solve the electromagnetic fields numerically.

2.3.1. Numerical modeling in induction heating

As mentioned before the trial and error method is an costly method to obtain a high performance IH system. The inductor load system where the coil and the piece that will be heated up can be extremely complex when need to describe the induction heating process. Due to multi physical phenomena and nonlinear material properties, based on the number of papers that are published on 'modeling induction heating" in the title a lot of effort is being paid to model the induction process. In the beginning only simple round geometries where being analyzed were simplifications could be made, up until now where whole structures are being optimized in terms of efficiency. Roughly three different types of research can be distinguished:

- Electrical equivalent parameter extraction
- Efficiency optimization
- Heat distribution optimization

In recent research has focused on the optimization part rather than on identifying certain process or material parameters [9].
Simplifications that are often been made are,[15]:

- Search for an axi-symmetric situation
- Assume materials are isotropic, non- magnetic (no hysterisis present) and have no net electric charge
- Displacement due current is neglected
- Distribution of electrical current in the coil is uniform
- Frequency is assumed equal in whole system

The simulations can be done in various commercial available simulation programs. The most used techniques are based on Finite Element Methods (FEM), Finite Difference Methods (FDM), Boundary Element Methods (BEM) and Mutual Impedance Methods (MIM) [22]. All these methods have their benefits and therefore are often used in a combination. The FEM method uses a node system which divides the object in, for example, triangular patches. FEM uses an energy method to solve all the data points (nodes) at the same time. In IH purposes often the air domain has to be taken into account to form the magnetic field. Which can be considered as non-useful information when for example only heating patterns have to be delivered. BEM or MIM methods can be useful because this methods do not have to take air into account which makes computation faster. Geometry can also be leading in the choice of method: For example in long slender parts when using FEM or FDM long and slender meshes are needed over the length of the part which results in a costly computational process, MIM is a better option which uses an integral equation approach instead of using differential formulation of the equations.

An example of a widely used method is disk induction [34], which is automated and optimized to uniformly heat a system. It can also be chosen to use the symmetry of the object. As can be seen in figure 2.8, the assumption is made that the current is running in the same direction in all of the cross sections of the coil and is pointing out of plane. In the same figure the magnetic field lines are displayed.

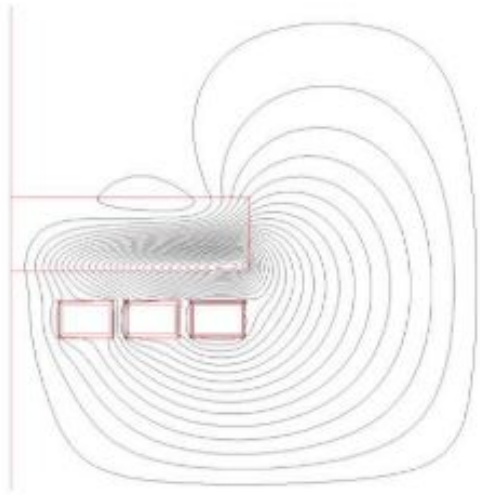

(a) Symmetrical cross-section, red; representation physical model, black lines; magnetic field lines

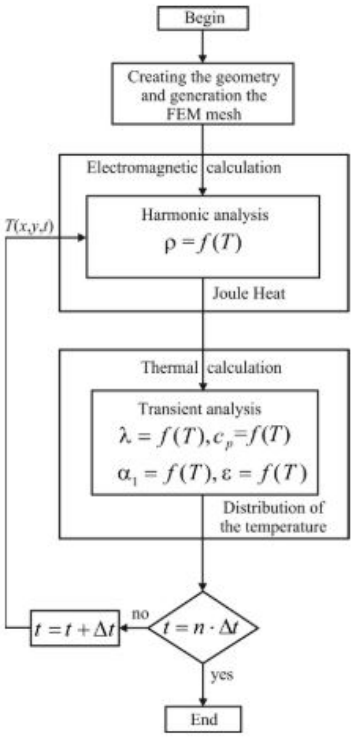

(b) Structure of the FEM model

Figure 2.8: modeling IH, a) symmetrical properties used ad advantage, b) structure of the FEM model[34]

Figure 2.8b gives an overview of the model structure in the commercial software Ansys. λ is the thermal conduction, ε the radiation and α the heat convection. After creating the model and the mesh the magnetic field lines are calculated and in this case only the Joule heating is calculated and magnetic hysteresis is neglected because of its lower contribution to the total The next step is to determine the distribution of the temperature as a result on the heat developed by the Joule heating in the first step. This will be a result of the convection of the heat through the material but also the radiation and so the cooling of the subject has a contribution that have to be taken into account. After this step the whole process has to be looped as a result of the non-linear properties in the system. In the research of [34] this model was used to make an optimization script where the position of the coil was taken as an variable to create an uniform heating profile.

In literature lots of similarities are seen in how FEM processes are approached, independent of which type of commercial package is used. In more recent literature the use of more than one coil and the dimensions or location of coils is used to optimize an heating profile. For example in [28] where the height to the subject is taken as an variable, or [14] where the shape of the coil is optimized for the most uniform temperature profile.

In the research of [13] the current density and the frequency of the power source are used as optimization parameters to optimize the heating rate. The effect of a flux concentrator was taken into account to point the heat at a certain location. Some choose to optimize for one single coil [20],in the case where quickly heating a small cavity is important for injection moulding. Others research the effect of multi layered induction coils on efficiency and uniformity of surface heating [12] or in multi coil optimization [6], where the optimization of a semiconductor wafer which had to be heated as fast as possible but still uniformly was investigated. Different coils were used with the same frequency but different amplitudes of current. In the research of [26] had to be optimized for its heating profile to eliminate cold spots for injection moulding. In this research multiple zones were created with different time of active heating to create an uniform heating profile of the surface. The goal was to use less power and heat up only the surface which, is more important for an high quality in case of injection moulding.

For the research in this master thesis the commercial software Abaqus CAE of Dasault systems is

used. Although not often seen in literature it is possible to make a co-simulation to model the induction heating with the use of Abaqus CAE. The fact that Fokker is using Abaqus CAE for simulation company wide makes the coupling from designing parts to manufacturing easier in the future if this simulation of the induction heating is made in the same software. Based on the literature review the following material- and process properties have to be found for the simulation, figure 2.9.

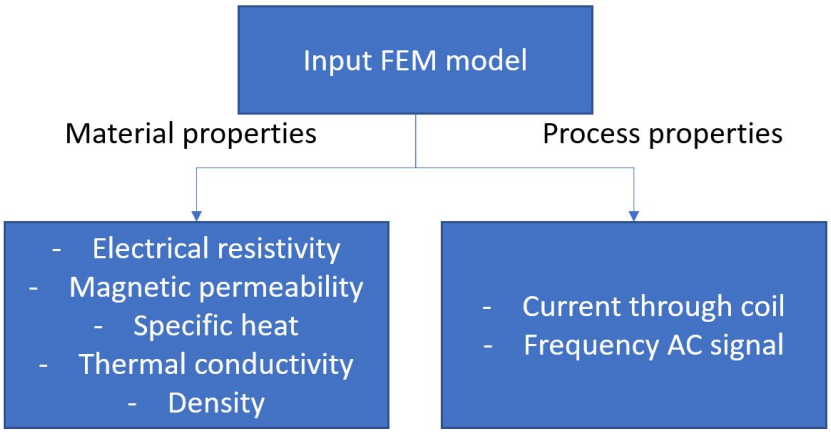

Figure 2.9: Material and process properties required as input for FEM model

2.4. Measure parameters

Based on the literature review the following parameters needed to be measured experimentally for the induction heating research, see table 2.2. Often parameters can be measured on different ways depending on the experimental setup and result required. The following parameters were found and are listed with their corresponding way of measuring as found in literature.

Table 2.2: Measurable parameters with their corresponding measurement devices

Parameter	Device		
Temperature	Thermocouples	Thermographic camera	-
Magnetic field	Magnetic field measurement sensor	-	-
Frequency	LCR meter (inductance (L), capacitance (C) and resistance (R))	Current clamp	Magnetic field measurement Sensor
Current	Current clamp	-	-
Voltage	Multimeter/ voltage meter	-	-

2.5. Research question

This master thesis is part of a project at Fokker where the goal is to technically secure a valid business case and accelerate implementation of the OoA Press (Co-)consolidation technology into aerospace applications. This thesis focuses on the heating of the (Co-)consolidating mould. Thermoplastics composites have proven to be suitable for this change in production process as mentioned in chapter 1.1. Consolidating of this thermoplastic composite requires a fixed recipe of pressure and temperature. In the OoA setup at Fokker, heat will be applied with use of an induction heating (IH) technology, IH has certain benefits; low cycle times, consistency and repeatability. The first steps were made in designing an testsetup as seen in figure 1.3, which was unsuccessfully used in verification of heating simulations in Abaqus CAE. The result of this research was that due to insufficient fundamental knowledge about the induction heating process the modeling with FEM software was not sufficient to converge results in experimental tests with results from simulations.

Together with the knowledge gained during the literature study the following main research question was formed:

What are the variables that influence the induction heating of the OaA mould and how can they be measured and verified to come to a reliable model?

2.5.1. Sub questions

This research question was divided in smaller sub question, together they will answer the main research question. The flowchart in figure 2.10 represents the structure of this thesis. The research is divided in three subjects also described via the three sub questions. First the material properties of both the mould and coil as a function of temperature is researched to find the contributing properties as well as their contribution to the accuracy of the simulation. As can be read in chapter 2.1.3, the electrical resistivity is one of the most varying parameters which means it has the largest contribution in verifying the heating as the temperature rises. This leads to the sub question:

1: What is the exact contribution of the non linear behavior of electric resistivity as a material property on the accuracy of the model?

The second sub question is about designing a simplified induction heating setup where process parameters can be measured and can be used to feed an Abaqus CAE model. It has to be mentioned that designing the FEA model itself is out of scope of this project, which means there will be focused on the input for the simulation model. This data will be divided into two streams; the verification of the input parameters like the frequency, current and voltage, cooling water temperature to verify the parameters used in the setup, and also the result like the temperature of the workpiece and the magnetic field at a given time:

2: How can with a simplified version of the mould and different configurations of the coil a test setup be designed where the coupling to a 3D FEM model can be made?

The last and third sub question is about optimizing the heating performance of the experimental setup. Therefore the model defined in research question 2 will be used to describe the necessary components to design an heating pattern for the use in the induction heating setup. The various parameters; process parameters, material properties, dimensions coil to mould and dimensions of the coil will be used to define an optimum in the heating pattern.

3: How can certain parameters be changed to end up with an desired heating profile of the mould?

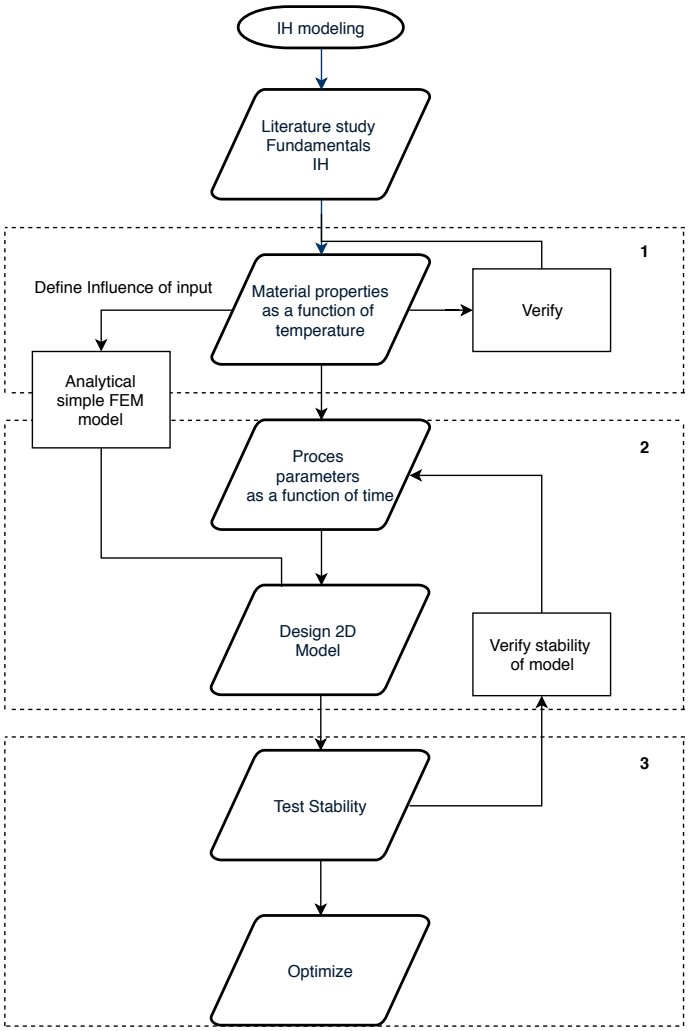

Figure 2.10: Flowchart thesis structure

2.6. Readers guide

This thesis is divided into three sections corresponding to the three sub-questions wit each sub-question has its own chapter 3,4 and 5 respectively. First, chapter 3 will answer sub-question 1. This chapter will look into the material and process properties contributing to the induction heating process. Also, the material properties will be found as a function of temperature for the mould material of the experimental setup used during this research. Thereafter chapter 4 will describe an experimental IH setup used to verify the FEM simulation. The chapter starts with an explanation of used assumptions during the design of the experimental setup and used the equipment during experiments. Thereafter is described how the simulations are performed, how the input data is generated and which assumptions are made when simulating. The chapter is finalized with a comparison of the experimental with simulated data. Chapter 5 gives a step by step solution to a simulation used for designing an induction heating setup. The final chapter will link information found in chapter 3, 4 and 5 to answer the main research question in chapter 6

3

Process properties

This chapter will answer research question 1: 'What is the exact contribution of the non linear behavior of electric resistivity as a material property on the accuracy of the model?' The research question and this sub research question 1 was based on the information gathered in the literature study. It was found that the electrical resistivity had the biggest variance as a material parameter in the temperature range of the production process. Because this production method will be designed for thermoplastic composites with an expected maximum melting temperature of 450 $^{\circ}C$ this was therefore kept as a operating range where the material properties have to be known.

In chapter 2.1.3 was found which material data and process data affects the IH simulation and it was assumed how much the parameters change as a function of temperature. But at what accuracy this material properties have to be known to have an useful simulation is not known.

These material properties were divided in electromagnetic and thermal properties. Four material properties were described as function of temperature, often these material properties are only known at room temperature and therefore used in simulations as a constant value. In table 3.1 it can be seen that the value of the material property can change substantially, in this case over a temperature range of 20-450 $^{\circ}C$. In the table '>' indicates an increase and '<' a decrease in the value compared to room temperature. From this table can be concluded that the electrical resistivity can introduce potentially the highest error in the simulation as it increases over 300 % compared to room temperature values.

Table 3.1: Material characteristics for induction heating for standard steel

	Symbol	Unit	Expected deviation
Electromagnetic properties			
Electric resistivity	ρ	$[\Omega \cdot m]$	300% >
Magnetic permeability	μ	$\left[\frac{J}{A^{(2)} \cdot m}\right]$	100% >
Thermal properties			
Specific heat	c	$\left[\frac{J}{kgK}\right]$	50%>
Thermal conductivity	k	$\left[\frac{W}{mK}\right]$	50%<
Density	ρ	$\left[\frac{kg}{m^3}\right]$	10%<
Cooling properties			
Convection	α	$\left[\frac{W}{m^2}\right]$	-
Radiation	C_s	$\left[\frac{W}{m^2}\right]$	-

This section defines the material data of the contributing components of the induction heating. The material properties of the mould will vary as a function of temperature, but the coil temperature will remain approximately 20 $^{\circ}C$ due to the cooling fluid. Therefore the material properties at room temperature will be used in the model for the coil, and the focus on this chapter will be on the material properties of the mould material as function of temperature. Table 3.2 gives the material data at room temperature of the mould material 'S355j2 +AR/m' which were found in the literature review.

Table 3.2: Materialdata S355j2 + AR/m at room temperature

	Value	Unit
Density	7800	$[kgm^{-3}]$
Specific heat capacity	460-480	$[Jkg^{\circ}C^{-1}]$
Thermal conductivity	40-45	$[Wm^{\circ}C^{-1}]$
Electrical resistivity	0.2-0.25	$[\mu\Omega m]$
Magnetic permeability	245	$[\mu_r]$

In chapter 3.1 the influence of the varying material data and their effect on the performance of the model will be described. This will be done with an analytical model and a propagation of error analysis. As the electrical resistivity was concluded to be the most varying material property this parameter was measured via an experiment in the TU Delft Aerospace Structures and Materials laboratory, described in chapter 3.2

In chapter 3.4 the material data will be verified with data from the software package 'JMatPro', which calculates the material data based on the element composition and behavior of element as function of temperature. Finally, research question 1 will be answered in section 3.5.

3.1. Influence of the accuracy of material data on induction heating simulations

In this literature study it was found that the value of material parameters can already differ substantially over the temperature range of room temperature till 450 $^{\circ}C$. For modeling it is useful to know which component influences the accuracy of the result. Therefore a propagation of error analysis is performed on the Maxwell equations as described in chapter 2.3.

Figure 3.1: Example of representation used in the research of Jankowski, left: representation of analytical model and FEM, right: verification setup, source: [21]

3.1.1. Analytical

Before designing a FEM analysis it is useful to determine the influence of the tolerance of the input to the output of the analysis. Therefore a propagation of uncertainty can be used.

$$s_f = \sqrt{\frac{\delta f}{\delta x}^2 s_x^2 + \frac{\delta f}{\delta y}^2 s_y^2 + \frac{\delta f}{\delta z}^2 s_z^2 ....} \tag{3.1}$$

This formula can be used for the function f where the components $x, y, z, ..$ are independent of each other, where s_f represents the standard deviation of the function f and $s_{x,y,z}$ the standard deviation of the independent variables.

Therefore an analytical equation is needed which describe the IH process as function of the material properties given in table 3.1. The Maxwell equations can be used to describe this, but are not analytical which makes it unusable for the propagation of error analysis.

An approximate analytical solution was designed by Jankowski [15] for a graphite cylinder with an coil with 'n' number of windings as shown in figure 3.1. This approximate solution describes the heating rate, the equivalent impedance of the associated tank circuit, and the frequency response of the frequency power of the tank circuit. A similar generator setup as in this thesis was used with the components placed in series. The research was done on a graphite cylinder with an 11 turn copper coil. During the validations the approximate solution shows a variation between the FEM and an analytical solution within 30 $^{\circ}C$ and a variation of frequency of 0.5 Hz. In this research all non magnetic materials were used and the magnetic permeability of vacuum was used as a constant $\mu = 4\pi \cdot 10^{-7} H/m$. Other material parameters as, electric conductivity, density, heat capacity and thermal conductivity were taken into account as function of temperature.

To be able to describe the IH process as an analytical equation Jankowski used a number of assumptions:

- Magnetic field purely axial, $\mathbf{H} = He_z$
- Electric field purely circumferential, $\mathbf{E} = Ee_0$
- Current through coil constant over cross section of coil
- Penetration depth below radius of cylinder
- Equal length of workpiece and coil, number of coil is represented as a density of coil according to the relation, n = N/L, N = number of turns and L = length workpiece.
- End effect at surface of cylinder is assumed as a result of the magnetic field between the coil and cylinder, H_s. For a short cylindrical current sheet is given $H_s = nIK_n$, where K_n is the modified Nagaoka coefficient corrected for finite length coil.
- $2\beta \leq 1$ with $\beta = b/l$, where the assumption of the Nagaoka coefficient is valid.
- $\varepsilon \leq 0.5$, where $\varepsilon = \frac{\delta}{R}$, is when the approximation of the δ is valid.
- thermal conductivity is assumed large enough so an lumped parameter model could be used where spatial temperature gradients are ignored. Ie; rise in temperature is assumed equal over the whole temperature at each point in time.
- non magnetic components, $\mu = constant = 4\pi x 10^{-7} H/m$

The temperature of the load was approximated with the following equation which is a first order fully explicit integration. The equation was simplified by using dimensionless variables, which are mentioned below.

$$\theta_{i+1} = \theta_i + \frac{\Delta\tau}{C^*_{p,i}}\Big[\frac{1}{\sigma^*_i}(\sqrt{\sigma^*_i \omega^*_i} - 0.5) - 2\varepsilon_R(1 + \frac{R}{l})(\theta_i^4 - 1)\Big] \tag{3.2}$$

$$\theta = \frac{T}{T_\infty}, \tau = \frac{t\sigma_b T_\infty^3}{(\rho c)_\infty R}, \sigma^* = \frac{\sigma\sigma_b R T_\infty^4}{n^2 I^2 K_n^2}, \omega^* = \frac{\omega\mu R n^2 I^2 K_n^*}{2\sigma_b T_\infty^*}, C_p^* = \frac{(\rho c)}{(\rho c)_\infty} \tag{3.3}$$

Table 3.3: Corresponding values of test #1, Jankowski, [15]

Sign	Unit	Description	Value
T_∞	Kelvin	Ambient temperature	293.15
t	seconds	Timestep	1
σ_b	$Wm^{-2}K^{-4}$	Stefan-Boltszmann constant	$5.67{\cdot}10^{-8}$
R	[m]	Radius	0.0451
N	[-]	Turns per unit load lenght (n/l)	55.56
I	[A]	Current at coil	467.72 (44%x1063)
K_n	[-]	Modified Nagoaka coeficient	0.86
$\bar{K_n}$	[-]	Nagoaka coeficient	-
ε_r	[-]	Surface emissivity	0.9

Table 3.4: Influencing variables with corresponding values

Sign	Unit	Description	Value
c	J/kgK	Specific heat	721
ω	rad/s	Radial speed frequency	$2\pi 15800$
ρ	kg/m^3	Density	1720
σ	Ω^{-1}	electrical conductivity	75250
μ	H/m	Magnetic permeability	$4\pi \cdot 10^{-7}$

As the values of the variables were verified by Jankowski et al and not all of the variables are known for the setup at Fokker, the variables and dimensions of Jankowski were used in this analyses. The variance between room temperature and actual values of the material properties is taken from the data in section 3.4 and is given as a percentage compared to the value at room temperature in table 3.5. The variance is the difference at 450 $^{\circ}C$ compared to RT. In figure 3.2 an example is given of how the difference is measured; blue is the material property when the value of room temperature is taken for the whole simulation and red when the material property is a function of the temperature. This values are used as deviation for the propagation of error analysis. For the analysis the derivative with respect to the particular variable has to be calculated, the full derivative can be found in Appendix A. To compare the influence per material property the standard deviation from table 3.5 of the particular variable is taken while the others is taken '0'. The standard deviation s_f represents the influence on the temperature increase of that variable.

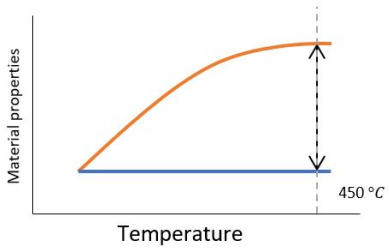

Figure 3.2: Input parameter error propagation analysis

Table 3.5: Input and result of propagation of error analysis

Material properties	**Input variance** [standard deviation]	**Ouput variance** [standard deviation]	**Temperature difference** [$^{\circ}C$]
Electric resistivity	1.87	$1.55{\cdot}10^{-2}$	4.55
Density	0.019	$3.91{\cdot}10^{-4}$	0.11
Specific heat	0.47	$9.67{\cdot}10^{-3}$	2.84
Magnetic permeability	0.01	$1.23{\cdot}10^{-4}$	0.036
Proces properties			
Angular frequency	0.01	$4.11{\cdot}10^{-4}$	0.12
Current at coil	0.01	$1.23{\cdot}10^{-4}$	0.036

3.1.2. Result propagation error analysis

In table 3.5, the results of the propagation of error analysis are given. At first the material properties will be discussed. As an input for equation 3.1, a value for s_x has to be given which represents the deviation of the value of the variable. The standard deviation of this particular variable was calculated and used in equation 3.1 and its percentage to room temperature is given in table 3.5. Per variable the effect on s_f was calculated while other variables were kept at $s_{variable} = 0$ to isolate the specific variable. The values in table 3.4 and table 3.3 where used which represents Jankowski's experiment #1[15] as the values were verified in the research. Since the rate of the change of the error is important compared to the error of the other variables, it was chosen to analyse at a timestep of 1 second in equation 3.2.

This means that the second part after the '-' sign remains relatively small due to $\theta = T/T_\infty$and can be neglected. It also means that the rates of change can be compared to find out which variable has the biggest effect on the total result. In column 3 of table 3.5 the effect of the variable as a percentage to the value of θ is given. In column 4 the increase of temperature is the result of the error of the variable after 1 timestep.

When looking at the numbers in column 4 the electric resistivity and after that the specific heat have the biggest influence on the induction heating process, which agrees with Rudnevs claim [21]. Therefore it was concluded that the electric resistivity has the biggest effect on the result of the simulation both due to the relatively big spread in value from room temperature and 450 $^\circ C$ and the effect calculated with the error propagation formula. Chapter 3.2 describes the process of measuring the electric resistivity in the temperature range needed for this production process.

Besides this in table 3.5 the process parameters are mentioned. The current is defined as at the coil, and the frequency is the radial frequency. As input for the error propagation analysis 1% of the measured value was taken. As result of the analysis the frequency shows 0.12 $^\circ C$ and the current 0.036 $^\circ C$ per 1% difference to the actual value. In practice the frequency is displayed by the generator itself and the current has to be calculated via input parameters on the generator. The frequency is often more important for the performance of the IH system as it directly influence the penetration depth and so the way the heat spreads over the workpiece, also the frequency is fixed by the hardware components of the tank circuit as later will be explained in chapter 4.1. The frequency is more important to know accurately compared to the current, as the current is a parameter which can be directly steered by the input parameters of the generator.

3.2. Electric resistivity measurements

The electric resistivity, also known as the specific electrical resistance or volume resistance is the reciprocal of the electric conductivity. Electric resistivity $[\Omega m]$ is a non-linear variable with respect to temperature, which contributes to the penetration depth, frequency and Joule heating in the case of induction heating of an object. In simulations the value of this material property is often taken as constant as the value at room temperature. This introduces a significant error in the results at high temperature (over a range of room temperature to 450 $^\circ C$ the value of electrical resistivity can rise by 300% [30, p.19]).

The electrical resistivity is a function of the resistance of the material and the dimensions of the workpiece according to the following relation:

$$\rho = R\frac{A}{l}[\Omega m] \tag{3.4}$$

Where 'A' is the surface of the cross-section of the sample in $[m^2]$ and 'l' the length in $[m]$. During the experiments the resistance 'R' is measured, which together with the volume dimensions allows the electrical resistivity 'ρ' to be calculated.
The resistance of the material can be measured and calculated via Ohm's law, which defines the relation between current, voltage and resistance. This principle is also used in multimeters and is called the 'two point technique' [7, section 43.3] due to the two contact point at the sample. Often this method is sufficient when measuring resistance. In figure 3.3 the electrical circuit is displayed which is also used in multimeters, where l is the length of the sample used in equation 3.4, and h and w the height and width of the sample used to calculate the area A also used in equation 3.4. A voltage is applied to the sample whereafter a current 'I' is flowing through the sample. The ratio of voltage over current is used to calculate the resistance which is displayed on the screen of the multimeter. In figure 3.4 it can be seen that for samples with low resistances this way of measuring introduces an error in the value. The resistance of this type of steel is in the range of $1.0{\cdot}10^{-3}$ Ω and not 0.1Ω as is displayed on the screen of the multimeter.

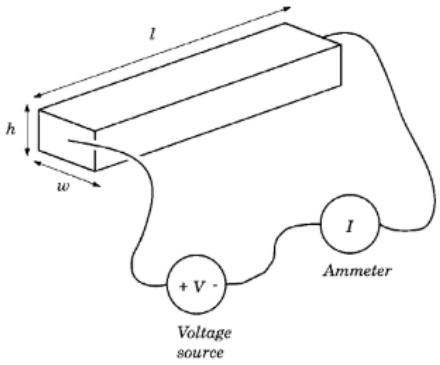

Figure 3.3: Two point measurement schematic

Figure 3.4: Resistance two point measurement on multimeter

This increase of the measured resistance is a result of:

- The resistance between the contact wires and the sample
- The resistance of the measuring wires and the internal circuit of the multimeter is added to the resistance of the sample
- The applied current modulates the sample's resistance

This increase in resistance when measuring with this two point method need always be taken into account when measuring resistance with a multimeter. To be able to measure without the influence of this parameter and so be able to measure lower resistances of samples the 'four point technique' is designed [7, section 43.3]. The four point techniques uses four points directly in contact with the measured sample. Two contacts are used to set up a current loop with the use of an current source and an ampere meter. The two other contacts are used to measure the voltage drop over the sample. The schematics of this electrical circuit can be seen in figure 3.5. The contact error is reduced as the current loop is separated and only the current is measured in this loop. Only the voltage drop over the sample is measured and not over the total circuit as is done when using the two point technique. The readings of both the current and voltage are used to calculate the resistance of the measured sample. This four point measurement is often used when the measurement of resistance has to be done with high accuracy. This is also found as a standard measurement option on various lab multimeters, for example the Keithley model 2701.

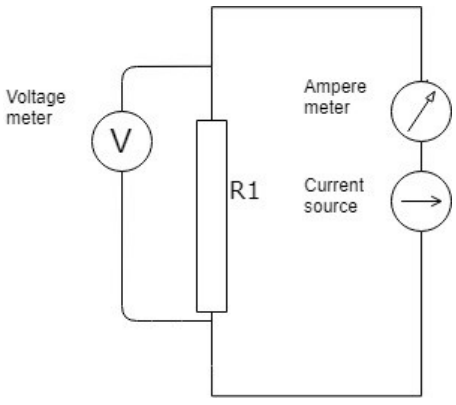

Figure 3.5: Simple electrical circuit 4 point measurement

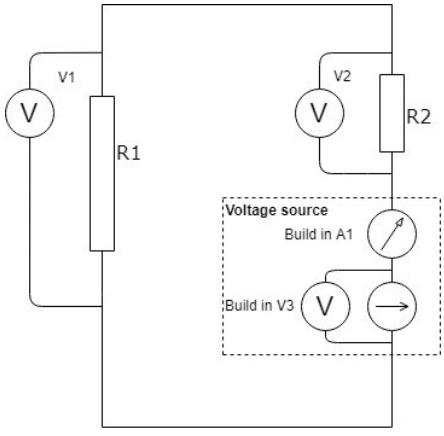

Figure 3.6: 4 point electrical circuit used in experiments

V1 is the voltage drop measured over the sample. R1 is the resistance of the sample during the experiment. V2 is the voltage drop measured over the resistance R2. R2 is the added resistance in

the circuit to lower the current and make a more stable reading possible. The voltage source in figure 3.6 has a built in current and voltage meter displayed by the A1 and V3.

3.2.1. Description of experimental setup

To measure the resistance a measurement setup is needed which: holds the sample, isolates the 4 contact points and is able to be placed in temperatures up to 450 $[^{\circ}C]$. A setup used before in research by K. Verwer [31, Appendix B] was used. This setup was previously used up to 250 $^{\circ}C$ and had to be adapted to cope with higher temperatures and to increase measurement accuracy and consistency. Therefore the contact points and the insulation material were changed. The two contacts of V1 were changed from a brazing to spot welds. Spot welding of the contacts is more reproducible as no filler material is used so the contact area is more constant, see figure 3.8. The isolator disks were made from foam that could resist the temperatures in the oven. The contact points for the current circuit were made from copper and shaped into cones to match the requirement of the minimal contact area. The final setup can be seen in figure 3.7.

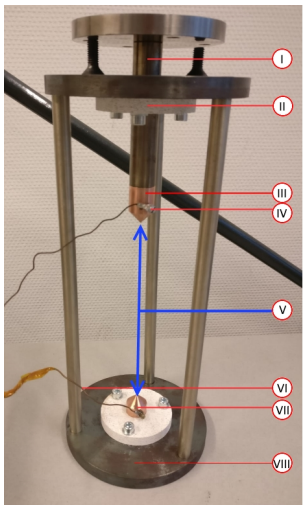

Figure 3.7: Measurement setup

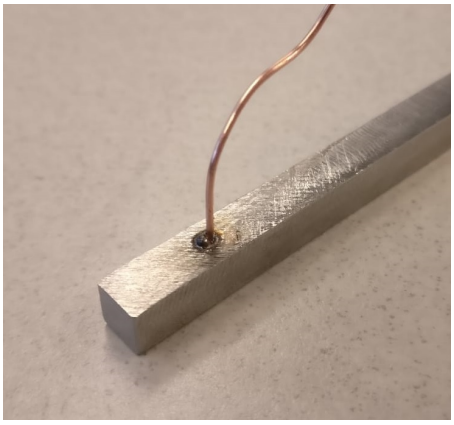

Figure 3.8: Spotweld of measurement wires to sample

In figure 3.7 the following components are listed: I Movable shaft to keep pressure on sample constant, II Isolator disk top, II Copper cone with minimal contact area, IV Screw on measurement point 'current circuit', V Place for sample in measurement circuit, VI Screw on measurement point current circuit, VII Lower copper cone with minimal contact area and VIII Steel support structure.

3.2.2. Equipment and accuracy

For the measurement the following measurement equipment was used. Their range and resolution is mentioned in table 3.8.

- Voltage: Keithley 2701 with an 7701 differential multiplexer
- Temperature: Keithley 2701 with an 7701 differential multiplexer
- Resistance: Keithley 2701, 4 wire resistance measurement with offset compensation on

Table 3.6: Accuracy of measurement equipment, Keithley 2701

Voltage		**Accuracy** [1]	
Range	Resolution	Reading	Range
100.0000 [mV]	0.1 [V]	30 [ppm]	35 [ppm]
Resistance		**Accuracy**	
Range	Resolution	Reading	Range
1.000000 [Ω]	1 [$\mu\Omega$]	100 [ppm]	40 [ppm]
Temperature			
Range	Resolution	Accuracy	
-200 + 760 [$^{\circ}C$]	0.001 [$^{\circ}C$]	1.0 [$^{\circ}C$]	

Measure resistance of R2

In[2] the electrical circuit an extra resistance R2 was added see 3.6, to reduce the current in the electrical circuit and measure the current flow through the circuit. For this current measurement the resistance of R2 has to be known. This resistance was measured by the Keithley 2701 by the four point measurement method. The measurement is schematically described in Figure 3.9. The measured value of the resistance with the corresponding accuracy is presented in Table 3.7. Also the current at one point[3] during the measurements is given to indicate the accuracy of the calculated current during the measurements. The current which is running through the sample is not constant and this value was taken into account during the measurements.

Table 3.7: Resistance value and accuracy R2,source [29]

Resistance R2 measured with Keithley 2701	
Resistance	102$\pm$0.05 [mΩ]
Current running through sample	285$\pm$0.1[mA]

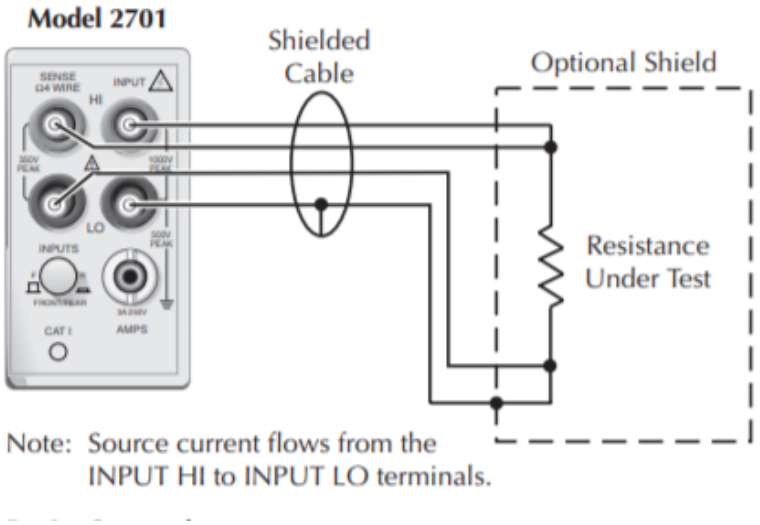

Figure 3.9: 4 ohm resistance measurement with Keithley 2701,source; [2, p.3.23]

[2]Ppm= Parts per million, 10 ppm =0
[3]Data used at 28 [°C]

3.2.3. Accuracy of measurements

The accuracy on the measured electric resistivity was calculated using a propagation of uncertainty analysis. The electric resistivity was measured 2.26$\dot{1}0^{-7}\pm$-9.84$\cdot10^{-10}$ [Ωm] at room temperature, and 5.64$\cdot10^{-7}\pm$2.039$\cdot10^{-9}$ [Ωm] at 410 [°C], which is 0.44% error at room temperature and 0.36% at 450 [°C]. The error between the different measurements is discussed later in section 3.2.8.

Table 3.8: Accuracy on measurement equipment, source [29]

Accuracy of measurement equipment	
20 [$^{\circ}C$], Room temperature	226$\pm$1.0 [nΩ]
450 [$^{\circ}C$]	564$\pm$2.0 [nΩ]

3.2.4. Sample dimensions experiment

For the sample dimensions the guidelines of the 4 point van der Pauw method was used. The sample has to be of constant thickness and the contact points have to be independent. Because the oven can have a temperature distribution it is useful to use a relative long sample so possible temperature variations along the length of the samples can be averaged out due to the length of the sample. Two samples were used during the measurements, with the orientation of the grain 90° rotated. Sample 1 has the grain orientated at 0° and Sample 2 has the grain perpendicular to this. The dimensions of the square cross-section are given in Table 3.9. L1 is the length between the two spot welded contact points.

Table 3.9: Dimensions of the sample

Sample	**I[mm]**	**II[mm]**
Width	5.98	5.76
Height	5.98	6.00
Length (L1)	166.72	156.33

3.2.5. Room temperature validation measuring setup

The calculation of the resistance $R = \frac{U}{I}$ relies on the fact that the current flowing through the resistor is directly proportional to the voltage across it; ohmic behavior. When this is proved the resistance R can be calculated with the relation $\frac{U}{I}$, which is used for both the calculation of the current running through the circuit as well as the resistance of the sample.

Metals are assumed to be ohmic when the temperature is constant, this was verified at room temperature. The voltage of the voltage source was increased in steps and the current was measured per step. This gave also the possibility to compare the values of the electric resistivity with values found in literature. For this test the voltage was set at 0.1 [V] and increased to 1.53 [V] in 8 steps. The current and the voltage drop over the sample was measured and used to plot an regression line through the data points. The line and relation in Figure 3.10 shows that the behavior of the material is ohmic. This measured data was used to calculate the electric resistivity, 2.26$\cdot10^{-70}$ [Ωm] which was found to be similar to literature values at room temperature (found values between the values: 2.0-2.5$\cdot10^{-7}$[Ωm]).

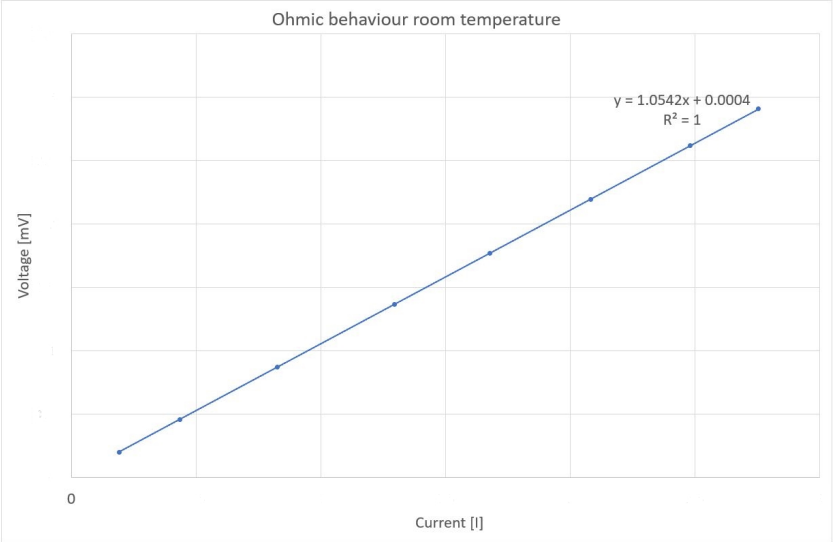

Figure 3.10: Ohmic behaviour sample

3.2.6. Heating during experimental setup

During preliminary testing it was noticed that the oven had an influence on the measured value of the electric resistivity see Figure 3.11. Directly after heating the value of the electric resistivity dropped below the value at room temperature. It was assumed that this was a result of the air flow activated by the hot air oven. For this reason all the experiments were performed with the oven cooling down. So first the oven was heated until 450 [°C] and then turned off. Therefore measurements were performed when passive cooling occuring without the oven influencing the results. The downside of this is that the measurement period was relatively long as the oven is insulated and the temperature does not drop fast.

Because of the long experiments at high heat there is a great chance that corrosion occurs at the contact points. At preliminary testing this occurred at the copper cones which interrupted the signal and let the measurement fail. For this reason it was chosen to put an extra weight on the movable shaft (indicated as no.1 in Figure 3.7.) which solved the problem. Figure B.5 gives an example of the corrosion on the copper tip.

The specifications of the oven do not affect the results of the measurements as the oven is only used as an insulating box. The full setup with measurement wires was placed in the oven and heated up. When the oven was at 450 $^{\circ}C$ the oven was turned off and the measurement start without opening the oven. This result in an reliable cooling down period without a minimum of air flow through the oven. The basic specifications of the oven used are given in Table 3.10:

Table 3.10: Important data of oven used during experiments

	WU600 Heraues
Temperature range	Room temperature-500 [$^{\circ}C$]
Dimensions inside wxhxd	475-475-420 [mm]
Rated power	5.4 [kW]
Rise up to 500 [$^{\circ}C$]	70 [min.]

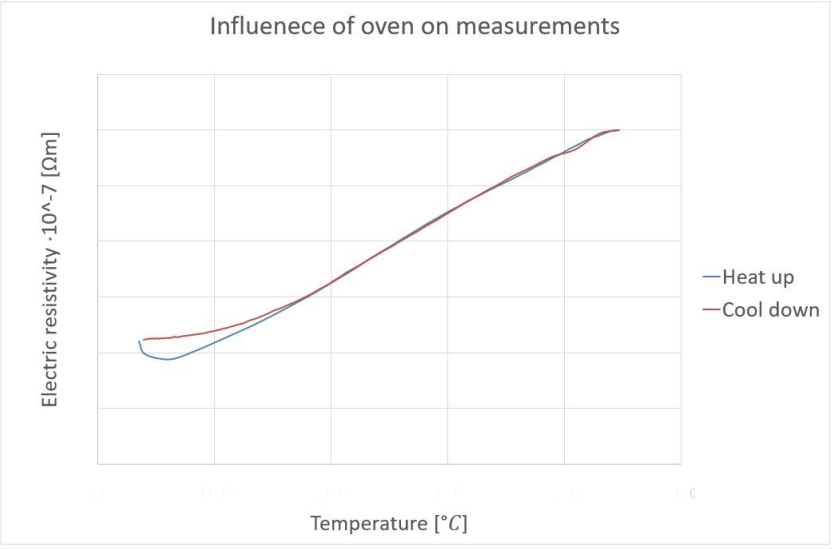

Figure 3.11: Influence of turning oven on and off

3.2.7. Temperature measurements

As mentioned in section 3.2.2, the temperature was measured with a K type thermocouple conntected to the Keithley 2701. Because this measurement of the resistance relies on small differences in voltages and because thermocouples measurements are based on potential differences between two different metals it was possible that this thermocouple measurement influences the measurement of the resistance of the materials. If the thermocouple is placed directly on the to be measured sample this could influence the resistance or the temperature measurements. Therefore an extra sample was used which was not placed in the electrical circuit to measure the temperature during the experimental test. The sample was placed at a distance of 10 [mm] from the sample in the electrical circuit so the temperature of the extra sample was representative to the sample in the electrical circuit.

3.2.8. Results electrical resistivity measurements

An average was taken of 8 measurements and the results are shown in Figure 3.12. The maximum difference between the average and largest error from this was 1.07 %. Together with the error on the equipment this will give an maximal error of 1.07+0.44 = 1.55% at the lower temperature readings and 1.07+0.36 = 1.43 % for high temperature readings. The accuracy on the electrical resistivity can be found in Table 3.11. A dependency of the grain direction was not observed in the measured values. This isotropic behavior is useful to know as it simplifies the experimental test in the future and simplifies the simulations.

Table 3.11: Accuracy electrical resistivity

Accuracy on measurement equipment	
20 [$^{\circ}C$], Room temperature	2.26E-7+/-5.93E-10 [Ω]
450 [$^{\circ}C$]	5.64E-7+/-6.98E-9 [Ω]

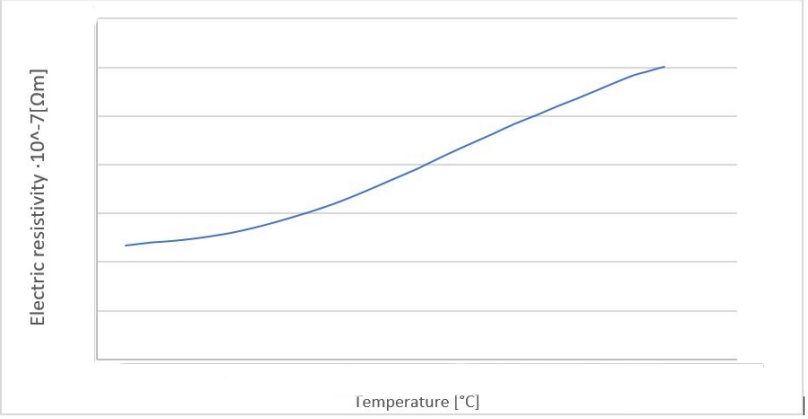

Figure 3.12: Electric resistivity as a function of temperature of S355j2

3.3. Recommendations for experimental setup

For a higher accuracy on the electrical resistivity test for future mould materials the following points will increase the accuracy on the measurements:

For high accuracy with the current setup:

- Use a weight to increase the pressure of the copper cone to the sample
- Clean or roughen up the surface of the sample and the copper cone
- Keep the temperature of the surroundings constant, specifically the temperature of resistance R2, as this can influence the resistance of R2 and wires.
- Bench test the setup to check the setup, this gives also an opportunity to verify with values found in the literature at room temperature.

To increase the accuracy on the measurement:

- Increasing the accuracy of the temperature measurement, in the case above a accuracy of 1.0 [$^{\circ}C$] was reached because an module had to be used which lowered the accuracy of the measurements.
- Spot welding the contact points is preferred to lower the chance on failing an experiment due to contact loss.
- A separate current meter can be used with an accuracy high enough, this eliminates the step of measuring R2 and calculating the current. This will not mean that R2 can be eliminated from the electrical circuit as it lowers the current in the circuit.

3.4. Material properties mould material

In chapter 3.2 the electric resistivity was defined by measuring it experimentally. In chapter 3.1 was mentioned that for the simulation model the following material parameters are required to end up with a reliable model. Which means that only for the electrical resisitivity the material data is available as a function of temperature (from room temperature until 450 $^{\circ}C$).

In chapter 2.1.2 it was mentioned that for electric resistiviy of pure materials their exists a relation (2.3) where, α the temperature coefficient defines how much the value differs from room temperature. The mould material 'S355J2 + AR/m is not a pure material but a low carbon steel which consists of a number of different elements in various percentages, as shown in table 3.12. This means that every element in this material has a certain contribution to the sum of elements. For this type of calculations software is available that can calculate the behavior of each elements as a function of temperature.

JMatPro® offers software which can calculate material properties based on physical principles instead of purely statistical methods [25, p.64]. JMatPro has been validated which can be found in [25] and per type of calculations on the website of the company. For the calculations of JMatPro the following information is needed:

- Exact composition in percentage of total
- Previous heat treatment of the alloy (During manufacturing and not during IH)
- For magnetic permeability:
  - The hardness of the material at room temperature or 0.2% proof stress or tensile stress.

– If the material has a course (lamellar or normalized) microstructure or fine (quenched and tempered).
– Estimated heating rate during the IH process.

The following data was used for the calculations in JMatPro for the material S355J2 + AR/m:

Table 3.12: Chemical composition S355J2 + AR/m

Element [%]	C	Mn	P	S	Si	Cu	Fe
S355J2 +AR/M	.20	1.60	.025	.025	.55	.55	97.05

- Thermal mechanical rolling
- Tensile strength of 480 $[N/mm^2]$
- Hardness 164 [HB]
- Microstructre is fine, quenched and tempered

For the model the following material data as function of temperature (from 0 till 1200 $^\circ C$) was generated with the software:

- Density $[\frac{g}{m^3}]$
- Electrical resistivity $[\Omega m]$
- Specific heat $[\frac{J}{g^\circ C}]$
- Thermal conductivity $[\frac{W}{m^\circ C}]$

The data found in section 3.2.8 were compared with the data calculated with JmatPro. The electric resistivity was measured until 450 $^\circ C$ so only this could be compared. The compared values can be seen in figure 3.13. In the figure the error during the measurements are taken into account are indicated with error bars in graph 3.13.

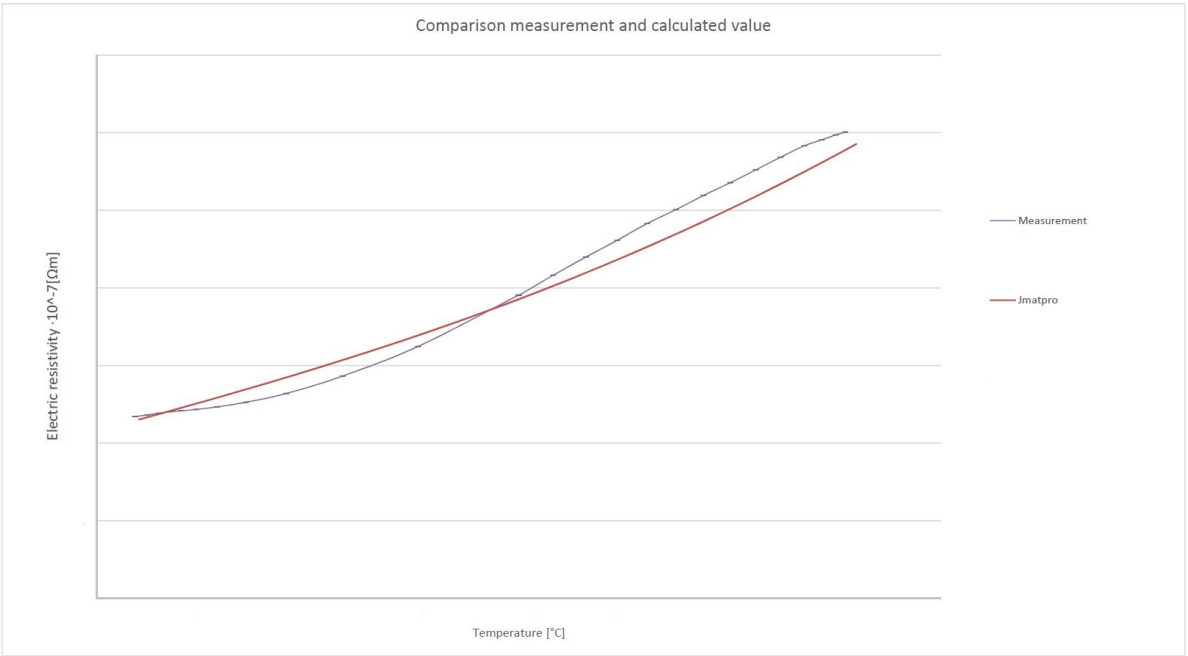

Figure 3.13: Comparison experimental measured data vs JMatPro, Electrical resistivity

Also required for the model but not as function of temperature is the magnetic permeability. As mentioned in chapter 2.1.2 the magnetic permeability can be defined as a relation between B/H or μ, so both are calculated. Different software packages require different input methods for the magnetic permeability. JmatPro defines the magnetic permeability as a function of heating rate during the IH. Different heating rates of 5,10 and 20 $^\circ C/s$ were calculated but there was much difference shown compared to the variance as function of ratio B/H field, as can be seen in figure 3.14. Therefore the

values at the heat rate 10 $^{\circ}C/s$ were used. Because there was no difference noticeable between the 5, 10 and 20 $^{\circ}C/s$ and 10 $^{\circ}C/s$ is a heating rate expected heating rate in production.

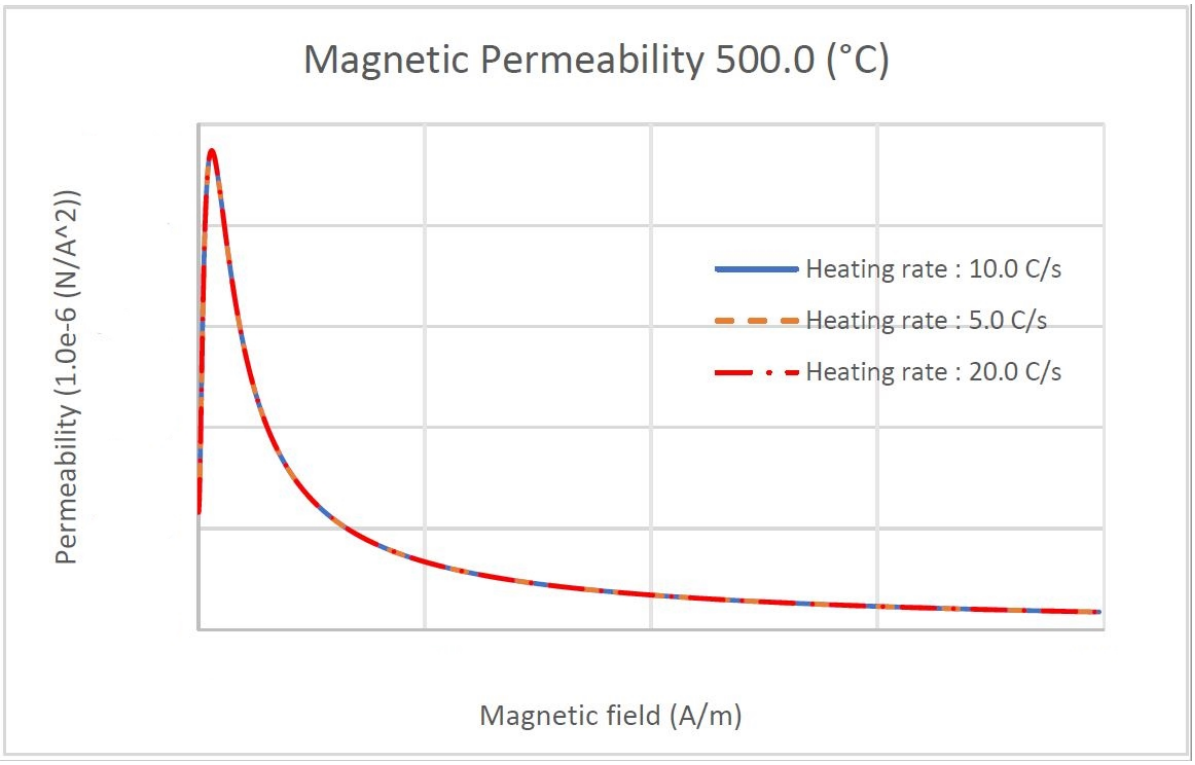

Figure 3.14: Comparison magnetic permeability different heating rates

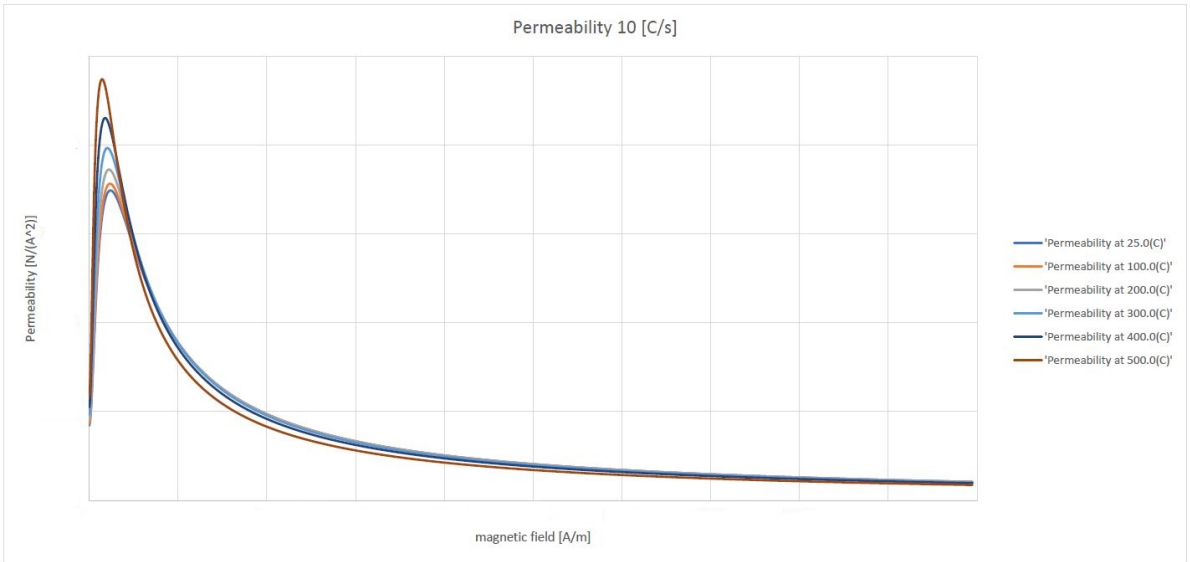

Figure 3.15: Magnetic permeability as function of magnetic field, at different temperatures

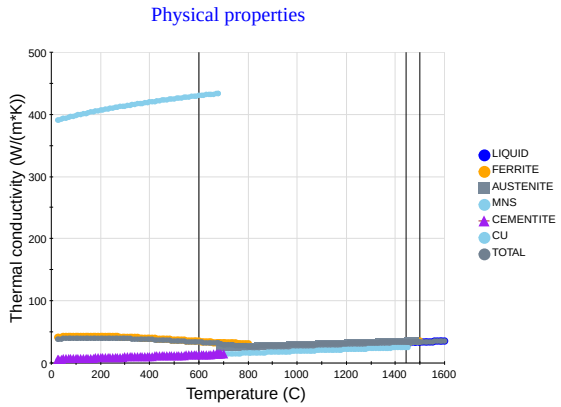

Figure 3.16: Thermal conductivity phase details visible

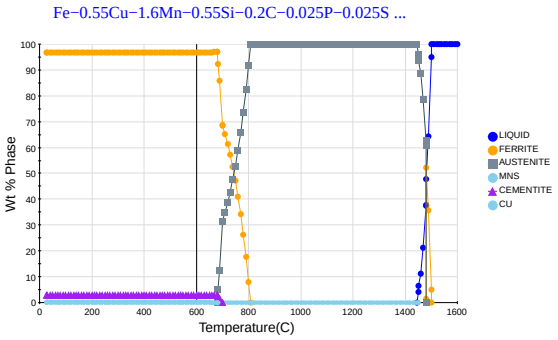

Figure 3.17: Thermal conductivity weight percentage of phase

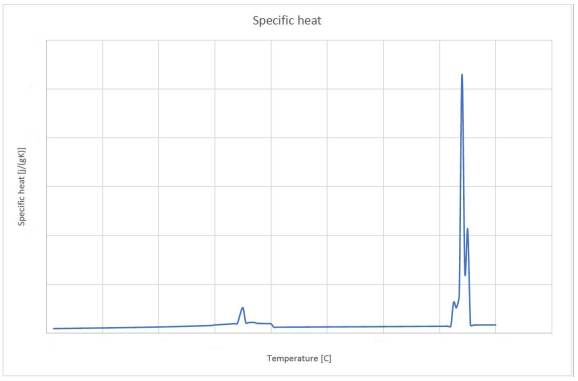

(a) Specific heat

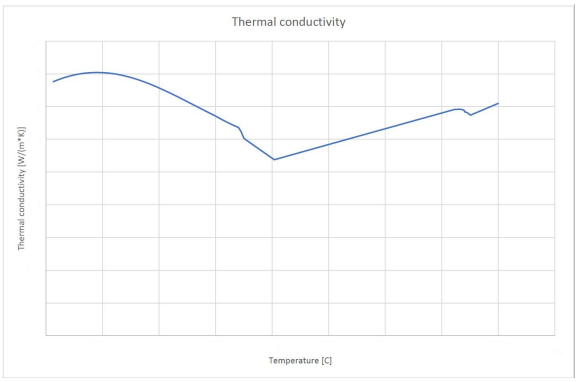

(b) Thermal conductivity

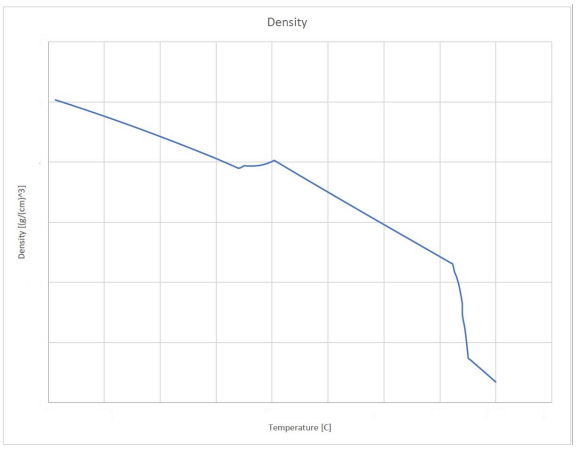

(c) Density

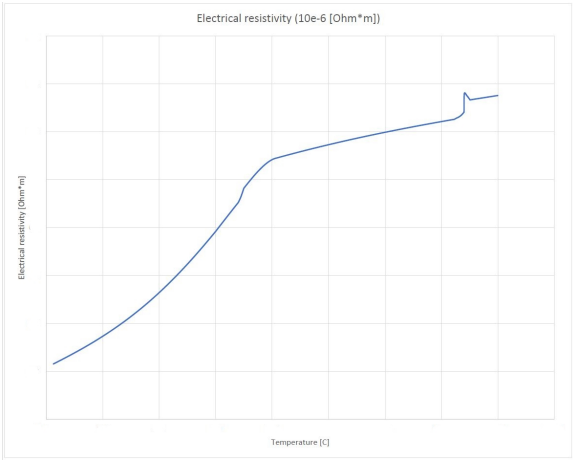

(d) Electric resitivity

Figure 3.18: Calculated material data JMatPro S355J2 + AR/m

3.5. Conclusion research question 1

Research question 1: 'What are the variables that influence the induction heating of the OaA mould and how can they be measured and verified to come to an reliable model?'. In the literature study was found that for a reliable model the following material properties need to be known for the mould material (conductor) as function of temperature:

- Thermal conductivity in $[W/m^{\circ}C]$
- Heat capacity in $[J/kg^{\circ}C]$
- Density in $[kg/m^3]$
- Electric Conductivity in $[S/m]$
- Magnetic Flux Density or B/H ratio

For the inductor the values of this parameter above are only needed at room temperature because coils are kept at a constant temperature. As the variation in temperature over the length of the coil is not influencing the material properties compared to the temperature changes in the conductor this is an valid assumption. Often in the FEM analyses the conductor is not analyzed in terms of temperature rise, as is assumed that the inductor is kept in the same temperature only the electromagnetic properties (electric resistivity and magnetic permeability) have to be known to form the magnetic field in and outside the inductor. It is possible to analyze the heating of the inductor, which is done when analyzing the efficiency of the cooling or generator. For this research, only the electric resistivity and magnetic permeability of the inductor at room temperature is sufficient to analyze the heating performance of the IH system.

In the literature study was found that in the range RT - 450 $^{\circ}C$ the electric resistivity had the biggest deviation from the low to the high temperature. Besides this was found that both magnetic permeability and electric resistivity had an influence on the skin depth when looking at the material properties. The influence of the material and process parameters were studied in section 3.1 via an propagation of error analysis, where was found that an error on electric resistivity had the biggest influence on the outcome of the simulation, directly after the specific heat.

Electric resistivity was measured during the experimental measurements described in chapter 3.2. Due to time limitations and earlier similar tests at TU Delft it was chosen to measure only the electric resistivity. The measurement setup was adapted to be able to measure reliable till 450 $^{\circ}C$. Multiple measurements show similar results. The grain direction did not show any measurable difference in or against the direction of the grain. This means that this does not have to be modeled in the final FEM model of the IH system.

During the research the software package JMatpro was used to find the missing material properties as function of temperature. The measured values of electrical resistivity were compared with the calculated values and are shown in figure 3.13. The figure shows that the values are comparable and that the data from JMatPro can be used for the FEM simulation model. The other material properties (heat capacity, density and thermal conductivity were compared at room temperature and showed similar values. The magnetic permeability is given by JMatpro as relation between; magnetic field and permeability (A/m and N/A^2), which are not compared with any other value.

The next chapter will compare measurements on an IH setup with FEM results. The chapter is divided into three parts: Firstly the IH setup will be described, and the choices made on the dimension and measurement setup will be explained. Secondly, the FEM simulation in will be explained. Finally the comparison between the experiment and FEM simulation will be presented.

4

Validation of simulation with small scale induction heating setup

Chapter 4 will answer research question 2: ”How can with a simplified version of the mould and different configurations of the coil a test setup be designed where the coupling to a 3D FEM model can be made?” The design of the test setup will be described in chapter 4.1, thereafter the used simulation for the verification is explained in chapter 4.2. The measured and calculated results are discussed and compared in chapter 4.3, and the answer to this subquestion is answered in chapter 4.5.

4.1. Experimental setup Induction Heating

The goal of this experimental IH is retrieving data to validate the simulation model. This means that a simple setup is chosen to make simulation easier, as this can be a difficult task with induction heating as discussed before in chapter 2.1.

For the experiments, the setup shown in figure 4.1 was used. Figure 4.2 displays a simplified representation with only the coil and the metal plate which acts as a mould surface. It was chosen to use this configuration for the experimental setup for two reasons: It is already available which is an important factor as this type of coil is costly in terms of cost and in time to produce was the fastest option, but thirdly other research on larger experimental setup is also been performed with this type of meander coil, which potentially makes it beneficial when scaling the simulation up to this mould.

The mould plate is constant in thickness and wider than the width of the coil, together with the relative long depth (300 mm) it makes this possible to simulate a 2D cross-section of this experiment. This makes it possible to neglect the edge effect 2.1.1 in the Z-direction, and to visualize the effect of the meander type coil, which results in an alternating direction of the current through the coil.

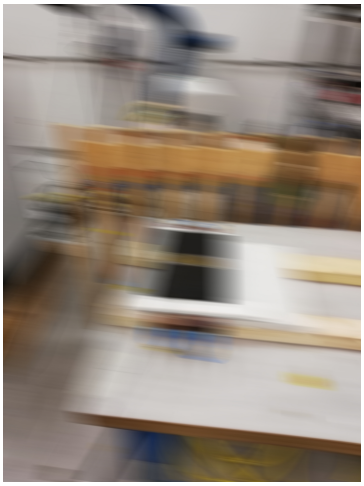

Figure 4.1: Experimental setup of induction heating

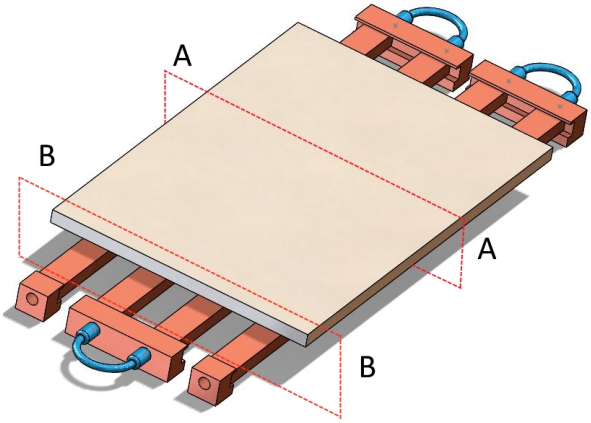

Figure 4.2: Representation experimental setup, a copper water cooled coil with an metal plate as mould surface

The hollow coil is made of copper, water cooled and kept at a temperature of $20 \pm 1°C$. The dimensions of the cross-section are 20x10x2 [mm], the dimensions of the whole coil and the full setup can be found in appendix D. The water cooling will be done by a separate cooling unit which also cools the IH generator.

The metal plate, which acts as a conductor, has the dimensions of 190x300x95 [mm]. In figure 4.1 the mould is painted black over the total surface with the exception of the center cross-section where the thermocouples are attached to the surface of the mould. The material of the mould will be low carbon steel, steel grade: 'S355J2 + AR/M'[1]. Chemical composition and material data as function of temperature can be found in chapter 3.4 and Appendix D.

The temperature of the mould during the experiments was measured with thermocouples at the location of the cross-section as visible in figure 4.4, the K-type thermocouples are fixed to the material with Kapton tape. Figure 4.4 and 4.3 gives a clear overview of the position of the 7 thermocouples, an extra thermocouple was placed on the blue water hose, which is also visible in figure 4.1. Although this does not give an exact reading of the water temperature during the experiments, it does give an indication of the generator showing an accurate reading of the water temperature.

Figure 4.3: Thermocouple location (after experiment)

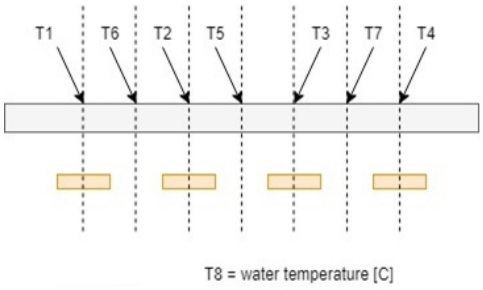

Figure 4.4: Location of thermocouples at cross-section

The heating of the setup was performed with an induction generator from Trumpf, model: TruHeat MF 3040, which was modified for control via an excel spreadsheet. This program was given a current or power signal as input for a given time. The generator is a mid-frequency range generator (5-10 $[kHz]$). Before IH generator inputs are discussed first a brief explanation of the generator principle will be given.

A general explanation will be given that is specific to this type of generator. The generator principle is shown in figure 4.5. The input for the generator is an AC current from the power grid. The next step is an ElectroMagnetic Compatibility (EMC) filter which ensures that the input in for AC-DC converter

[1] according to NEN-EN 10025-2:2018

will be according to electromagnetic standards. The AC-DC converter supplies a DC signal which has sufficient capacity and stability for the inverter bridge to work with. After this step, there is room for a controlled step to steer the output of the generator. This can be done in a number of ways, some IH generators, for example, have an extra power factor correction to increase voltage and ensure a sinusoidal input current before the inverter bridge. The inverter or DC-AC converter takes care of the increase in frequency that will be fed through the coil.

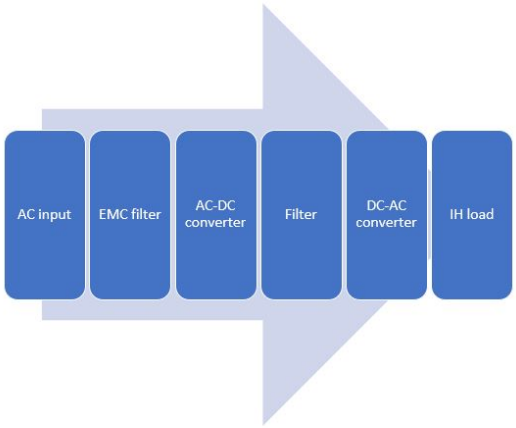

Figure 4.5: Typical power conversion in an IH system, source [17]

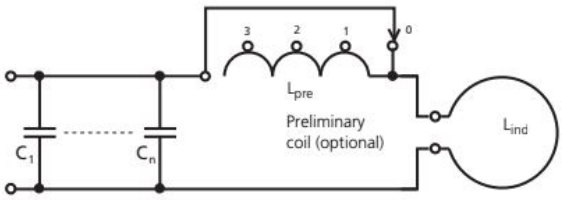

Figure 4.6: Tank/Oscillating circuit, parallel RLC, figure from technical manual Truheat generator [3]

The output frequency is a function of all the components in the induction system as in figure 4.6. Often referred to as the tank circuit or oscillator circuit. This tank circuit is in the case of this Truheat 3040 set up as a hardware setup which cannot be actively controlled. The tank circuit is a parallel oscillating circuit which is often modeled as in figure 4.6. The frequency is a function of the following relation:

$$f = \frac{1}{2\pi\sqrt{L_{ges} \times C_{ges}}} \tag{4.1}$$

Where L_{ges} is the sum of the inductances in the tank circuit, from the coil and an optional preliminary coil, C_{ges} is the sum of individual capacitances of the capacitors (as they are placed in parallel). In practice, the inductance of a used coil is given and fixed by the geometry which means that only the capacitors are used to tune the frequency to a certain value. The frequency will be tuned to retrieve a certain penetration depth in the workpiece. It has to be mentioned that the position of the cables feeding the coil also have an effect on the value of R_{ges} and so influences the frequency of the current through the coil, this will be in the order of $\pm 0.5\ [kHz]$ variance. If equation 4.1,and 2.2 are analyzed, it can be concluded that when an increase in penetration depth is required, an extra capacitor has to be added and vice versa.

As the frequency is a function of the tank circuit the generator measures this frequency and adapts it to match the input of the generator. This is done on the DC signal in a variable rectifier via a chopper unit and makes the output power controllable from 0% to 100% of the maximum 40 $[kW]$. The maximum output voltage will be a percentage of the 600 or 300 volts depending on the setting on the generator.

4.1.1. Current and frequency

During the initialization steps in creating this experimental setup, the output was checked to verify the input data for the simulation model. Therefore, a multimeter (Fluke 3000FC) was used to measure the voltage and frequency. A separate current clamp was used to verify the current running through the coil. The choice of the current clamp was made based on two arguments: Firstly, breaking the circuit and introducing an ampere meter will influence the performance of the IH and as the tank circuit is kept as small as possible this will influence the IH significantly. Secondly often ampere meters are not

designed for both this high frequency and high current for this type of measurements. A current clamp works in a similar way to transformers where the circuit acts as the primary coil and the current clamp as the secondary coil. When the number of wounds is known the ratio of the transformation is used to calculate the current through the coil.

During initial measurements it was visible that the purchased current clamp did not measure the expected current and the measurement equipment started to heat up extensively, although it was specified to measure in this range. The sinusoidal shape of the current was verified with an oscilloscope, as an imperfect sinusoidal it could 'charge' the current clamp and therefore influence the measurement as the current clamp was heated instead of a perfect transformation. The sinusoidal shape of the current is visible in Appendix D.7

A current clamp works similar to a transformer. Figure 4.8 gives a simplified figure of a current clamp. A current carrying wire will induce a magnetic field around itself, the ferrite core will become magnetized and the secondary winding will also experience this magnetic field. Due to the difference in windings; 1 in the primary and n in the secondary the current will be transformed by the following relation:

$$I_s = \frac{I_p}{n_s} \tag{4.2}$$

The stepped down current can then be measured with a oscilloscope or multimeter with a appropriate sample rate. A better-suited measurement device would be a current meter based on the 'Rogowski coil' principle, see figure 4.7. This meter, also provides an indirect measurement but differs in the core that is used in the coil. In an often plastic core, a current carrying conductor is placed and this same wire is looped around the core 'n' times. By not using a high permeability steel core the Rogowski coil has a linear characteristic which means that measurements from milliampere to mega-ampere are possible[24]. The absence of high permeability steel core also results in a reliable measurement result when the input current signal is not perfectly sinusoidal. An added benefit of the Rogowski is that the coil is flexible and that the ends do not have to be attached to each other, as long as the coil is in the magnetic field of the conductor the measurement is reliable which makes it useful when maneuvering around an induction coil.

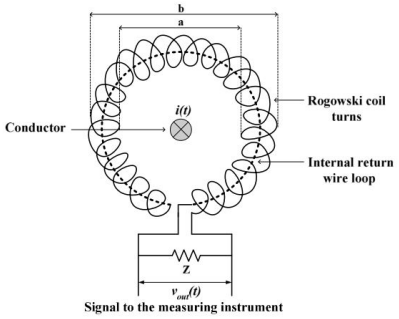

Figure 4.7: Rogowski coil structure,[24]

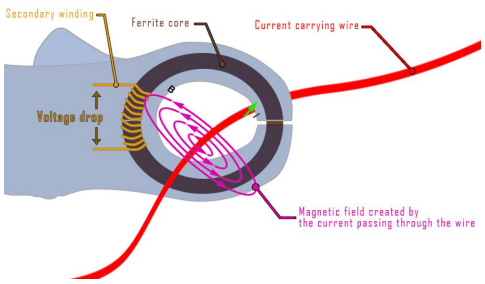

Figure 4.8: Simplified representation current clamp, magnetic field from the source wire will be magnetize the ferrite core in the current clamp.

In figure 4.7 i(t) represent the current source, a and b are the internal and external radius of the coil. Z is the representation of the external impedance of the measurement device and coil terminals, including damping resistor and coupling cable capacitor. An alternative to measuring the current running through the coil is estimated the current through the coil via a calculation. For this type of generator, it is not possible to read the current through the coil because the tank circuit is not actively controlled and the output is only corrected on the measured frequency at the tank circuit. Trumpf supplied a calculation sheet to do this according to the following steps. Trumpf supplies the DC signals of the generator on the display of the generator itself U_DC and P_DC represent the voltage and power before the oscillator circuit.

$$\text{Actual generator output voltage , } U_G[V] = \frac{U_{DC}[\%]}{100} \times 600V(300V) \tag{4.3}$$

$$\text{Actual output power , } P_{MF}[kW] = P_{DC}[kW] \times 0.9 \tag{4.4}$$

$$\text{Actual output current , } I_G[A] = \frac{P_{MF}[kW] \times 1000}{U_G[V]} \tag{4.5}$$

$$\text{Actual capacitive reactive current , } I_C[A] = U_G[V] \times 2 \times \pi \times f[kHz] \times \frac{C_{ges}[\mu F]}{1000} \tag{4.6}$$

$$\text{Quality factor of the oscillation circuit , } Q = \frac{I_C}{I_G} \tag{4.7}$$

$$\text{Actual current through the coil , } I_{ind}[A] = I_G[A] \times \sqrt{1 + Q^2} \tag{4.8}$$

This calculation of the current is an estimation based on a number of estimations: (I)The tank or oscillating circuit is a parallel coupled RLC circuit. (II)The inverter has an estimated loss of 10 % which influences the effective power in equation 4.4. (III)The Q factor is an imaginary number j, the actual current through the coil I_{ind} gives an absolute value and therefore the absolute value of the imaginary number Q have to be used, equation 4.8. (IV)This calculation assumes a loss of 10 % in the inverter, according to the manufacturer Thrumpf, this is accurate when the tank circuit is optimized for the induction heating job and the workpiece is made of a magnetic material. In this research the workpiece is a magnetic material but the tank circuit is not optimized for the specific IH geometry as the generator is used for multiple setups. Therefore a loss of 10% might be optimistic and a higher loss can be expected. However it was found when a higher loss is taken into account the current will not change substantially (an extra 10% would result in an less than 0.1% difference in current at the coil), makes the calculation still use full as an indication of the current through the coil.

The benefits of this type of Parallel RLC circuits for induction heating are clear when analyzing the equations: At first the magnetic field strength is an function of the current running through the coil which can be changed by increasing the quality factor Q. Secondly, the load and generator can be matched by changing the value of the capacitors.

4.1.2. Temperature measurement

During the test, temperatures was measured on two ways: directly via a K-thermocouple and indirectly via a thermographic camera (Flir e50). The direct measurements were placed on the mould as described in figure 4.4, this collected data will later be compared to the same points in the FEM model. Because it is impossible to measure at all points it is useful to see the progress of the heating over time, to compare to the simulation model. To be able to measure with the thermographic camera there are limitations to the reflective properties of the object, for that reason parts of the plate were sprayed with black heat resistant paint. It was chosen to not paint the location of the thermocouples for the fastest response of the temperature rise of the mouldsurface during the measurement. The cooling system should keep the temperature of the cooling water within $20 \pm 1\ ^\circ C$ and this was checked with a thermocouple at the blue connection tube on the coil. This does not give an accurate reading of the water inside the coil but can give an indication if the water temperature was changing when running through the coil.

4.1.3. Used process parameters

During the experiment the process properties in table 4.1 were used. These were read from the generator display. The current through the coil was calculated according to the formulas above. The percentages are percentages of the maximum values the generator can deliver. These values were required for the calculations of the coil current.

Table 4.1: Input data as displayed by generator

Input	Value	Unit	Percentage [%]
Current (I_{DC})	30	[A]	25
Voltage (U_{DC})	309	[V]	72
Power (P_{DC})	9.2	[kW]	22
Frequency	58.2	[kHz]	
Time	300	[s]	
Calculated current at coil (RMS)	834	[A]	
Calculated current at coil (Peak)	1178	[A]	

4.1.4. Safety

When operating the induction heating experimental setup, special attention to safety has to be taken. As the setup works with high power electronics, high frequency, magnetic waves, and hot items. Because the generator is used for multiple coil systems there is no special fixed fence for the setup as the setup has to be flexible in use. Therefore a red/white cord was used when operating the setup and when the setup was cooling down, as someone can seriously injure himself/ herself when touching the mould when hot. The cord was placed at a radius of 2 [m] from the coil so that nobody could reach the IH setup when operating. During testing rubber gloves and eye protection were worn.

4.2. Simulation model

Modeling this induction heating was initially not considered part of the scope of this master thesis. Within Fokker Aerostructures Abaqus CAE is used in both design of products as for the design of production processes. From literature review it was clear that Abaqus CAE might not be the most logical choice to simulate the induction heating process as it is possible to simulate this process according to Abaqus his user guide. For the simulation model in Abaqus CAE, Sebastiaan van den Berg helped to set up the model and did the simulations according to the material and process data found in this master thesis. In parallel the simulation software CENOS was used to get a feel of the induction heating process. The results presented below are those obtained from the Abaqus CAE model.

4.2.1. Abaqus CAE eddy current analysis

To simulate the induction heating process in Abaqus CAE a co-simulation was performed combining eddy current analysis and heat transfer analysis. The eddy current analysis defines the coupling between electric and magnetic fields which are solved simultaneously. The eddy currents in the conductor are the result of an oscillating magnetic field and are converted to thermal energy. The process can either be simulated as time-harmonic and time-transient. For time-harmonic the assumption is made that both electric and magnetic fields oscillate at the same frequency. In the time transient simulation they are decoupled and can be specified individually. In a time-transient process, the input current which is a sinus signal has to be described with at least 8 data points over the sinus shape to represent the shape correctly, as the time of one oscillation is 1/T = F, where T is the period of 1 sinus with a frequency around 60 [kHz] this becomes to computational costly running a simulation for multiple years for a similar length to compute with a time-transient process.

In the eddy current analysis, Abaqus CAE uses the Maxwell equation with the assumption of low frequency which neglects the displacement current correction. This is valid when the wavelength of the electromagnetic waves corresponding to the frequency of the source is large compared to typical length scales of the IH system.

A magnetic vector potential **A** was introduced so that the magnetic flux density vector $\mathbf{B} = \nabla \times \mathbf{A}$. Abaqus finds the time harmonic electromagnetic response $\mathbf{A}_0 e^{i\omega t}$ when the system is subjected to a time harmonic excitation of the same frequency. By $\mathbf{J}_0 e^{i\omega t}$. Where $J_0$and A_0 are the amplitudes of the magnetic vector potential and applied volume current density [27, section 6.7.5 Eddy current analysis]. Under these assumptions Maxwell's equation reduces to:

$$\nabla \times (\mu^{-1} \cdot \nabla \times \mathbf{A}_0) + i\omega\sigma^E \cdot \mathbf{A}_0 = \mathbf{J}_0 \tag{4.9}$$

Where μ is the magnetic permeability tensor, σ^E the electrical conductivity tensor and ω the angular frequency. For the time-harmonic analysis in Abaqus CAE it is only possible to assume the magnetic permeability as linear magnetic behavior that is independent of the magnetic field. In figure 4.9 is visible how the maximum values were taken of the different temperature lines indicated with an red line. The average of this line is indicated with a red dot which indicates the final value of the magnetic permeability that was used. The other material properties both thermal and in the electrical analysis are put in the analysis as a function of temperature.

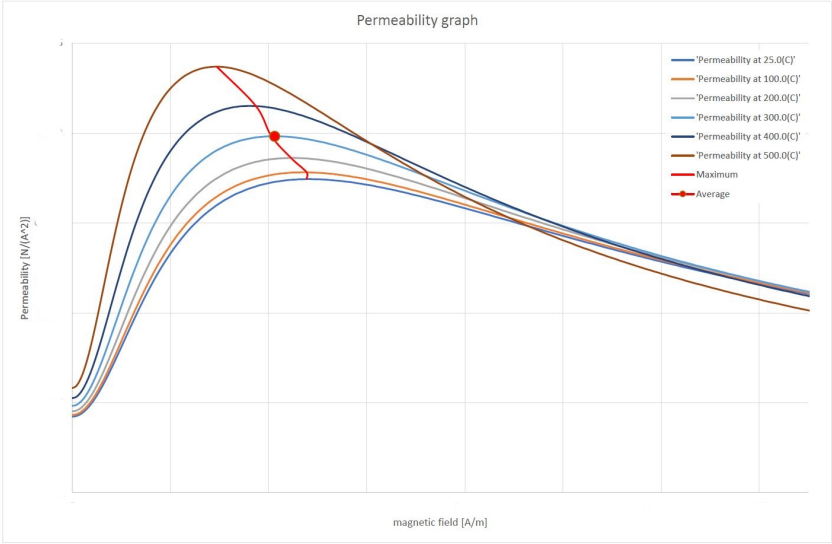

Figure 4.9: Average magnetic permeability

4.2.2. Model representation of experimental setup

The assumptions mentioned before are limitations as a result of the software. Therefore the following assumptions were made in building the model for both the simulations in Abaqus CAE and CENOS. As mentioned in section 4.1 a 2D representation was modeled, using the following assumptions:

- Cross-section that is analyzed (A-A in figure 4.2)is far enough from the sides of the plate so the edge effect, ring effect and slot effect due to the bending of the coil has minimal influence on the heating performance at the cross-section.
- Coil has a constant temperature due to water cooling, which will be verified with a separate temperature measurement on the coil. This constant temperature results in constant properties of the coil.
- Contribution due to cooling is only radiation by a constant parameter $e = 0.8$, verified in experiments performed on cooling slope of this material.
- Thermal properties of the mould material are known as a function of temperature
- Magnetic properties of material are known as a linear relation between the B and H field.
- Process properties are considered constant; the frequency which is indicated by the generator and is verified via a RLC measurement, and the current through the coil, which is estimated via the calculation described in chapter 4.1.1.

To make these assumptions a relatively low power setting and heat up time was chosen. Also, the temperature of the mould was kept below the Curie temperature, this is because above the Curie temperature the behavior of the IH process changes because the material is not magnetic and the driven heating force is purely Joule heating. The first goal is to verify the simulation model where the effect created due to the Curie point makes this more difficult.

To place the Boundary Conditions (BC) on the setup the following groups were used visible in figure 4.10. The groups are coupled to the mesh and boundary conditions. The dimensions of the coil, mould and offset can be found in Appendix D. As mentioned in section 2.1.1, the skin effect has a major contribution to the heat propagation in the mould, as it defines the penetration depth of the magnetic field. When the mesh is not small enough at the skin of the conductor, the skin effect will not be predicted accurately.

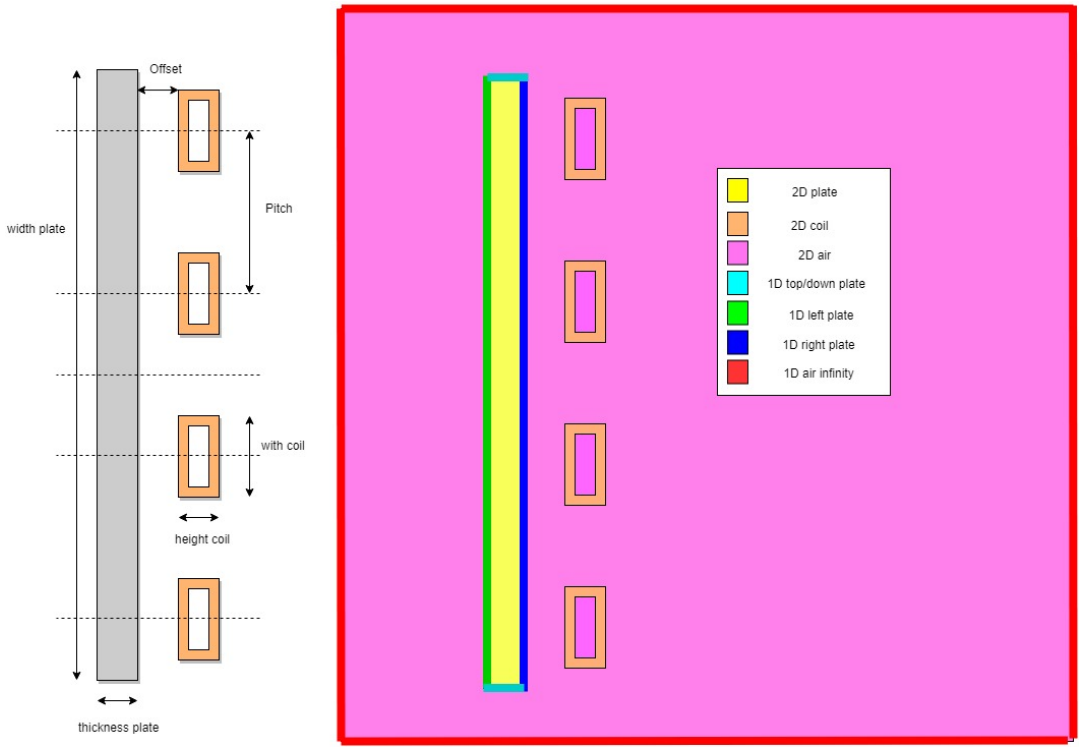

Figure 4.10: Created groups for Boundary Conditions

This means that the size of the mesh at the skin of both the coil and mould affects the accuracy of the simulation model. When looking at equation 2.2 and using material properties from the material properties a penetration depth of below 1 $[mm]$ is reached. This means that the increase in mesh density has to be as a maximum in this depth range. Figure 4.12 shows the increase of the mesh at the skin of the mould. Deeper than this skin depth the mesh can be bigger as the heating of this part is mainly due to convection from the skin.

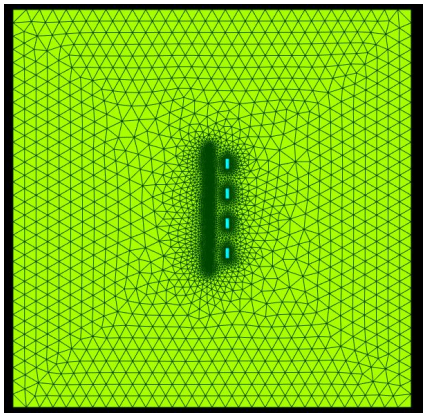

Figure 4.11: Global mesh representation

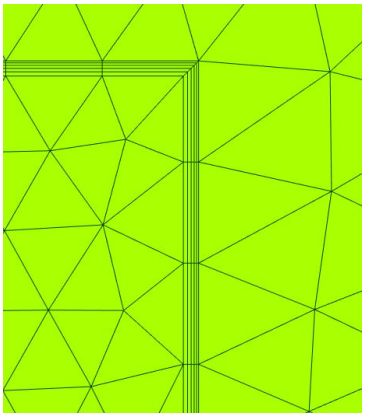

Figure 4.12: Local mesh representation at corner of conductor

4.3. Compare experiment with simulation

In this chapter, the results of both the experiment and the Abaqus CAE simulation are discussed. The temperatures of the top surface were measured with thermocouples during the experiment. Because the thermocouples only show the temperature at one point an IR camera was used to follow the propagation of the temperature in time. The data from the IR camera were only used to check the heating behavior. As the IR camera is not accurate enough to compare measured data this could only give an indication.

Top surface

In figures 4.13, 4.15, 4.14 and 4.16 the temperatures measured during the experiments are compared with simulated data of Abaqus CAE. When designing this setup there was assumed that the heating performance was symmetrical, to validate the thermocouples were used in pairs placed on the mould as is visible in figure4.4, the temperature readings T1=T4, T2=T3 and T6=T7 should be similar. As the Abaqus model showed identical temperature readings at the locations of the pair only 1 reading per location is displayed. The reading of T5 could not be checked with a reading at a symmetrical location. The IR camera and the simulated data showed that the thermocouple at location 5 showed a lower temperature than location 2 and 3. Which makes the temperature reading in T5 in figure 4.16 a logical reading when compared with the other measured data.

In the FEM model was also assumed that the temperature of the coil remains at room temperature, to be able to use material data only known at room tempeature for the coil. To accommodate this the coil was cooled an external water cooling unit at a set temperature of 20 $\pm$ 1 $^{\circ}C$ at a minimum rate of 16.5 l/min. There was assumed that with this flow rate and cooling performance there was no chance of evaporation in the cooling channels. To validate the performance of the cooling a thermocouple was placed on the cooling channel of the coil. The thermocouple at the coil was showing a reading of 22.6$\pm$0.5°, from the start to finish of the simulation. This demonstrated that the temperature of the coil is kept constant and the assumption of material properties of the coil at room temperature is valid.

The thermocouples were applied with Kapton tape to the top surface of the mould, Kapton tape was used as it was the tape which could withstand the highest temperature and was available. Unfortunately, the tape released at some places during the measurements as is visible by the burned look in figure 4.3 This results in temperature readings that show a tooth-like profile. This is visible in the readings of the thermocouples at location T3, T4 and T7.

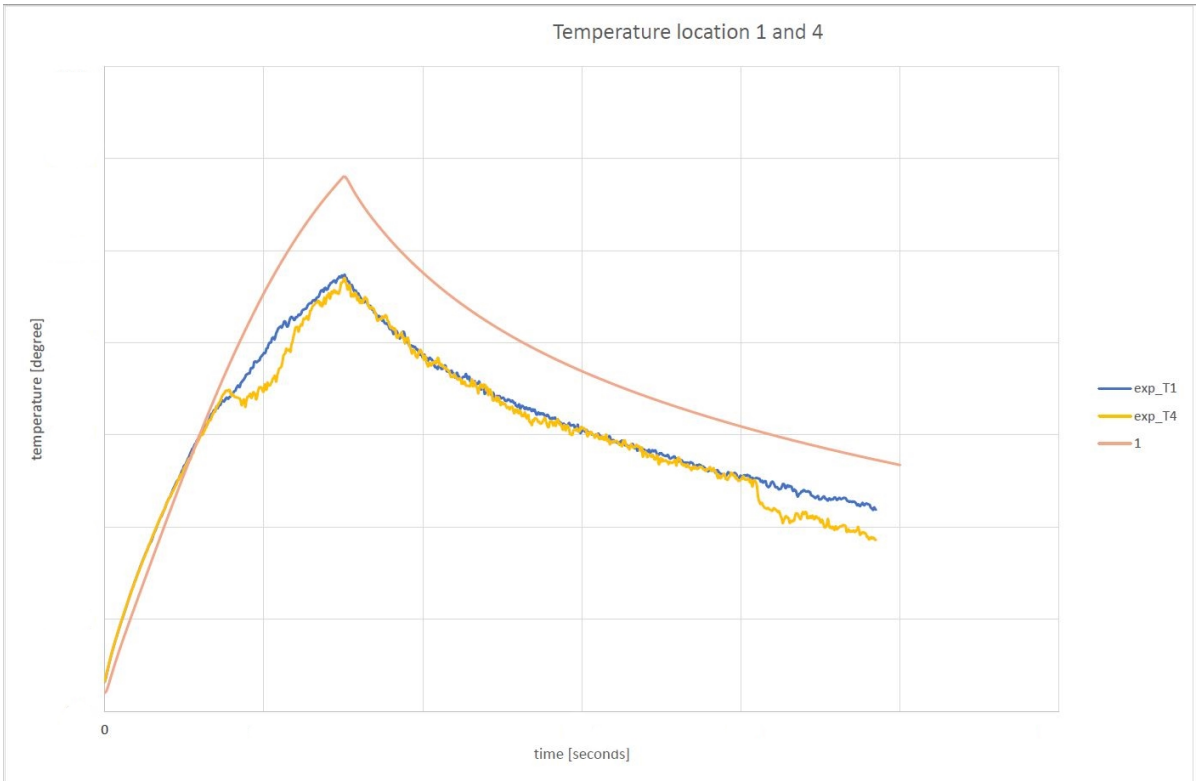

Figure 4.13: Temperature at location 1 and 4

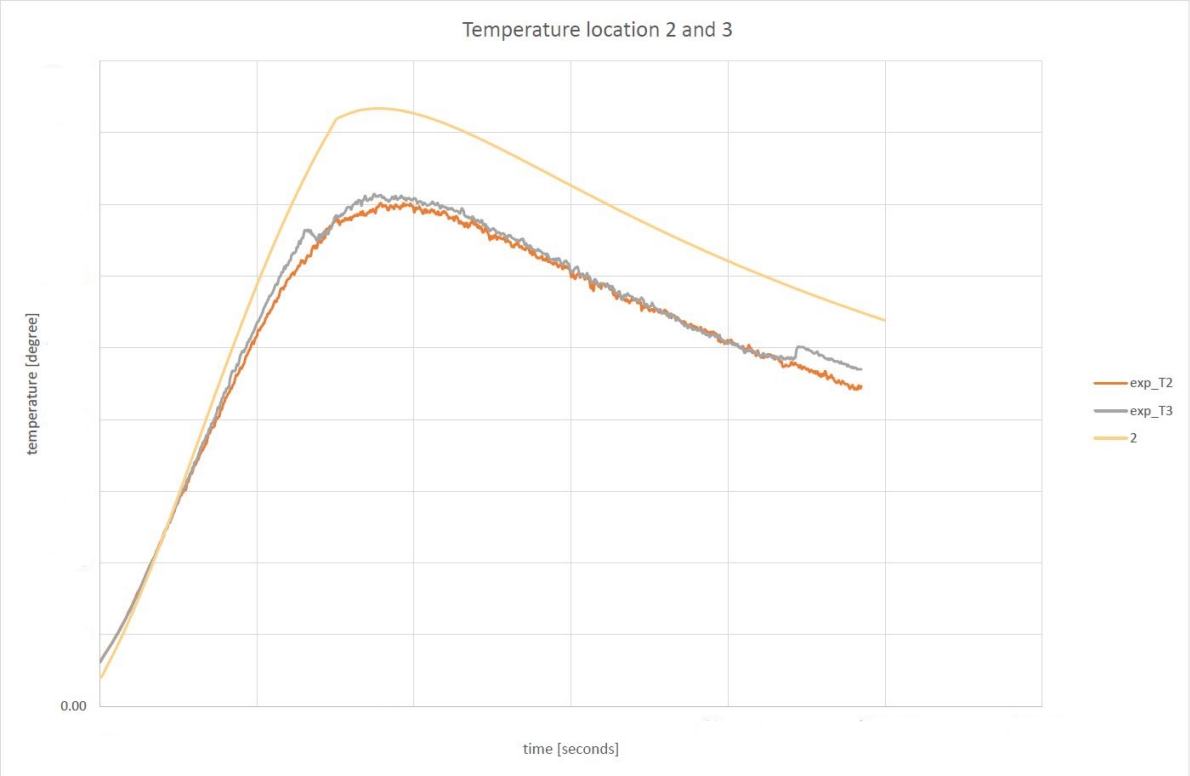

Figure 4.14: Temperature at location 2 and 3

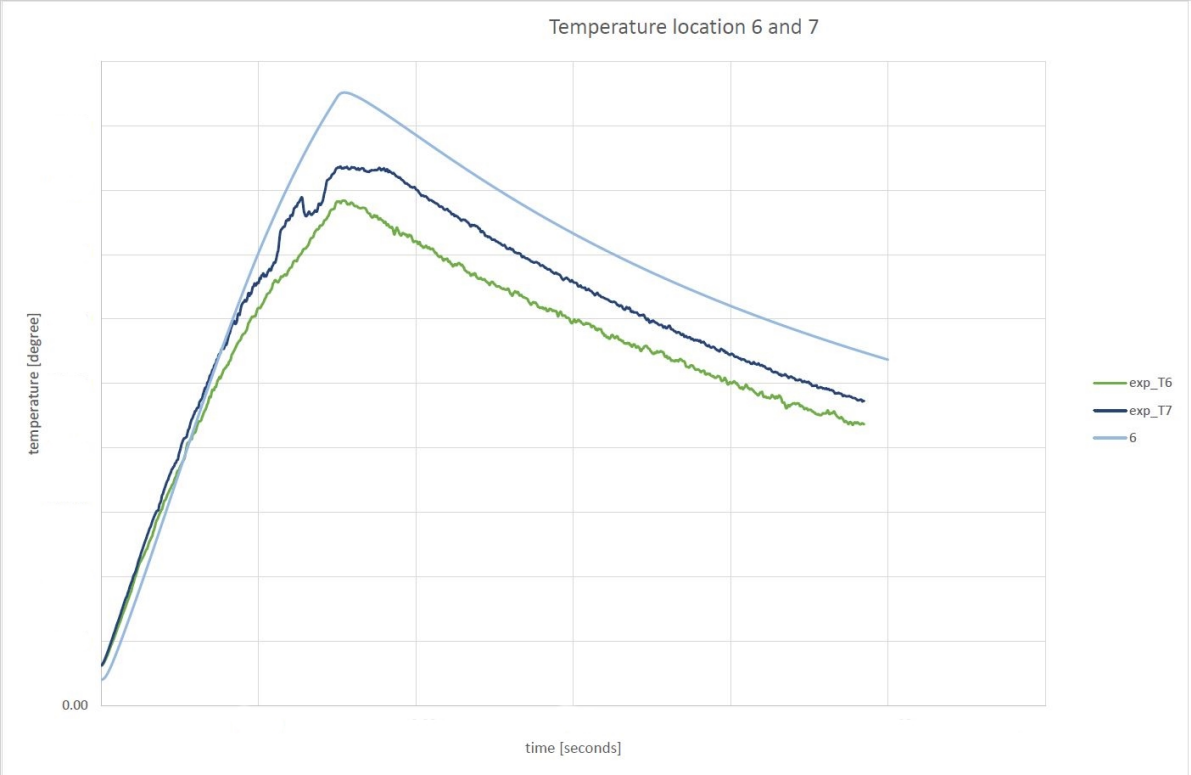

Figure 4.15: Temperature at location 6 and 7

The symmetrical behavior is visible in measurements in figures 4.13 and 4.14 by a similar temper-

ature at T2=T3 and T1=T4. Figure 4.15 shows an exception with an higher temperature measured at location 7 compared to 6. When analyzing the coil and mould after the measurements there was visible that the thermocouple was not placed directly in the middle between two coils as displayed in 4.4. The thermocouple was shifted 2 [mm] of center. This was the result of an different distance between the two outer coils. The coils showed an pitch which was 2 [mm] smaller than the other pitches.

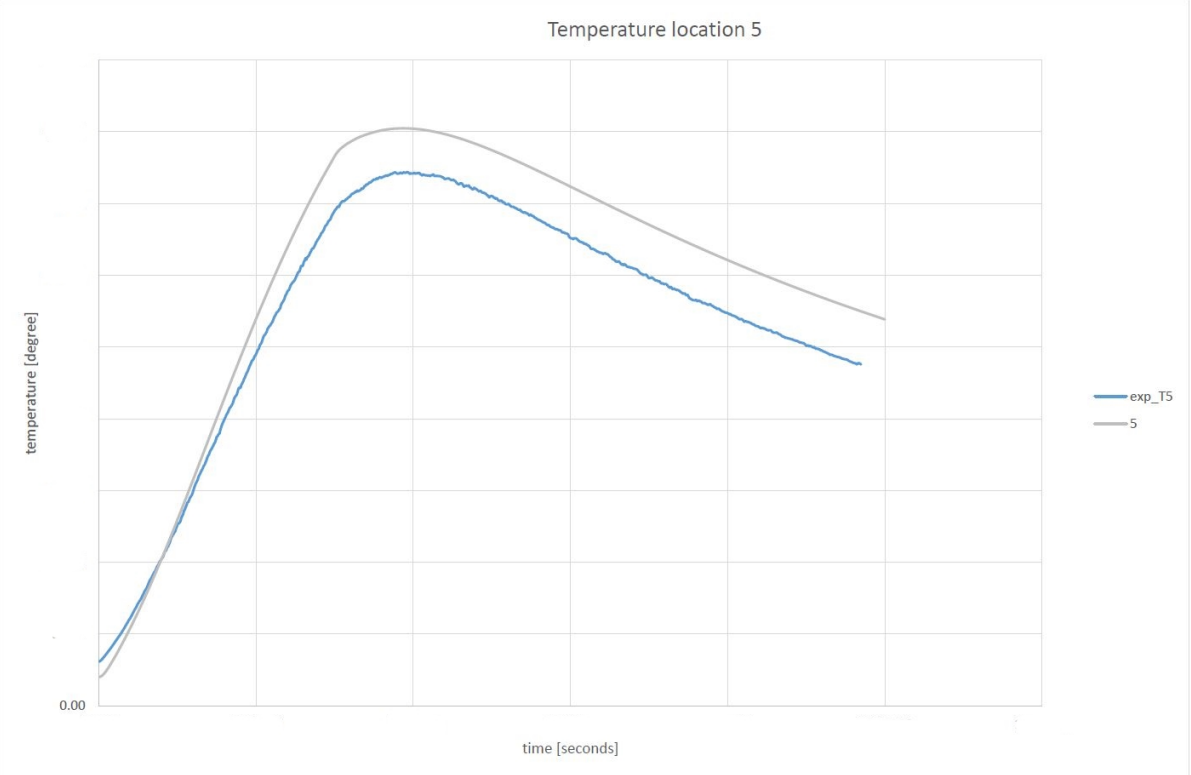

Figure 4.16: Temperature at location 5

In the temperature readings, there is visible that the IH system heats for 300 seconds whereafter the mould cools down for almost 700 seconds. The analysis of the data can be divided into two parts, cooling and heating. When looking at the cooling temperature lines there is visible that the lines remain parallel although the lines are at an offset. The properties that influence this simulation are: dimensions of the mould, start temperature and material properties influencing thermal properties. The thermal properties, thermal conductivity, specific heat, and density, are calculated with JmatPro and validated at room temperature so could be assumed correct. The radiation property was used from earlier research at Fokker so could also be assumed correct. As the dimensions of the mould were directly measured with a caliper, this could also be estimated as correct. Only the start temperature is estimated too high in the simulations at every location. Still, there can be assumed that the thermal material properties and the analysis of the cooling was estimated correctly by Abaqus CAE based on the parallel curve.

When analyzing heating phase there is visible that for the first 100 seconds the simulations are almost exactly similar to the measurement. All of the measurements are within 4% of the simulations. It is also visible that between 100 and 300 seconds the simulations show a higher temperature than the measurements. Based on the cooling phase was concluded that the thermal properties were estimated correctly. Which means that difference in simulated and measured temperature could be the result in an error in the estimated electromagnetic properties, electric resistivity, and magnetic permeability. The electric resistivity was measured and verified with room temperature data and the calculated data from JmatPro. Based on this is assumed that the difference in temperature was not based on the electric resistivity. This error could be the result of an error in the magnetic permeability, this could be the result of one of the following estimations made: firstly the magnetic permeability could only be used

as a constant value instead of a non-linear value calculated by JmatPro, due to the limitation to only be using time-harmonic analysis discussed in section 4.2.1. Secondly, the magnetic permeability data calculated by JMatPro are based on the chemical composition and some material properties based on the production of the material, see section 3.4 given by the supplier of the base material. This magnetic permeability was not verified similar to the other properties to a value at room temperature as this is not possible for this material property. Although JmatPro claims that their models are verified there can still be a potential error in the data obtained from the material supplier.

Based on these arguments was assumed that the calculated magnetic permeability was estimated wrong and that a measured data could increase the accuracy of the simulation in a way that the simulations have the same low $\leq$5% accuracy.

Propagation of heat trough the surface
This inaccuracy of the simulation compared to the experiment does not mean that the simulation is not useful for the design of an IH setup. How the heating pattern changed as a function of time was not known before. In the figures, it is visible that the same heating pattern is reached in both the experiments and simulation. For the OoA production process, the surface temperature will be required result of the simulation. In figure 4.17 the temperature distribution of the top surface at 27, 105, 221 and 288 seconds are displayed. In this figure is also visible that if a thermocouple is placed on a location 5 [mm] different that read from the simulation data it would give a relative big error. For example at location T1 and T4 which is indicated with a blue dotted line, a 5 [mm] shift to the center would decrease 15 $^{\circ}C$ in temperature. This is also the result of the error between the measurements of T6 an T7 which supposed to be equal due to symmetry.

The measurement of the thermocouples only shows data of a specific location, an IR camera was used to check the thermal image as a function of time during the experiment. For the IR camera to work the same value of emissivity was used as in the Abaqus simulations $\varepsilon = 0.8$. During the experiments, The IR camera was used to see the propagation of the temperature of the top surface compared to the simulation model. It was concluded that the simulations show similar heat propagation of the mould as a function of time. However, it could not be used to measure a certain location and collect data points to compare with the simulation data. Two reasons are the result of this: The camera was positioned at an angle similar like visible in 4.1 this caused the camera to focus on the front face of the plate instead close to the thermocouples. Secondly, the relative motion between the camera and the plate made it impossible to retrieve data at certain locations which would introduce a similar error as between thermocouple 6 and 7.

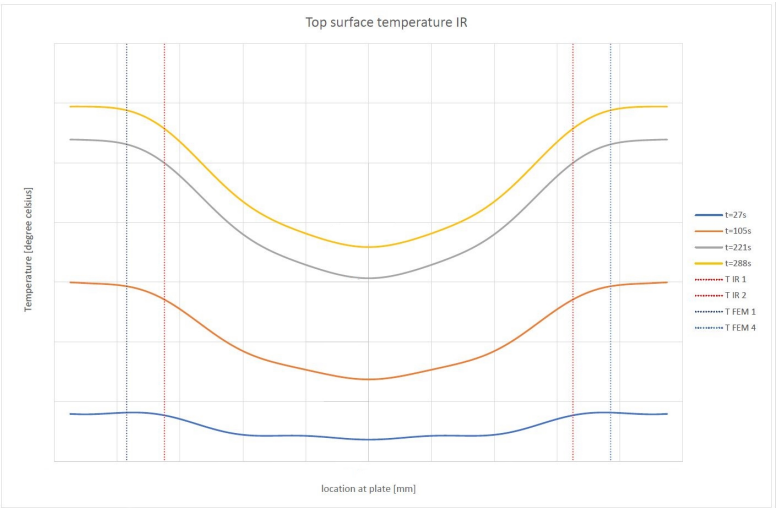

Figure 4.17: Temperature of top surface Abaqus CAE model

The temperature profile shown in this experiment is a result of the direction of the current through the crosssection. This different direction of current flow results in a canceling of magnetic field around

the middle two coils. Which results in a temperature difference of almost 250 $^{\circ}C$ difference between the middle and the edges of the plate.

In figure 4.17 the temperature of the top surface is visible but does not indicates how the heat propagates through the thickness. In figure 4.18 the heat propagation through the thickness is visible at the same timestamps as in figure 4.17. These figures give a better indication of how the heat is propagating through the thickness. In the figure, it is visible that at t = 27 seconds the highest temperature is visible above the outside coils. There is a temperature difference of 60 $^{\circ}C$ visible between the center and the hottest point directly above the outer coil.

The opposite direction of the current in the cross-section results in the conflicting area as a consequence of a canceling of the magnetic field around the middle two coils. The maximal temperature difference at the top surface is then 250 $^{\circ}C$.

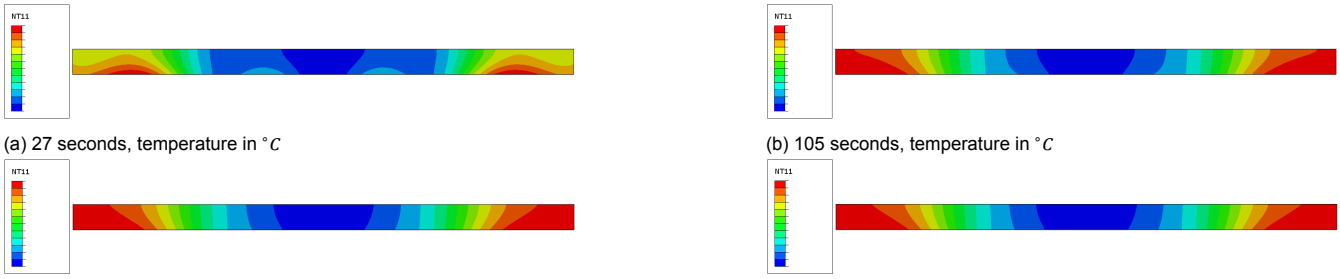

(a) 27 seconds, temperature in $^{\circ}C$

(b) 105 seconds, temperature in $^{\circ}C$

(c) 221 seconds, temperature in $^{\circ}C$

(d) 288 seconds, temperature in $^{\circ}C$

Figure 4.18: Heat profile of cross-section Abaqus CAE model

4.4. Discussion

This research was mainly based on finding a solution in Abaqus CAE for an experimental setup. Because there was no thorough understanding of the behavior of the induction heating process. It was chosen to simplify the experimental setup till a point where the solution would still be useful for further research. The coil was taken from an setup earlier used at Fokker, because a coil is expensive and time consuming to produce. The mould material was simulated with a metal mould of equal thickness and known material parameters and chemical composition. The dimensions were chosen so it was wider than the coils and shorter than the length of the coils so it would not experience the magnetic fields excited in the corners of the coil. In this way the edge, ring and slot effect where not taken into account.

The opposite current affected due to the meander type of coil was thought to be very important to Fokker to simulate as it is used in many of the designs of other experimental setups at R&D of Fokker. The material was chosen as S335J2 AR/M. Mainly because this is a widely used material which has known material properties and chemical composition. Added benefit is that the Curie temperature lies well above the target temperature of 450 $^{\circ}C$ at a temperature of 800 $^{\circ}C$. Above the Curie temperature the magnetic properties are lost which result in a higher power input required to keep equal temperature gradient in the mould.

The material properties retrieved from research question 1 in chapter 3.5 were used in the simulations. The magnetic properties (electric resistivity, magnetic permeability)and thermal properties (thermal conductivity, specific heat capacity and density) as a function of temperature. Due to the limitations of Abaqus CAE in terms of computation time it was not possible to simulate in a time-harmonic simulations but only time transient analysis which results in the linear magnetic permeability parameters, which was chosen to be the average of the maximum values at the known temperatures retrieved from the data found in chapter 3.4.

In chapter 4.3 it was visible that thermal properties such as specific heat capacity, thermal conductivity and density were assumed to be estimated accurately as the slope of the cooling curve was equal on all measured points. When the heating period was analyzed, the first 100 seconds the temperature of the experiment and simulations are relatively close. After that, the simulation results predict a higher temperature than the experiments. This indicates that there could be an error in the material properties, assumed that the material properties which define the thermal behavior of the simulations are correct. This is the result of the electrical resistivity or the magnetic permeability. As the electrical resistivity was

measured in section 3.2.8 and verified in section 3.5. The limitations of Abaqus CAE for time-harmonic eddy current is that only a constant can be taken as the magnetic permeability instead of the non-linear calculated in section 3.4 the magnetic permeability is not linear for this type of material. Given that the magnetic permeability could not be verified with any value as was done with the other material properties which were compared with room temperature values and experimental measured data there will also be a change that the magnetic permeability is not estimated correctly with the calculated data from JmatPro found in section 3.4. It is expected that the simulations in Abaqus CAE will be more accurate when the correct constant value of magnetic permeability is used and even more accurate if the non-linear value is used in the simulation.

4.5. Conclusion research question 2

Reaserch question 2: ”How can, with a simplified version of the mould and different configurations of the coil, a test setup be designed where the coupling to a 3D FEM model can be made?”

A simplified set was designed where edge effect, end effect, slot effect and ring effect contribute to the minimal to the setup. A design with a flat plate with a constant thickness in combination with a meander type of coil was used, see section 4.1. The meander type coil is used in other research at Fokker and was therefore useful to use in the experimental setup. The temperatures were measured directly with thermocouples and indirect with the use of an IR camera. There was chosen to analyze the specific cross-section mentioned in figure 4.2 to minimize the effect of the edge effect and ring effect of the loops in the coil. The material properties as a function of temperature that were found in chapter 4.1.2 were used in the simulation.

For this specific situation was found that the time-harmonic analysis had to be performed to use Abaqus, assumptions made are discussed in 4.2. In section 4.3 the data of the experimental test and the simulation are compared and discussed. It was concluded that the material properties based on heat flow and radiation were correct based on the cooling phase of the temperature readings. During the early heating phase, there were similar results visible in both the experiment and simulation. After 100 seconds the simulation showed a higher temperature than the experiment indicating that the material properties or the model were not exactly correct in these regions. Based on the verification of the material properties with the values of room temperature and the measured values of the electrical resistivity was concluded that these properties were assumed correct. Together with the fact that the magnetic permeability was taken as a linear value instead of a nonlinear and the property was not verified in a way that the other material properties were verified was concluded that there is an error in the estimation of the magnetic permeability.

There was proven that the heat propagation analysis of the simulation is useful for designing an IH setup as the heating patterns were similar in the simulation as the experiment. Also, the cause of the heat pattern on the mould could be verified and traced back to the direction of the current through the coils.

There was concluded that the location of the thermocouple is particularly important when comparing heat propagation with simulation as it can influence significantly as was visible in figure 4.15.

There was discussed that the accuracy of the simulation could be higher when the magnetic permeability was directly measured as a constant. Additionally, the magnetic permeability could be used as a non-linear relation as found in 4.1.2, this does require verified material chemical composition for the input for the material calculation software JMatPro and another software package than Abaqus CAE.

5

Design of induction heating setup

The following subquestion will be answered in this chapter: ”How can certain parameters be changed to obtain the desired heating profile of the mould?” This will be explained with a step by step solution to design the new induction heating setup in section 5.1. The design solution will be explained using the current Fokker IH system as described in section 5.2. Thereafter the influence of another coil strategy on the heating performance is explained in section 5.2. Section 5.4 will give a recap of the chapter and a conclusion on the subquestion of this chapter.

5.1. Design of IH system

The performance of an induction heating system is a combination of the specifications of the conductor, inductor and generator, see figure 5.1. All have their requirements and different limitations to the system. This chapter explains the decisions that have to be made when designing an induction heating setup for the out of autoclave co-consolidation method. The steps in the list below will be taken to come to a final design.

Steps in designing an induction heating setup

1. Define type of thermoplastic material which defines the maximum heating rate of the material.
2. Define mould material and rough volume needed required to withstand clamping force and accommodate eventual cooling channels. The chosen cooling method will also influence the critical volume of the mould.
3. Estimate the maximum power required for the generator and pick a generator based on this estimation.
4. Measure, retrieve material data as a function of the temperature of mould material. Material properties at room temperature for the coil.
5. Write material in correct SI units and form for the input of the Abaqus CAE co-simulation
6. Simulate and optimize heating pattern to TP composite requirements based on the variables stated in table 5.3.
7. Manufacture mould and coil, optimize generator to coil and mould to a specific frequency.

5.1.1. Define production parameters of specific TP composite

Thermoplastic composites have the typical consolidation cycle, shown in figure 5.2. The plastic has to be molten in the heating phase, then kept under a certain temperature under pressure for a given time specific for a type of plastic required to retrieve the mechanical properties of the composites. After the consolidation phase, the plastic has to be cooled down till a certain temperature before it can be released from the mould. The rate of the heating and cooling steps are specified and required to get the desired quality of the composite.

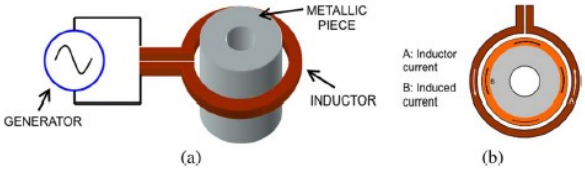

Figure 5.1: a)Typical representation IH setup, b) top view with current in inductor and induced current in workpiece

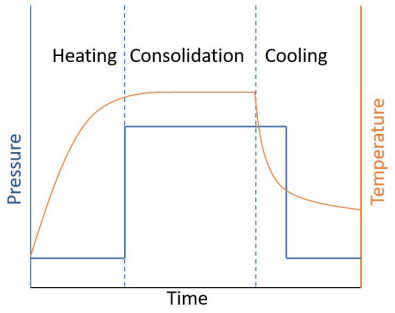

Figure 5.2: Typical heating profile of Thermoplastic composites

The melting point and heating rate of the TP is the input for the design of the induction heating. This defines at what heating rate the mould has to be heated and therefore defines the maximum power required by the generator. The induction heating generators are limited in their maximum power, maximum effective current at the coil and maximum frequency which are important parameters for the induction heating.

5.1.2. Pick mould material and cooling method

The way the mould is cooled in the cooling phase has to be decided before the estimation of the generator can be done. At Fokkers research to OoA Press (Co-)consolidation technology, there are two principles used to cool the mould, see figure 5.3. Version A, has separate cooling channels in the mould and version B which use the cooling capacity of the coils to cool down the mould.

For the design of the mould there will be started with a minimum thickness or volume of the mould. As the amount of mass to be heated defines the rate a mould can be heated. This minimal thickness is defined by the cooling method just mentioned and the stiffness the mould has to have during the production process to remain his shape and so ensures the correct dimensions of the to be produced product.

Figure 5.3: Two types of cooling of the mould, a) separate cooling channels in mould, b) coil placed directly to mould surface

There have to be mentioned that during the experiments and the verification process, the material properties of the coil were taken only at room temperature assumed was that the coil was kept cool during the heating via cooling method A. This was verified during the experiment and the coil was kept at 22.6 $\pm$0.5°. When using option B the coil will not stay at room temperature and the material properties of the coil also have to be known as a function of temperature for the simulation.

The weight of the mass that has to be heated is in this case largely defined by the material and mass of the mould material. For the production of composites, a preferred metal is Invar, due to a similar expansion coefficient as a function of temperature in the temperature range the TP composite is consolidated. The volume, density and the specific heat at room temperature will be needed for this estimation of the power of the generator. There are different types of Invar available, a different type can be the result of a required curie point which can be beneficial for a certain type of TP.

At this point the cooling method, required stiffness of the mould and mould material are chosen. At this point the required minimal volume can be calculated. How stiff the mould has to be is out of scope of this research.

5.1.3. Estimate size of IH generator

When the minimal volume of the mould is defined together with the maximal heating rate of the TP the capacity of the generator can be calculated. A rough estimation can be done with the following equations 5.1 and 5.2. As this is an estimation there is no contribution of heat loss due to radiation, convection or conduction. It does give an indication of the size of the generator to start with.

When looking at equation 5.1, the amount of work in joule needed to heat up a certain critical mass between a ΔT can be calculated. Use this in equation 5.2 and divide the work by time the power consumption in [watt] can be calculated which is the parameter that can be found at the datasheets of generator manufacturers.

In section 4.1.1 has been shown that there will be a 10 % loss at the inverter bench, Trumpf indicates that for copper coils and magnetic mould material there will be another 20 % loss from the coil to the mould when describing in terms of power. Thereof 20% will be heating the coil and 80% will heat the mould itself, the 20% heat generated at the coil will be cooled via the cooling water of the cooler. In case of a nonmagnetic material there will be more loss in the step between the coil and the mould. In total there will be 28% extra power needed to overcome the loss generated in heat in the coil and inverter which is taken into account in equation 5.2.

$$\text{Work, } Q = mc\Delta T \ \ [Joule] \tag{5.1}$$

$$\text{Power, } P = \frac{dW}{dt}\frac{1}{0.72} \ \ [watt] \tag{5.2}$$

Where Q is the worked energy in the mould in joule, m the mass of the mould [kg], c the specific heat $[J/kgK]$ and ΔT the temperature range the material has to be heated. P is the power needed to heat up the mould at a certain time, dW the work delivered and t the time in seconds.

The choice of generator can be based on this calculated power, do not limit the generator to pick for example a 5 kW generator if the calculation brings 5 kW and pick a heavier version to be more flexible in future processes with the same generator. It have to be mentioned that this method of calculating the required power for the generator is rough estimation and can be estimated with a higher accuracy with a FEM model. As the final shape, volume, potential zones with separate generators are not known this process can give an indication of the generator size.

5.1.4. Material properties as a function of temperature

When the mould material is known the following material properties have to be known as a function of temperature in the temperature range: Room temperature until 500°C. This is about 100 °C higher than the mould surface during the press consolidation, there is accounted for the peak at the bottom of the mould during heating.

- Thermal conductivity in $[W/m°C]$
- Heat capacity in $[J/kg°C]$
- Density in $[kg/m^3]$
- Electric Conductivity in $[S/m]$
- Magnetic Flux Density or B/H ratio

In section 3.1.1 was shown that a correct estimated electrical resistivity/ conductivity has the biggest contribution to a correct estimated induction heating simulation. Therefore an experimental method to measure the electrical resistivity as a function of temperature described in section 3.2.

As mentioned in section 3.4 this data can be retrieved from JMatPro® when the following data is known of the material: there have to be mentioned that the accuracy of the data is fully dependent of the accuracy of the input data

- Exact composition components in percentage of total
- Previous heat treatment of the alloy (During manufacturing and not during IH)
- For magnetic permeability:
  - The hardness of the material at room temperature or 0.2% proof stress or tensile stress.
  - If the material has a course (lamellar or normalized) microstructure or fine (quenched and tempered).
  - Estimated heating rate during the IH process.

There has to be mentioned that the accuracy of the data is fully dependent on the accuracy of the composition of the material. A verification step with measured data from the electrical resistivity data

and values at room temperature found in literature is recommended. Material properties at room temperature of the copper used for the coil can be found in Appendix E.1.

5.1.5. Input data Abaqus CAE

The input for the simulations can be divided into two parts, material data and process data. The input data will be specific for an induction heating simulation in Abaqus CAE.

Material data in Abaqus CAE

For the time-harmonic co-simulation of the induction heating process the following material data is used in the following units, table 5.1. The co-simulation consist of the eddy current analysis and a heat transfers analysis, Abaqus needs two separate input files for both analyses.

As the eddy current analysis is time harmonic the absolute magnetic permeability Hm^{-1} can only be put in the analysis as a constant [27, section 6.7.5]. Chapter 4.2.1 explains how an average of the nonlinear variable can be found. There has to be special attention to the unit of the magnetic permeability as not all software packages require the μ absolute magnetic permeability which is the relative magnetic permeability of the material times the magnetic constant $4\pi \times 10^{-7}[Hm^{-1}]$, $\mu = \mu_r\mu_0$. The surface emissivity is a unit less variable with a value between 0 and 1. The value 1 represents the radiation of a perfectly black surface, which emits 448 $[wm^{-2}]$ of energy due to thermal radiations at room temperature. All other material parameters can be put in the analysis as a function of temperature as found in section 3.4. The data have to be offered as a list of datapoints with the value of the material property at the corresponding temperature.

Table 5.1: Required material data for Abaqus CAE simulation

Variable	SI unit	Note
Eddy Current analysis		
Magnetic permeability	$[Hm^{-1}]$	Absolute magnetic permeability $\mu = \mu_r\mu_0$
Electric conductivity	$[Sm^{-1}]$	
Heat transfer analysis		
Density	$[kgm^{-3}]$	
Specific heat	$[Jkg^{-1}K^{-1}]$	
Thermal conductivity	$[Wm^{-1}K^{-1}]$	
Surface emissivity	$[-]$	Dimensionless quantity

Process data in Abaqus CAE

For the time-harmonic co-simulation of the induction heating process the following process data is used in the following units, table 5.2.

The body current is the current divided over the cross-sectional area of the coil, this analysis assumes an constant current as a function of time. In the time transient analysis Abaqus CAE requires an RMS signal of the current. In case of the sinus-shaped frequency the this can be calculated via: RMS $=$ max.amplitude$/\sqrt{2}$. This RMS stands for the Root Mean square of the signal and represents the average amplitude of a signal. In this way a representative signal can be used for the time transient analysis. In case of an transient analysis both the frequency and current signal will be given in one value which is a function of time.

The current is depending on the frequency and capabilities of the generator. It is recommended to base the frequency on the required skin depth during the heating. As the heating has to flow through the mould the skin depth is preferably large to put more energy deeper in the mould which makes the heating of the top surface faster compared to a small skin depth. As the skin depth is a function of material properties, frequency and inductance of the coil this can be roughly estimated. Often the generator manufacturer gives a range of frequency that can be reached by a specific type of generator independently of the coil. The frequency and so the penetration depth can later be optimized via the capacitors in the generator.

Table 5.2: Required process data for Abaqus CAE simulation

Variable	SI unit
Frequency	$[kHz]$
Body current (RMS)	$[I/A^2]$
Time of analysis	$[s]$

Note
The input file of the geometry, used elements and nodes in the simulation is not discussed as it is out of the scope of this master thesis. Also, the cooling method is out of the scope of this research and discussed as two options and the effect it has on the simulation.

5.1.6. Simulate and optimize

At this point the time-harmonic co-simulation can be performed and the temperature profile can be simulated. At this moment the process has to be optimized for two objectives; homogeneous temperature and speed. The following parameters have influence on this objectives, see figure 5.4 for a schematic representation of the terms.

- Current in the coil
- Shape of the cross-section of the coil
- Pitch of the coil
- Distance to from coil to mould
- Thickness of the mould

The fastest system will have the thinnest mould, the smallest pitch, the smallest distance from the coil to mould and the highest body current. However this would result in large temperature deviation at the top surface of the mould. Parameters that influence the heating pattern through the mould are all of the above except the body current as it only increases the speed of heating but not necessarily increase the temperature deviation at the top surface.

The most homogeneous heating pattern would be retrieved if the magnetic field created at the coil has a homogeneous density at the underside of the mould. This could be obtained by using: wide thin coil, low distance between coil - mould, low pitch distance and thicker mould. The downside is a less efficient heating system in terms of power consumption and heating speed. An example of the effect of the shape of the coil on the heating pattern is given in figure 5.5.

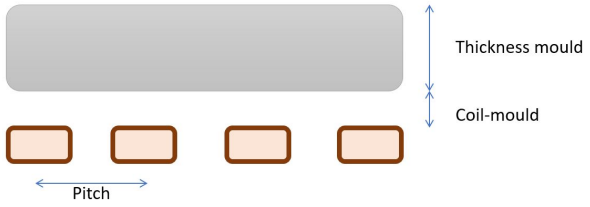

Figure 5.4: Influencing parameters of induction heating system

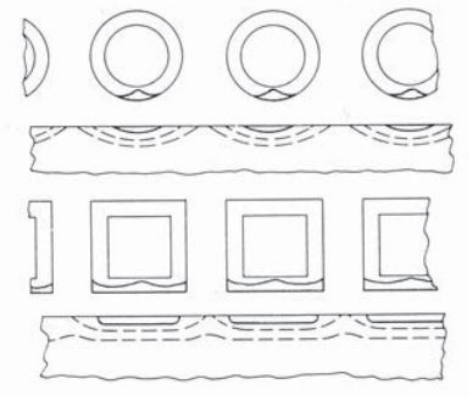

Figure 5.5: Compare heating pattern coil shape, source [35]

My advice is to start with a small volume of mould and the minimum requirements in terms of stiffness, to start with a producible coil with low pitch distance place closed to the mould. Note, in practice this small pitch distance bring extra challenges in manufacturing of the coil. Then to simulate this setup and to check the heating pattern by varying the thickness of the mould, pitch, and distance to from the coil to the mould to optimize the heating pattern on the top surface.

After that, increase the power to find the process setting of for the generator. When the coil is produced the inductance has to be measured to tune the tank circuit to the desired frequency. If it is

not possible to measure the inductance of the coil in advance, this tuning process can also been done in an iterative way.

Table 5.3: Effect of variables on heating performance

	Speed	Uniform heating
Pitch increase	Slower	Less
Increase thickness mould	Slower	More
Increase ofset	Slower	More
Increase body current	More	No effect

5.1.7. Manufacture IH setup and optimize generator

The generator has to be optimized in terms of frequency and power output as the coil which is part of the induction heating setup influence the efficiency of the generator. This is described in appendix E.3. This will not decrease the performance of the heating directly as it optimizes the efficiency of the generator. It can be a limit when the generator is used on its maximum level and the generator cannot deliver more power because it is not efficient enough. When the frequency is determined the maximum body current can be estimated with the formulas in section 4.1.1 by using 100% for U_{DC} and the maximum power output from the datasheet of the generator.

5.2. Dimension of coil to mould and effect

In the research at Fokker, the meander type coil is often used in the out of autoclave thermoplastic composite press see in figures 5.6 and 5.7. As the coil is produced by brazing by hand this is a fast way to produce a coil that can heat larger surfaces. The square cross-section is used because of their benefit in terms of heating pattern in the mould. The downside to the meander type coil is the direction of the body current is opposite in the parallel parts of the coil, which causes a canceling effect of the magnetic field between the coils. This effect was visible in the experiment and delivers a large temperature difference at the mould side as can be seen in figure 4.17.

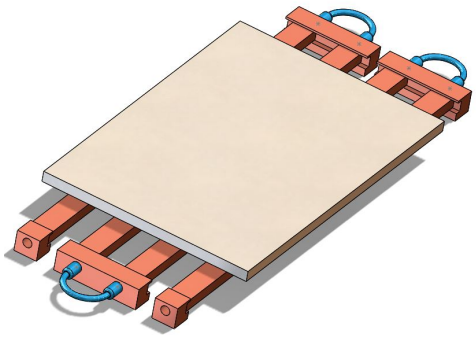

Figure 5.6: Meander type coil on flat mould

Figure 5.7: Meander type coil on curved mould

To indicate the potential benefits of a type of coil where the current does not run in the opposite direction two separate simulations were performed. Both have the same dimensions, material and process properties except for the direction of the current. In figure 5.8 a) the direction of the current points in the same direction while in figure b) the current points in the opposite direction. In figure 5.8 it is visible that a) reaches a higher temperature compared to situation b). The figure shows two potential benefits for this type of heating: efficiency and homogeneity of the temperature.
The efficiency can be explained by the higher temperature of the mould surface with the same process parameters, which means that for the same temperature a smaller current could be used and so more efficient. The homogeneity of the temperature is indicated by a ratio of the highest to the lowest temperature of the left side of the mould (as this is the surface in contact with the composite). In table 5.4 this temperatures are given, the fourth column gives the ratio between the highest and lowest temperature.

The ratio of 1.13 compared to 1.74 indicates that the coil where the direction of the current is in the same directions is easier to tune to a constant temperature at the mould surface.

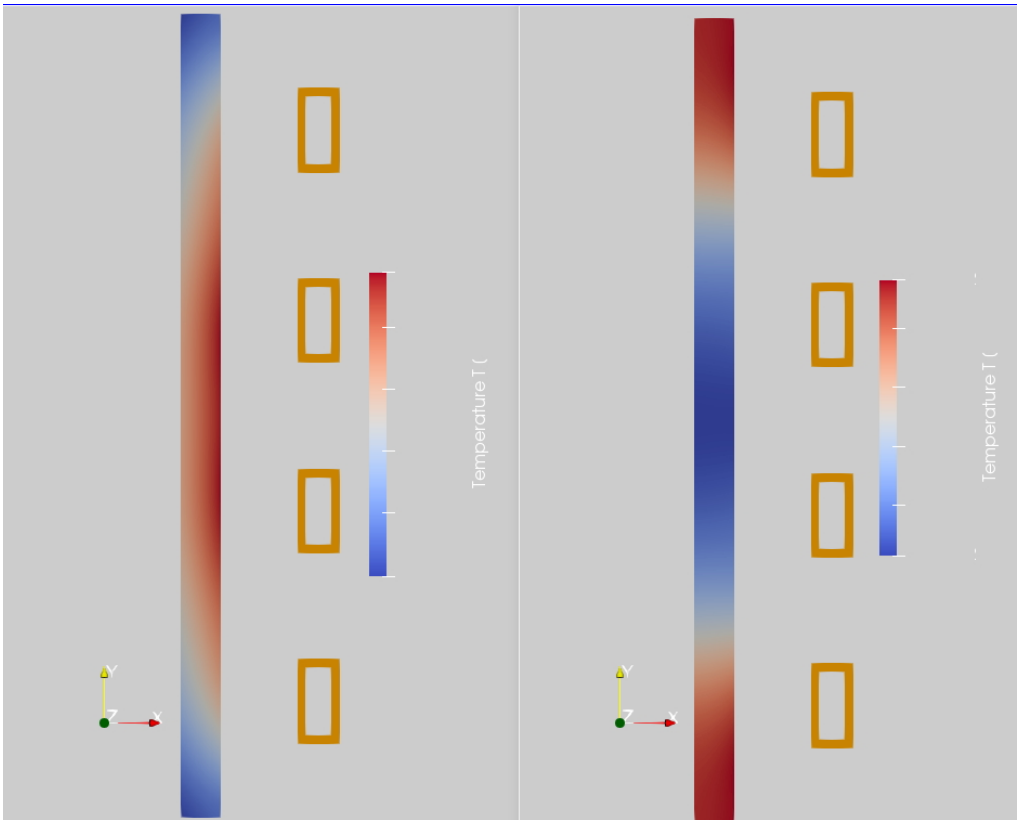

Figure 5.8: Result different current direction, a) current in same direction, b) current in opposite direction

Table 5.4: Effect of direction of the current in the coil

	High temperature $[^{\circ}C]$	**Low temperature** $[^{\circ}C]$	**Ratio**
A) Current same direction	xxxx	xxxx	1.13
B) Current opposite direction	xxxx	xxxx	1.74

A more constant heating pattern of large surfaces could be reached with a coil where the direction of the current is equal to its parallel coil. This type of coils are called pancake coils and are often used in induction cooking as indicated in figure 5.9. This would result in more complex coil shapes. Also, there have to be multiple sets of this type of coils next to each other to cover bigger surfaces. For larger more complex moulds, it is almost impossible to prevent neighboring coils with the opposite current direction. Another solution would be magnetic shielding in these conflicting areas. In [26, p.6] a ferrite core was used to shield the conflicting areas resulting in a more even temperature distribution on the mould as seen in figure 5.10. In the figure a cross section of 2 sets of 3 coils can be seen, left side the current pointing inwards and the right side is pointing outwards. The top figures (a and b) show the situation without a ferrite shield and the lower figures (c and d) shows the heating pattern more equally distributed inside the mould.

Figure 5.9: Pancake coil type, source [35]

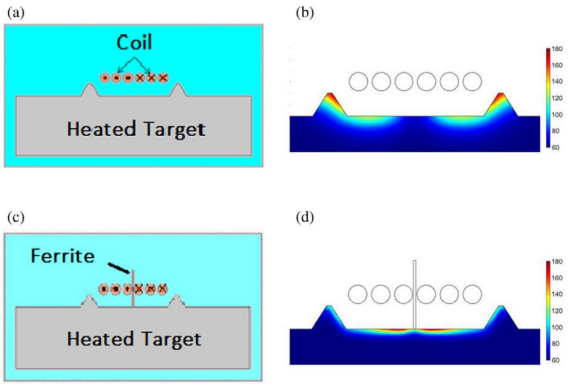

Figure 5.10: Use of ferrite core to shield conflicting areas, source: [26]

This makes it also possible to use a combination of the design used at Fokker and the pure pancake type of mould as one of each alone is not feasible. Figure 5.11 gives an example of an induction heating coil used for a bumper of a car. The green parts in the figure represent the ferrite core and the yellow the configuration of the coil.

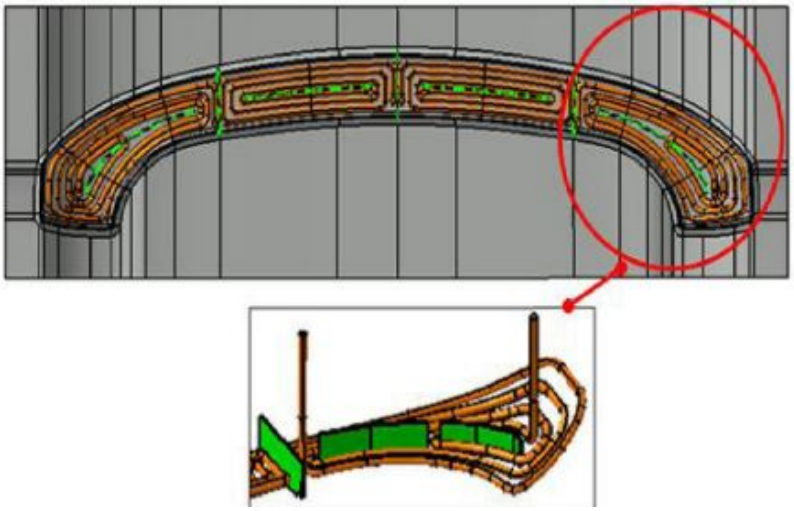

Figure 5.11: Ferrite shielding used in complex curved mould to divide sections, source [26]

5.2.1. Potential design coil

With these findings in mind, two potential designs can be proposed. It might be straight forward to propose one for the particular size used in this research, see 5.6. Given that this research is performed to develop a method to simulate bigger a more complex mould it would be unrealistic to state that a pancake coil would be the solution for every mould. Figure A is a version of a pancake mould design with the current running in one and the same direction, Figure B is a version of the meander type coil with ferrite (indicated by green blocks) shielding used in conflicting areas.

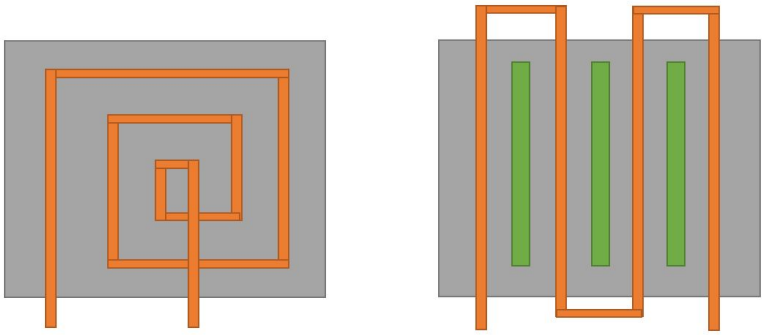

Figure 5.12: Potential design, A) pancake based mould, B) improved meander type mould

Design A is based on the pancake mould, ideally, the coil would be made out of one piece and bent into shape. This result in a constant cross-section over the whole length. The benefit of this type of design is that the direction of the current through the coil remains in the same direction. This results in an efficient heating system due to a homogeneous magnetic field above the coil. The downside is the complexity in producing this type of coil in the correct shape, as the induction system benefits from a high tolerance this could potential difference between a simulated version and produced coil.

The second type (B) is an improved version of the meander type. In situations where there it is not possible to manufacture a coil so the direction of point in the same direction. This could be the case in complex moulds or when different zones are used in the mould, both visible in the example given in figure 5.11. In the design blocks of ferrite are placed at the location where the current is running in the opposite direction to improve the heating in this conflicting areas. The benefits of this solution would be that the coil design can be simple, it also offers a solution when the geometry of the coil causes a conflicting area. The downside of this method is the loss in efficiency as the ferrite blocks absorb a part of the heat. Also, it is not proven that the ferrite cores does not degrade over time, which means that the heating performance is less reproducible.

5.3. Discussion

In section 5.1 the parameters that influence the heating profile of the mould were described. This was explained by describing the steps needed for the design of an IH system. As this suits the needs within this project and research question: ”What are the variables that influence the induction heating of the OaA mould and how can they be measured and verified to come to a reliable model”. It was explained that the IH system is a product of the requirements that follow from the consolidation cycle of the TP composite, the maximum heating, and cooling rate. This maximum heating rate was taken as an input for the estimation of choice of power of the generator. Moulds used for composite production are often made from Invar due to their similar expansion coefficient in this production temperature range. Together with the preference of high penetration depth when the mould is heated from below an estimation of the frequency of the IH system can be formed with the use of equation 2.2. This frequency range will be an estimation for the system but a requirement when selecting the IH generator.
The next step was selecting material properties of the mould as a function of temperature, the required material properties with their corresponding SI units can be found in table 5.1. JmatPro offers software to retrieve this material properties as function of temperature based on the chemical composition of the materials as described in detail in section 3.4. Measuring the electrical resistivity is recommended as is was proved that it showed the biggest variance in value over the temperature range in section 3.1 and has the biggest contribution to the IH process in section 3.1.2. Therefore an experimental setup was designed and verified for the measurement of this property, used in this research in section 3.2.8. Magnetic permeability is a nonlinear material property but used linearly in the Abaqus CAE simulation due to the limitation of the time-harmonic analysis described in section 4.2.1. Therefore the data calculated using JMatPro has to be taken at one point which is described and used in the verification of the experimental setup in section 4.2.1. When all this data is retrieved the Abaqus co-simulation can be used to simulate the IH process. This information can be used to adapt the mould

and coil to find the most equal temperature at the top surface of the mould. The properties influencing this temperature profile and performance are listed in table 5.3.
The advice is to start with thin mould stiff enough to not deform under the closing pressure of the press and thick enough for the cooling method of choice, see figure5.3. The coil dimension can start from a pitch equal to the width of the coil cross-section. The coil to mould distance is a function of the choice of cooling but is recommended to be placed as close as possible for efficiency purposes.

When a mould and coil design has been made the tank circuit has to be tuned for the correct frequency described in appendix E.3.

Section 5.2 explained the effect of the meander type coil often used in research at Fokker. A comparison was made where was shown that not only the temperature at the mould surface is more equal but also the IH system work more efficient when the current runs in similar direction in parallel coils. This effect caused due to the conflicting areas between coils with opposite current direction can be reduced by using a ferrite core between the coils. The ferrite core shields the conflicting areas which result in a more gradual heating pattern as was displayed in figure 5.10. Still, the pancake type coil has a preference as it is more efficient as the ferrite core absorbs part of the magnetic field. In complex coil configurations it will be almost impossible to have coils where the current is running in the same direction, which makes the ferrite cores a useful solution as displayed in figure 5.11.

5.4. Conclusion research question 3

Research question 3: ”How can certain parameters be changed to end up with a desired heating profile of the mould?” This question was answered by giving a step by step solution to design an induction heating setup. This can be summarized by the following steps:

Steps in designing an induction heating setup

1. Define type of thermoplastic material which defines the maximum heating rate of the material.
2. Define mould material and rough volume needed required to withstand clamping force and accommodate eventual cooling channels. The chosen cooling method will also influence the critical volume of the mould.
3. Estimate the maximum power required for the generator and pick a generator based on this estimation.
4. Measure, retrieve material data as a function of the temperature of mould material. Material properties at room temperature for the coil.
5. Write material in correct SI units and form for the input of the Abaqus CAE co-simulation
6. Simulate and optimize heating pattern to TP composite requirements based on the variables stated in table 5.3.
7. Manufacture mould and coil, optimize generator to coil and mould to a specific frequency.

The parameters that influence the behavior of the induction heating and are useful for optimizing the setup were formed in section 5.1.6 and coupled to two parameters, heating rate of the mould and uniformity of the temperature at the mould. As these objectives are both relative but contradicting the effect of the variables were given as a function of these two objectives, see table 5.5.

Table 5.5: Effect of variables on heating performance

	Speed	**Uniform heating**
Pitch increase	Slower	Less
Increase thickness mould	Slower	More
Increase ofset	Slower	More
Increase body current	More	No effect

A potential optimum mould design was purposed in section 5.2.1 based on the findings of the effect of the current direction on the heating performance and the ferrite shielding used to solve conflicting areas two designs were purposed, see figure 5.12. Ideally, a pancake type design would be used as much as possible as this has the benefit of high efficiency and homogeneous temperature distribution. However, it is not realistic that when designing complex moulds the coil can be formed in a way that all the current is running in the same direction. Therefore a second design was purposed based on

the meander type coil, ferrite blocks will be used as a magnetic shielding in conflicting areas to smooth out heating profiles. Potential downsides of these ferrite blocks are: less efficient system due to the absorption of energy and the ferrite block tend to degrade over time which results in a changing heating pattern over a longer period.

6

Conclusion

This master thesis describes the development of what is needed for induction heating simulation of the 'out of autoclave co-consolidation press' researched at Fokker to use as a future production technique. Earlier research at Fokker did not deliver the required results in terms of simulation about the induction heating and simulation process. The research question of this thesis "What are the variables that influence the induction heating of the OaA mould and how can they be measured and verified to come to a reliable model?" helps as guide through the research and is divided into three sub questions. The motivation and questions can be found in section 2.5.

Sub question 1

The literature review investigated the fundamentals of IH a summarized version of the literature review can be found in chapter 2. The variation of contributing material parameters as a function of temperature was studied by comparison of available data in the literature. A list of material properties and their expected variance can be found in section 2.1.3. Electrical resistivity was found to be the most varying parameter as a function of temperature. In section 3.1.1 an error propagation analysis was performed to find the contribution of the material and process properties on the heating performance of the IH system. Electrical resistivity was found as most contributing material property and most useful to measure exactly as a function of temperature. An experimental measurement setup was designed, used, and verified in chapter 3.2. Other material properties which were also proven to be necessary for the simulation were still only known at room temperature.

Due to time constraints, it was not possible to measure all material properties as a function of temperature. The software package JmatPro, was found which calculates the material parameters based on their chemical contribution of the elements and some additional production-related information which can be found in section 3.4. Of all the material properties the calculated data, measured data, and room temperature values were compared. The magnetic permeability was compared with a linear value known from literature.

Sub question 2

Chapter 4 describes the validation of the simulation in Abaqus CAE with the use of an experimental IH setup. First the experimental setup was described in section 4.1, where a simplified IH setup was designed without edge effect, end effect, slot effect and ring effect contributing which makes it possible to analyze the result and relate the effects to the input parameters. How parameters are measured, with motivation can be read in section 4.1.2.

The assumptions used to simulate in Abaqus can be found in section 4.2. In section 4.3 the data of the experimental test and the simulation are discussed. It was concluded that the material properties based on heat flow and radiation were correct based on the cooling phase of the temperature readings. During the early heating phase, there were similar results visible in both the experiment and simulation. After 100 seconds the simulation showed a higher temperature than the experiment indicating that the material properties or the model were not exactly correct in these regions. Based on the verifications of the material properties with the values of room temperature and the measured values of the electrical resistivity was concluded that these properties were assumed correct. Together with the fact that the

magnetic permeability was taken as a linear value instead of a nonlinear and the property was not verified in a way that the other material properties were verified was concluded that there is an error in the estimation of the magnetic permeability.

Still, the simulations are more than useful in designing the IH system. As the heating pattern was exactly predicted as the experiment. Verified with thermal camera images as visible in section 4.3.

When the magnetic permeability is defined more exactly this will increase the accuracy of the simulation. A possibility to use the nonlinear values of the magnetic permeability would also increase the accuracy of the simulation. It was concluded that the simulations are useful when designing an IH setup, the heating pattern can be simulated and the temperature distribution gives an indication of the temperature gradient on the mould surface. When comparing initial simulations with current simulations at thermocouple location 1 the result are much more accurate as is visible in figure 6.1

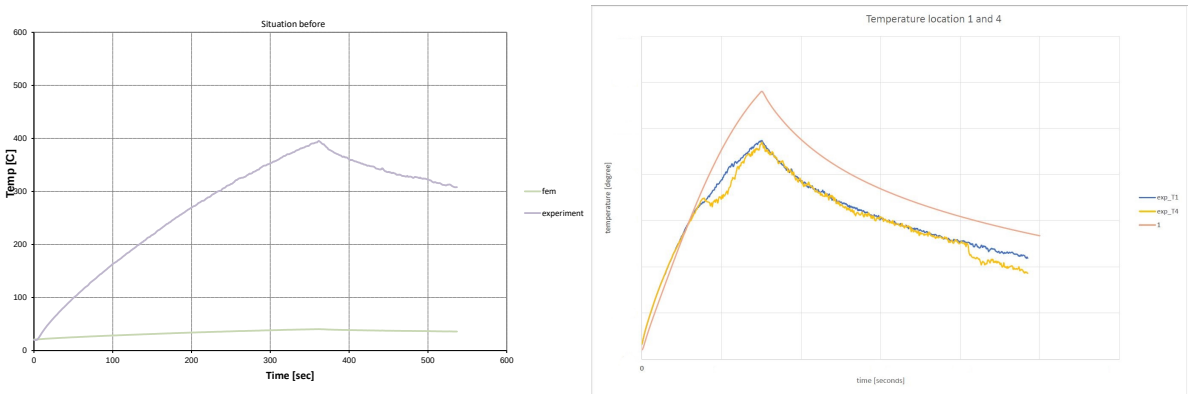

Figure 6.1: a) Initial simulation IH setup, b) Current simulation IH setup both at location T1

Sub question 3

In section 5.1 a step by step solution was given for the simulation of a new IH system. A summary of the steps to be taken are given below:

Recap

- Define type of thermoplastic material which defines the maximum heating rate of the material.
- Define mould material and rough volume needed required to withstand clamping force and accommodate eventual cooling channels. The chosen cooling method will also influence the critical volume of the mould.
- Estimate the maximum power required for the generator and pick a generator based on this estimation.
- Measure, retrieve material data as a function of the temperature of mould material. Material properties at room temperature for the coil.
- Write material in correct SI units and form for the input of the Abaqus CAE co-simulation
- Simulate and optimize heating pattern to TP composite requirements based on the variables stated in table 5.3.
- Manufacture mould and coil, optimize generator to coil and mould to specific frequency.

Also, advice was given on coil design for future IH systems at Fokker. In current setups, a meander type coil is used. The downside of this type of coil is the direction of the current which is opposite in neighboring cross sections, which creates conflicting areas between the coils resulting in big deviations of temperature at the top surface of the mould. This was demonstrated with a small simulation where it was shown that not only the temperature difference on the top was sufficient but also the efficiency of the heating system was influenced by the opposite current directions. A pancake type or any coil where the current in neighbor coils is equal in direction would be recommended.

For complex mould strategies, this could be a problem as it would be impossible to have only similar direction current in the whole system. A solution for this could be ferrite cores which function as a magnetic shield and improve the temperature distribution. The downside is a decrease in efficiency as the core absorbs some of the magnetic field. Still, it would be an option as it is more efficient than

a meander type of coil.

6.1. Recommendations

With the above-described conditions, the simulations can be used for a new design of an IH system. The proposed recommendations will increase the accuracy of the simulations.

6.1.1. Material properties

A much-heard term in simulations is ”Garbage in, garbage out”, aiming at that the computer software can only produce meaningful information if the input information is correct. Two material properties will be pointed out; magnetic permeability and radiation heat transfer.

Define Magnetic permeability

In section 4.5 was concluded that there was an indication that the magnetic permeability was not determined correct. Other material properties could be verified with room temperature values and electrical resistivity even with measured data. Also, the fact that Abaqus CAE could only use the property as a linear value as a result of the high frequency. Given that request from Fokker was, to use Abaqus CAE for the simulations for implementations with other processes another software package where the nonlinear values of the magnetic permeability can be used not an option. My advice would be to measure the magnetic permeability values of the mould material to increase the accuracy of the simulations when using Abaqus CAE for the heat simulations. Another option would be to use a simulation software package than can use this nonlinear values in his simulations for example: Cenos, a specific written software for induction heating or Comsol multhiphysics which was also found in the literature review [30]. When this is done it would be recommended to verify the chemical composition or the results of the material property calculation software JMatPro.

Radiation Heat Transfer

The heat transfer of the simulations in this report were estimated based on earlier results at Fokker. Based on the temperature comparisons these were estimated at $\varepsilon = 0.8$. This was estimated in other tests on the cooling temperature curve, as similar material was used this was relatively easy to define and verify. As for future mould design, Invar materials will be used where thermal radiation is not known from former data. Thermal radiation is a function of the material properties, texture, colour and surface area of the mould [23, p.530] which makes it complex to measure separately.

Because the radiation loss is a small term in the heating curve it will be possible to estimate a value for initial IH design and later define the thermal radiation based on cooling down test.

6.1.2. Finite plate simulations

In this research, the experimental setup was chosen to be relatively simple to be able to verify the IH with simulation data. A complex setup would make it impossible to distinguish the different effects and makes drawing conclusions impossible. As at this moment, it is clear that what is needed to set up a useful IH simulation. Also it is known which material properties are already known and which can further be explored. In the experiments, a cross-section of the plate was analysed where only the edge effect in the width direction was taken into account, Figure 6.2 (A-section). The following magnetic effects are minimally effecting the analysis.

- Edge effect
- Ring effect
- Slot effect

My recommendation will be that the areas where the coil stops and turns also need some verification as in figure 6.2(B-section). Especially if this area lies beneath the plate. It is expected will be that the effect of these corners in the coil will be able to simulate with the current setup. But it is also expected that this will have a big effect on the homogeneity of the temperature profile especially when a meander type of coil will be used.

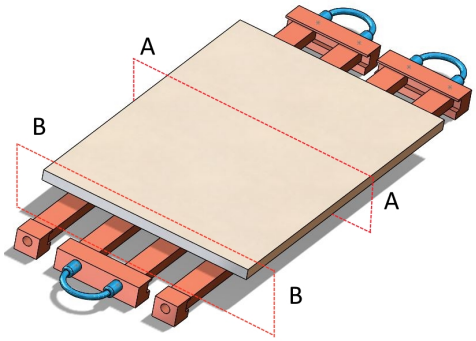

Figure 6.2: Cross-section analysis vericus edge effect

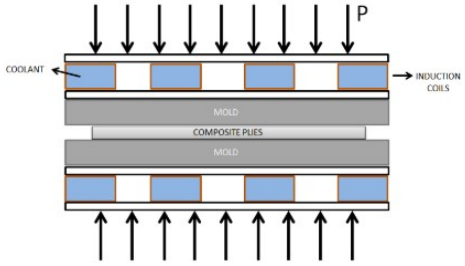

Figure 6.3: Configuration of mould and induction coil

6.1.3. Field concentrator

When producing TP composites the composite has to be pressed between two metal moulds. In this case it is not possible to place the induction coil inside the mould where is would be more effective as it could directly heat the surface, also one coil could directly heat up top and bottom surface. Logically this is not possible with this configuration, figure 6.3. This means that only a small portion of the magnetic field generated by the IH system is used for heating the surface, see figure **??**.

This is not only inefficient but also potentially heats the surrounding structure of the press mould. Therefore it would be highly recommended to use a magnetic field concentrator to increase the efficiency of the heating performance of a production mould. An example was given in chapter 5.2 where ferrite cores were used to direct magnetic field to specific areas.

An example of a magnetic flux concentrator is given in figure 6.4. The graph indicates the power concentration under the coil with and without the magnetic concentrator. The concentrator will decrease the efficiency of the generator but will increase the efficiency of the heating.

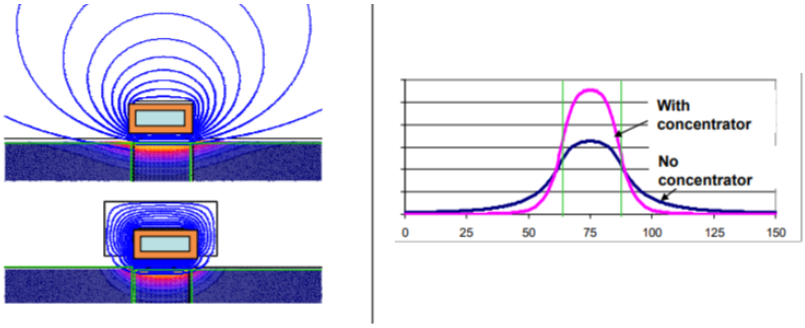

Figure 6.4: Effect of magnetic flux concentrator a) top no concentrator used, bottom a concentrator is placed on top of the coil b) normalized power distribution on vertical axis, distance over coil horizontal axis,source (Fluxtrol)

Appendix

A

Propagation of error analysis

For the propagation of error analysis in section 3.1 the approximate analytic equation from Jankowski was used [15]. The analytic approximation of the Maxwell equation is used to produce a first order fully explicit integration method to approximate the average temperature of the load at the surface. The subscript i represent to a point in time and $\Delta\tau$ the fixed dimensionless time step. The relation allows to calculate the temperature as function of time from $\theta_0 = 1$, with required material and process properties.

$$\theta_{i+1} = \theta_i + \frac{\Delta\tau}{C^*_{p,i}}\left[\frac{1}{\sigma^*_i}(\sqrt{\sigma^*_i\omega^*_i} - 0.5) - 2\varepsilon_R(1 + \frac{R}{l})(\theta_i^4 - 1)\right] \tag{A.1}$$

The following dimensionless variables are implemented to simplify the energy equation:

$$\theta = \frac{T}{T_\infty}, \tau = \frac{t\sigma_b T_\infty^3}{(\rho c)_\infty R}, \sigma^* = \frac{\sigma\sigma_b R T_\infty^4}{n^2 I^2 K_n^2}, \omega^* = \frac{\omega\mu R n^2 I^2 K_n^*}{2\sigma_b T_\infty^*}, C_p^* = \frac{(\rho c)}{(\rho c)_\infty} \tag{A.2}$$

The general error propagation relation will be used to define the propagation of variance in material and process parameters. s_f is the variance of the function f as result of the variance at the variables in the equation(s_x, s_y, s_z). The equation assumes linear characteristics neglecting correlations and assume independent variables. This relation will work when variation of the variables is relative small, because the variance at some material parameters is relative big this result can only be used as an estimation of the error of the function f. When the partial derivatives are compared still an indication can be given of the rate the specific variable and the effect on function f.

$$s_f = \sqrt{\frac{\delta f}{\delta x}^2 s_x^2 + \frac{\delta f}{\delta y}^2 s_y^2 + \frac{\delta f}{\delta z}^2 s_z^2 \cdots} \tag{A.3}$$

For the propagation of energy analysis the partial derivative has to be taken to several variables. Which will be used to relate the influence of the variable to the output of the analytic equation. In other words; what has an increase in variable value in temperature of the workpiece. Although in chapter 3.1 is looked at material properties also the partial derivative to the process properties are analyzed.

$$\frac{\delta f}{\delta \rho} = \frac{t\sigma_b T_\infty^3\left(n^2 I^2 K_n^2 \frac{\sqrt{2}\sqrt{\sigma R^2\omega\mu}-0.5}{2\sigma\sigma_b R T_\infty^4} - 2\varepsilon_R(1 + R/l)(\theta^4 - 1)\right)}{R\rho^2 c} \tag{A.4}$$

$$\frac{\delta f}{\delta c} = \frac{t\sigma_b T_\infty^3\left(n^2 I^2 K_n^2 \frac{\sqrt{2}\sqrt{\sigma R^2\omega\mu}-0.5}{2\sigma\sigma_b R T_\infty^4} - 2\varepsilon_R(1 + R/l)(\theta^4 - 1)\right)}{R\rho c^2} \tag{A.5}$$

$$\frac{\delta f}{\delta \sigma} = \frac{t\sigma_B T_\infty^3\left(\frac{-n^2 I^2 K_n^2\sqrt{(2)}\sqrt{(\sigma R^2\omega\mu)}-0.5}{2\sigma^2\sigma_b R T_\infty^4} + \frac{.353 R n^2 I^2 K_n^2\omega\mu}{\sigma\sigma_B T_\infty^4\sqrt{(\sigma R^2\omega\mu)}}\right)}{\rho^2 c^2 R} \tag{A.6}$$

$$\frac{\delta f}{\delta \mu} = \frac{0.353 t n^2 I^2 K_n^2 \omega}{T_\infty \rho c \sqrt{\sigma R^2 \omega \mu}} \tag{A.7}$$

$$\frac{\delta f}{\delta \omega} = \frac{0.353 t n^2 I^2 K_n^2 \mu}{T_\infty \rho c \sqrt{\sigma R^2 \omega \mu}} \tag{A.8}$$

$$\frac{\delta f}{\delta I} = \frac{t \sigma_b T_\infty^3 \left(n^2 2 I K_n^2 \frac{\sqrt{2}\sqrt{\sigma R^2 \omega \mu} - 0.5}{2 \sigma \sigma_b R T_\infty^4} \right)}{R \rho c} \tag{A.9}$$

Results of the propagation of error analysis are discussed in chapter 3.1. Also the expected variances that are used for the analysis are explained.

B

Test Plan

Test plan for measuring electrical resistivity in metal samples as function of temperature

This chapter describes the steps necessary to perform the measurement of electric resistivity on metals as a function of temperature. This chapter is written to use separate as a guideline during testing. More in depth information is given in section 3.2. This Appendix should give sufficient information to perform the electrical resistivity test on any metal from room temperature until 450 $[^{\circ}C]$. The electrical resistivity ρ is calculated with the following formula:

$$\rho = R\frac{A}{l}[\Omega m] \tag{B.1}$$

Where 'A' is the surface of the cross-section of the sample in $[m^2]$ and 'l' the length in $[m]$. When the resistance 'R' is known the electrical resistivity can be calculated as the dimensions remain constant. This resistance will be measured by performing a 4 point measurement also known as a van der Waal resistance measurement[27]. A voltage will applied on a sample, hereafter a current is running through the sample, the voltage drop over the sample combined with the current running through the sample will be used with ohms law to calculated the resistance. This technique avoids contact resistance problems due to different electrical properties between the sample and measurement wires and eliminates the effect measurements wires have on the measurement. This is especially relevant when measuring low resistances as expected for this type of material. To find the resistance of the sample as a function of temperature the following electrical circuit will be used:

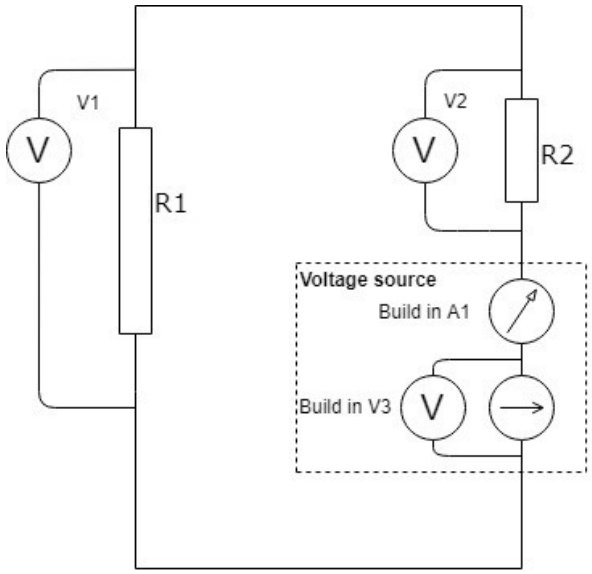

Figure B.1: Electrical circuit used for measurements electrical resistivity

In this circuit R1 is the sample and the resistance that will be the main result of this experiment. R2 is an added resistance for two reasons: to lower the current in the circuit to increase the accuracy of the measurements and to calculate the current in the circuit by measuring the voltage over a known resistance.

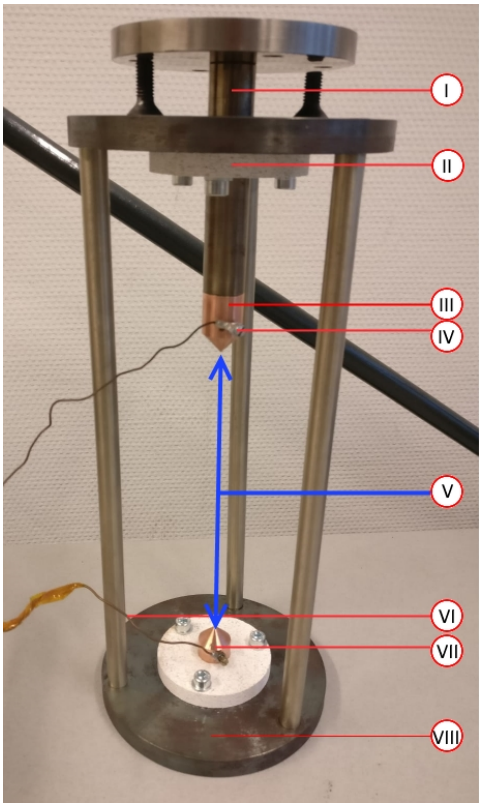

Figure B.2: Measuring setup

In figure B.2 the following components are listed: I Movable shaft to keep pressure on sample constant, II Isolator disk top, II Copper cone with minimal contact area, IV Screw on measurement point 'current circuit', V Place for sample in measurement circuit, VI Screw on measurement point current circuit, VII Lower copper cone with minimal contact area and VIII Steel support structure.

B.1. Specifications of equipment required

Electrical equipment:

- Accurate multimeter with 4 point resistance possibility to measure R2, resolution: 1$[\mu\Omega]$, Accuracy 140 PPM [1]
- 2x Accurate voltage meters, resolution 0.1$[\mu V]$, accuracy 65 PPM
- 1x K-type thermocouple, resolution 0.001 $^{\circ}C$, accuracy 1 $[^{\circ}]$
- Voltage source, 0.05 [V] constant

Use the voltage meters in combination with an computer to automate the measurements when the setup is placed in the oven. So that the measurement is not unnecessary lengthy. Other equipment:

- Oven with minimal internal dimension of 400x100x100 [mm] HxWxD, and a temperature range of room temperature to 450 $[^{\circ}C]$.
- Measurement setup described in Figure 3.5
- Extra resistance (R2) around 0.1Ω
- Spot welder[2]
- Copper wires to facilitate electrical circuit, 1 [mm] minimal diameter
- File or rough sandpaper

[1] Parts Per Million

[2] A spot welder used for preparing thermocouples can be used for this purpose

- Kapton tape (or other heat resisting isolating tape)
- Weight of 1105 gram (This specific weight is used before and worked)

B.1.1. Requirements sample

- Constant thickness
- 200 [mm] long
- Square or round cross-section both possible.
- Area of cross-section has to be 2 orders higher than the contact surface copper pin to sample

The sample size that was used before (6x6x200 [mm]). The square surface makes it easier to spot weld the measurement wires.

B.2. Steps to be performed during experiment

1. Measure resistance R2
2. Spot weld measurement wires
3. Roughen up surface
4. Prepare setup for Ohmic behavior test at room temperature
5. Test in oven

B.2.1. 1. Measure resistance of R2

Ohms law is used to calculate the current running through the electrical circuit during the measurements $(I = U * R[a])$. Therefore the resistance of R2 has to be known which can be done with a digital mulitmeter, Keithley 2701 with the 4 points resistance function. The Keithley 2701 has an build in voltage source and ampere meter. The ratio voltage over current is used to define the resistance of R2. Figure B.3 shows schematically how R2 has to be wired to the Keithley 2701. The resistance will be measured with a resolution 0.1 $[\mu V]$ and an accuracy of 65 PPM. The measurement can be done at room temperature.

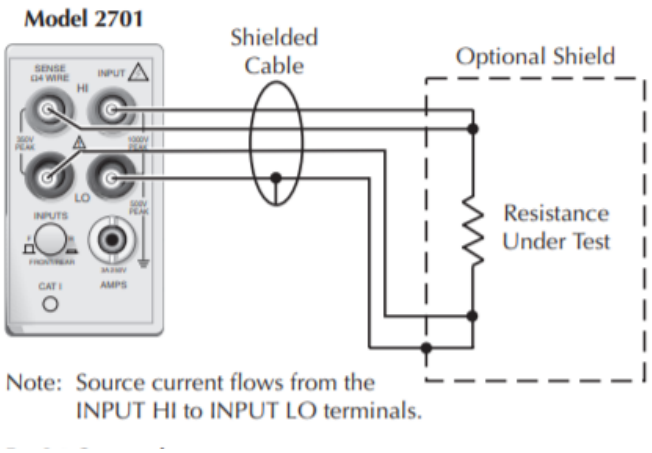

Figure B.3: Electrical circuit of resistance test of R2. The shielded cable was not used as their was none available that can withstand the temperature in the oven. The measurement setup was electronic shielded from its surroundings.

B.2.2. 2. Spot weld measurement wires

The connection to the sample is important for an accurate and consistent measurement. In this experiment it is chosen to use spot welding to connect the two wires of the measurement loop (voltmeter) to the sample. A spot weld has the benefit of making a connection without having to add extra material (which is the case for welding, soldering) which makes the cross-sectional area small and consistent. After the spot weld the distance between the spot welds can be measured and filled in the measurement sheet: (L1 in [mm]).

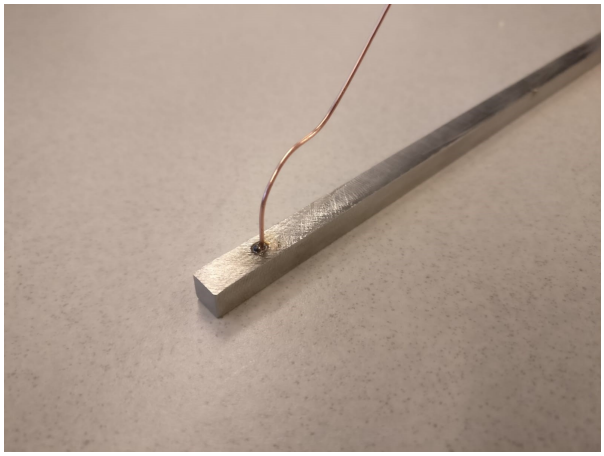

Figure B.4: Example of a connection of the voltmeter with the use of spot welding

B.2.3. 3. Roughen up surface

The connection is very important for the accuracy of the measurements. Therefore the top and bottom surfaces of both the sample and copper cone have to be sanded/ filed to remove corrosion from earlier tests. A weight of about 1100 [gram] was used to take care of the right amount of force on the contact point. This weight is placed on top of the setup on the tray which is connected to the movable shaft. This weight will prevent contact loss due to the forming of corrosion at the contact points. Figure B.5 shows an example of an sanded tip and sample.

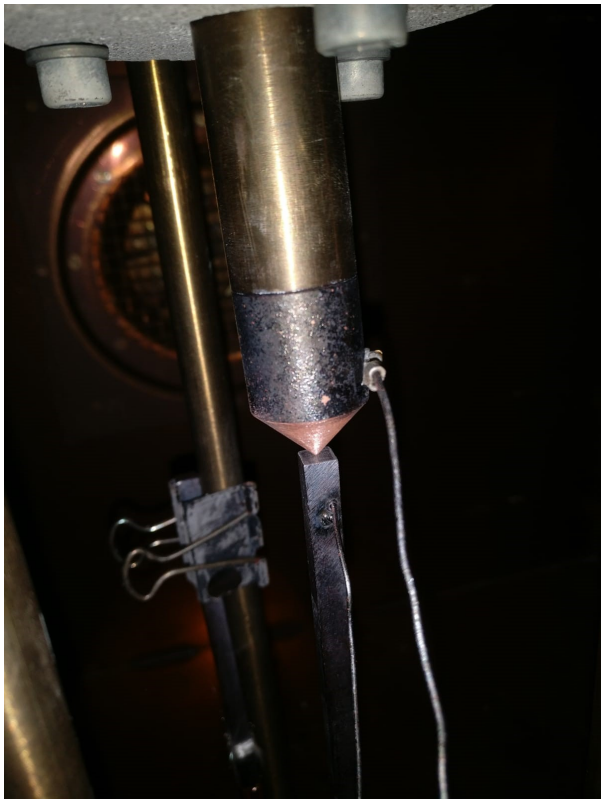

Figure B.5: Example of sanded contact point, this figure shows an sanded tip which is in contact with an sanded top surface of the sample.

B.2.4. 4. Prepare setup for validation at room temperature

The electric resistivity test is based on Ohms law. To verify this behavior this test will be done at room temperature. An added benefit of this check is that the electric resistivity can be checked with data from

literature and so the setup can be checked. Often the electric resistivity is known at room temperature in various sources (preferably the manufacturer of the material otherwise a general database for example; CES Edupack). Fill in the following data sheet from the measurement sheet. Plot the data in a graph to check the linearity over different voltage settings. A best-fit linear line can be fitted through the data point to find the average resistance at room temperature. Table B.1 can be used to set up the ohmic behavior test.

Table B.1: Example graph testing Ohmic behavior

Set	**Measured**		**Calculated**	
Voltage power source	Current	Voltage, measured at sample	Resistance	Electric resistivity
[v]	[A]	[V]	$[\Omega]$	$[\Omega m]$
0.1	-	-	-	-
0.2	-	-	-	-
0.4	-	-	-	-
0.8	-	-	-	-
1.0	-	-	-	-
1.2	-	-	-	-
1.4	-	-	-	-
1.5	-	-	-	-

In table B.1 the resistance 'R' is calculated by $\frac{U}{I}$, and the electrical resistivity with the relation found in equation B.1. An example of the graph which is formed in the ohmic beheviour test is found in figure B.6. This graph is made with an spreadsheet program were the best-fit linear function is used to form a graph through the data points found in the experiments, based on the value of $R^2 = 1$ is concluded that the data is linear.

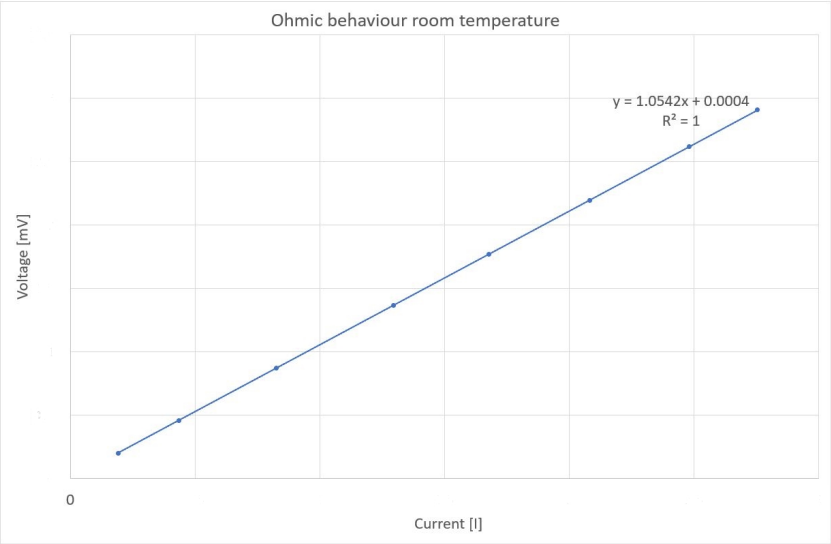

Figure B.6: Example plot of data test ohmic behavior

B.2.5. 5. Test in oven

The tests in the oven are in theory the same as the measurements at room temperature. What makes it different is that the setup is not visible and the test is performed at high temperature. To make sure that the test is performed successfully it is recommended to make sure that the connection to the sample is rigid and will last for the whole heating cycle. Before the test start it is recommended to check if the measured values are in the same range as the measured values at room temperature. To make it possible to check the setup it is recommended to start the measurements already in the heating part of the experiment. A low voltage is recommended as it heat up the electrical circuit as less as possible.

Recommended is 0.05 [v]. As the process is Ohmic a higher voltage will also work but will introduce an extra heat source in the measurement wire due to high currents. An example of the setup placed in the oven is given in figure B.7. Here is visible that to prevent a short circuit with the oven door glass fabric was used to cover up the measurement wires. In the figure the weight is placed next to the setup but this will be placed on the setup during measurements.

Figure B.7: Test setup placed in oven

When performing the experiment pay extra attention to the following points:

- The R2 resistance has to be at a constant temperature, connect to a heat sink
- The connection between the copper cone and the sample is extremely important for the accuracy, make sure to make this connection properly
- Because cooling down can take a while it is not likely that you will be present the whole experiment. Monitor the voltage over the R2 or current at the voltage source to check if the connection is still as expected.
- Place the sample on a way in the setup so it cannot fall out and break the circuit and damage your experiment

The data retrieved from the experiment can be loaded into a spreadsheet program to check the electric resistivity throughout the experiment. For an accurate result the test has to be repeated at

least 3 times per sample. Any variations between the different measurements can than be spotted. It is recommended to check values of resistance at room temperature before start heating of the oven, if the resistance is to low check the contact surfaces in contact with the sample. Any during the inaccuracy during the measurements comes from both the measurement error from the equipment and the variance between the different measurements.

C

Measurement sheet electric resistivity test

Measurement sheet

Sample description: _____

Before measurements

Parameter	Value	Unit
L1		[m]
Width		[m]
Height		[m]
Cross-sectional are		$[m^2]$
Resistance R2		[[Ω]

Check Ohmic behavior

Set	Measured		Calculated	
Voltage power source	Current	Voltage	Resistance	Electric resistivity
[v]	[A]	[v]	$[\Omega]$	$[\Omega m]$
0.1	-	-	-	-
0.2	-	-	-	-
0.4	-	-	-	-
0.8	-	-	-	-
1.0	-	-	-	-
1.2	-	-	-	-
1.4	-	-	-	-
1.5	-	-	-	-

$$R = \frac{U}{I}\,[\Omega]$$

$$\rho = R * \frac{A}{L1}\,[\Omega m]$$

Measured parameters during test

V[rod]	V[current]	Temperature	Calculated current	R1	Electric resistivity
			calculated	calculated	calculated
[mV]	[mV]	[C]	[I]	[Ohm]	[Ohm*m]
-	-	-	-	-	-
-	-	-	-	-	-

D

Experimental setup IH

D.1. Experimental setup

Figure D.1: Setup experimental induction heating experiment

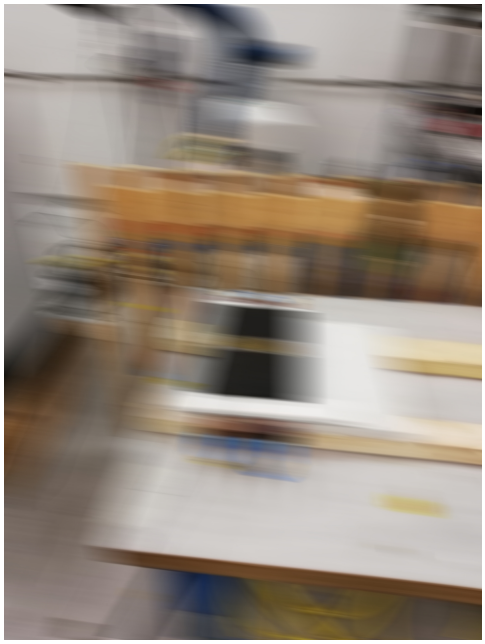

Figure D.2: Location of thermocouples on mould

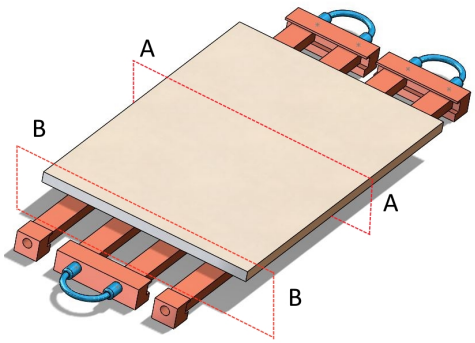

Figure D.3: Representation of mould and coil

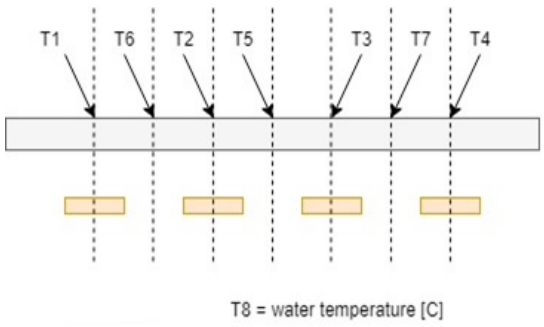

Figure D.4: Cross-section A and location of thermocouples

Figure D.5: Dimensions plate and coil

D.2. Raw data

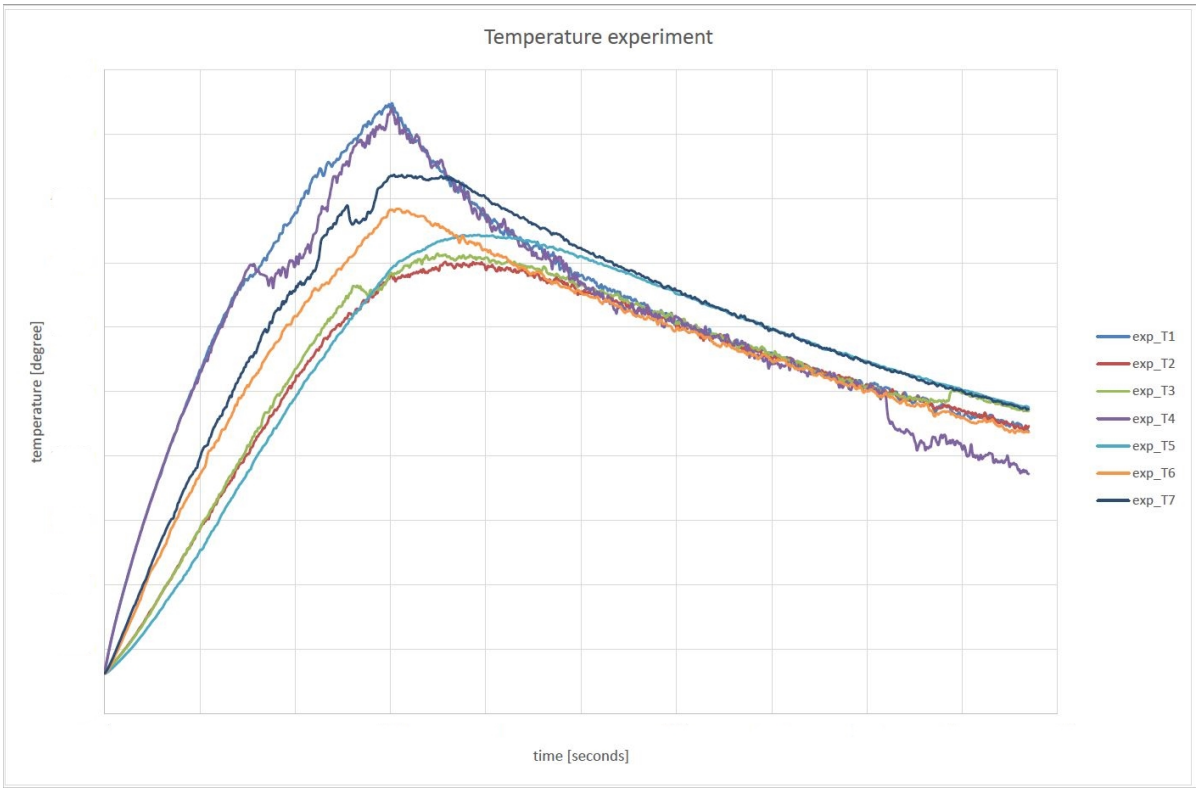

Figure D.6: Temperature readings thermocouples, location corresponds to figure D.4

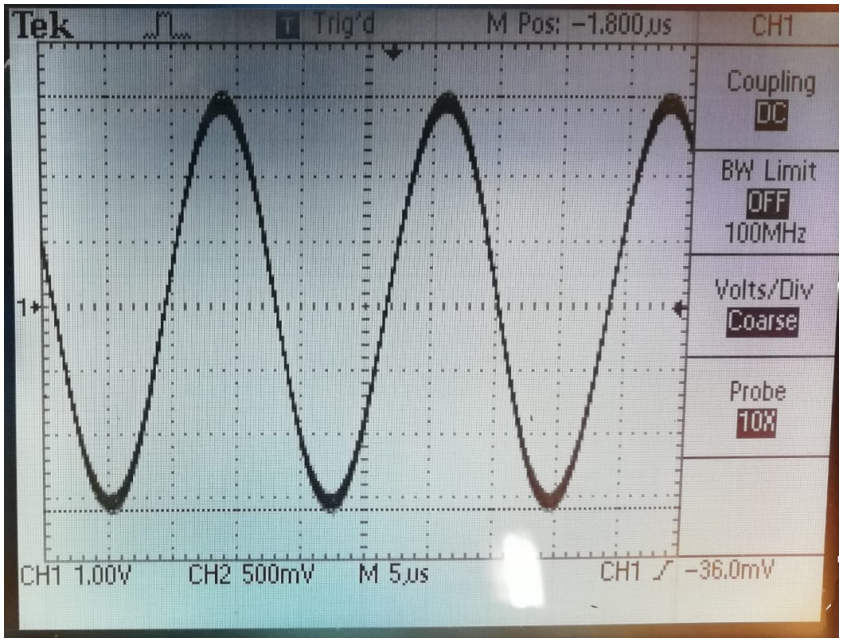

Figure D.7: Shape current signal during experimental test, verification of sinusoidal shape.

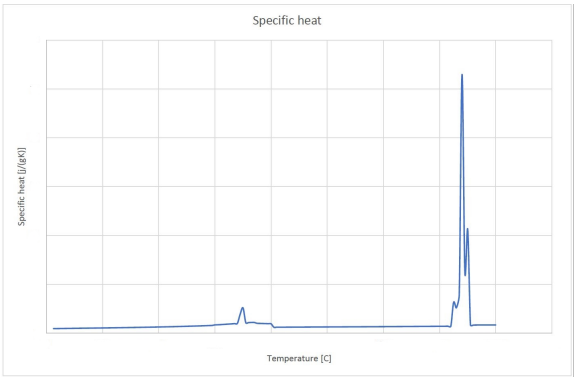

(a) Specific heat

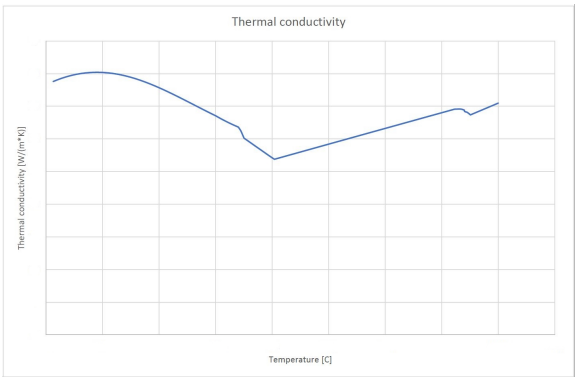

(b) Thermal conductivity

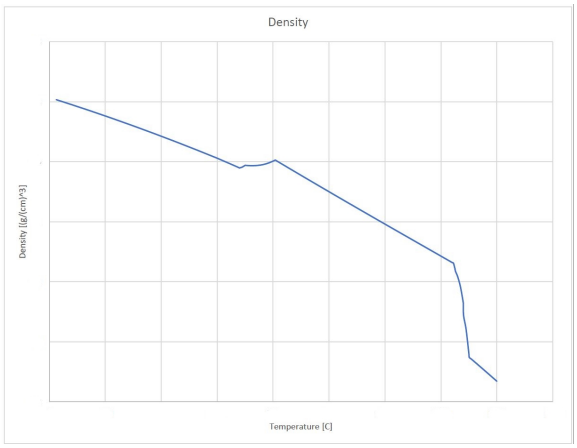

(c) Density

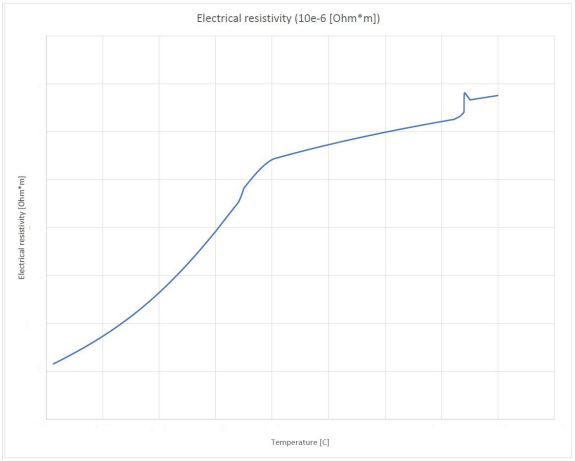

(d) Electric resitivity

Figure D.8: Calculated material data JMatPro S355J2 + AR/m

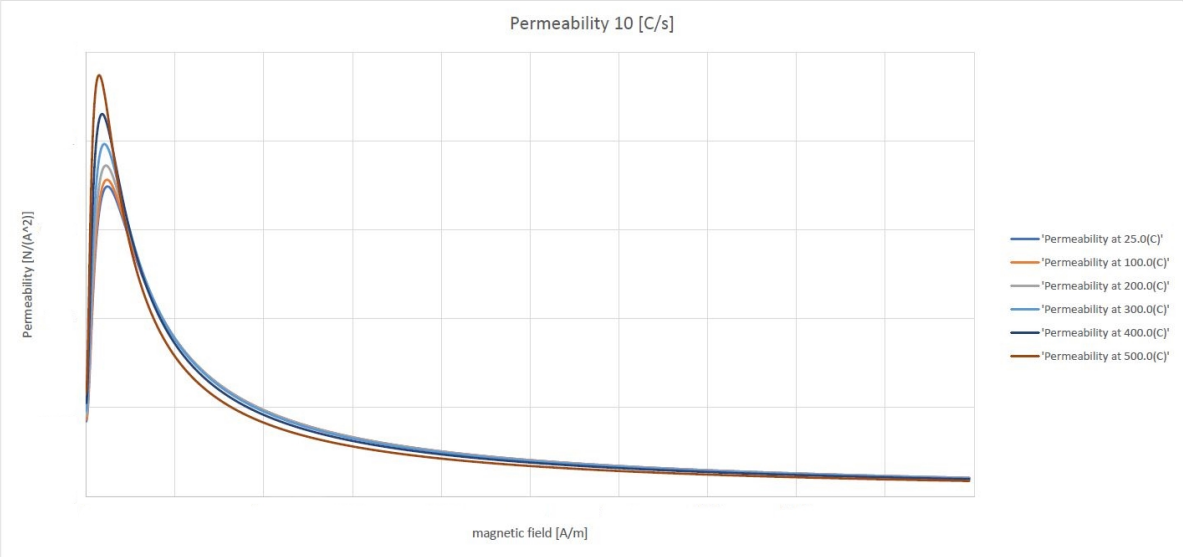

Figure D.9: Magnetic permeability as function of magnetic field, at different temperatures

Table D.1: Material properties S355 +AR/m, 0- 200

Temperature	**Value**	**Unit**	0	50	100	150	200
Specific heat	c	$[Jkg^{-1}K^{-1}]$	xxxx	xxxx	xxxx	xxxx	xxxx
Thermal conductivity	k	$[Wm^{-1}K^{-1}]$	xxxx	xxxx	xxxx	xxxx	xxxx
Electric resistivity	ρ	$[\Omega m]$	xxxx	xxxx	xxxx	xxxx	xxxx
Electric conductivity	σ	$[Sm^{-1}]$	xxxx	xxxx	xxxx	xxxx	xxxx
Density	ρ	$[kgm^{-3}]$	xxxx	xxxx	xxxx	xxxx	xxxx

Table D.2: Material properties S355 +AR/m, 250-450

Temperature	**Value**	**Unit**	250	300	350	400	450
Specific heat	c	$[Jkg^{-1}K^{-1}]$	xxxx	xxxx	xxxx	xxxx	xxxx
Thermal conductivity	k	$[Wm^{-1}K^{-1}]$	xxxx	xxxx	xxxx	xxxx	xxxx
Electric resistivity	ρ	$[\Omega m]$	xxxx	xxxx	xxxx	xxxx	xxxx
Electric conductivity	σ	$[Sm^{-1}]$	xxxx	xxxx	xxxx	xxxx	xxxx
Density	ρ	$[kgm^{-3}]$	xxxx	xxxx	xxxx	xxxx	xxxx

Table D.3: Material properties S355 +AR/m, 500-600

Temperature	**Value**	**Unit**	500	550	600
Specific heat	c	$[Jkg^{-1}K^{-1}]$	xxxx	xxxx	xxxx
Thermal conductivity	k	$[Wm^{-1}K^{-1}]$	xxxx	xxxx	xxxx
Electric resistivity	ρ	$[\Omega m]$	xxxx	xxxx	xxxx
Electric conductivity	σ	$[Sm^{-1}]$	xxxx	xxxx	xxxx
Density	ρ	$[kgm^{-3}]$	xxxx	xxxx	xxxx

E

Detailed material properties IH system

E.1. Coil material

Table E.1: Material properties Cu-HCP/CW021A room temperature

Property	Value	Unit
Density	xxxx	$[kgm^{-3}]$
Thermal conductivity	xxxx	$[Wm^{-1}K^{-1}]$
Magnetic permeability	xxxx	$[Hm^{-1}] = [NA^{-2}]$
Specific Heat	xxxx	$[JKg^{-1}K^{-1}]$
Electric conductivity	xxxx	$[Sm^{-1}] = [A^2s^3kg^{-1}m^{-3}]$

E.2. Mould material

Conditions necessary JMatPro

Table E.2: Composition metal S355 + AR/m

Element	Percentage [%]
C	0.20
Mn	1.60
P	0.025
S	0.025
Si	0.55
Cu	0.55
Fe	97.05

- Thermal mechanical rolling
- Tensile strength of 480 $[N/mm^2]$
- Hardness 164 [HB]
- Microstructre is fine, quenched and tempered

Table E.3: Material properties S355 + AR/m room temperature

Property	Value	Unit
Density	7800	$[kgm^{-3}]$
Thermal conductivity	40-45	$[Wm^{-1}K^{-1}]$
Specific Heat	460-480	$[JKg^{-1}K^{-1}]$
Electric resisitivity	0.2-0.25·10^{-6}	$[\Omega m]$

E.3. Generator

Table E.4: TruHeat MF 3040 important parameters

	Value	Unit
Rated power	40	$[kW]$
Maximum output voltage	600	$[Veff]$
Nominal operating frequency	5-200	$[kHz]$
Total efficiency	87	$[\%]$

Table E.5: Process properties generator

Input	Percentage [%]	Value	Unit
Current	25	30.0	$[a]$
Voltage	72	309.0	$[v]$
Power	22	9.2	$[kW]$
Frequency		58.2	$[kHz]$
Calculated values			
Current at coil	RMS	834.32	$[a]$
Current at coil	peak	1179.91	$[a]$

E.3.1. Generator matching

For an optimal induction heating system the induction heating system has to be optimized for the correct frequency and efficiency. This oscillator circuit matching is a function of the impedance and capacitance of the components in the tank circuit E.1.

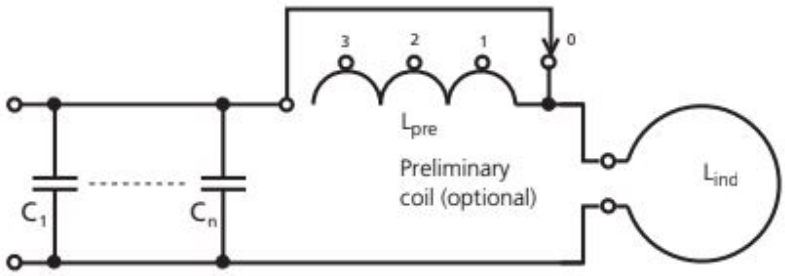

Figure E.1: Tankcircuit of induction heating system

The inductance of the coil is a function of the shape and material properties. As the coil is made as a function of the simulation the impedance has to be measured after manufacturing. This impedance has to be used to tune the oscillator circuit for the correct frequency. The frequency can be calculated with the following relation

$$f = \frac{1}{2\pi \times \sqrt{L_{ges} \times C_{ges}}} \tag{E.1}$$

Where the total capacitance C_{tot} can be calculated from the sum of the individual capacitances:

$$C_{tot} = C_1 + C_2 \ldots\ldots + C_n \tag{E.2}$$

The total inductivity L_{tot} can be calculated from the sum of the individual inductances:

$$L_{tot} = L_{ind} + L_{pre} \tag{E.3}$$

The inductivity of the inductor (inductor) can be measured with an LCR meter of a multimeter. The capacitors can be used to adapt for the required frequency.

After correcting for the frequency the process parameters have to be matched to find the most optimal setting for the efficiency of the IH process. Ideal IAC = UAC (percentage values). When IAC<UAC the impedance of the tank circuit is to large. When IAC>UAC the impedance of the tank circuit is to small. The manual of Trump gives options to vary this setting without (de)crease the frequency[3]. A summery of the effect on changing the parameters is given in table E.2.

EFFECTS				
Changed values		**Effect**		
Capacitance C_{tot}	Inductance L_{tot}	Output frequency f	Output current I	Oscillator circuit impedance
+	=	−	+	−
−	=	+	−	+
=	+	−	−	+
=	−	+	+	−

Figure E.2: The effect of changing the parameters on the IH system

Bibliography

[1] Theory of Heating by Induction chapter 2. Technical report, 2001. URL www.asminternational.org.

[2] Model 2701 Ethernet-Based DMM / Data Acquisition System Users Manual, 2002.

[3] Operating Instructions TruHeat MF 3040, 2016.

[4] J Acero, R Alonso, J M Burdio, L A Barragan, and D Puyal. Analytical Equivalent Impedance for a Planar Circular Induction Heating System. *IEEE TRANSACTIONS ON MAGNETICS*, 42(1), 2006. doi: 10.1109/TMAG.2005.854443. URL https://ieeexplore.ieee.org/ielx5/20/33149/01561506.pdf?tp={&}arnumber=1561506{&}isnumber=33149.

[5] Jesús Acero, Pablo J Hernández, José M Burdío, Rafael Alonso, and Luis A Barragán. Simple Resistance Calculation in Litz-Wire Planar Windings for Induction Cooking Appliances. *IEEE TRANSACTIONS ON MAGNETICS*, 41(4), 2005. doi: 10.1109/TMAG.2005.844844. URL https://ieeexplore.ieee.org/ielx5/20/30696/01420684.pdf?tp={&}arnumber=1420684{&}isnumber=30696.

[6] Rajaneesh Acharya. *Modeling and Simulation of Multi Coil Induction Heating System for Semiconductor Wafer Processing*. IEEE International Conference On Recent Trends In Electronics Information Communication Technology, India, 2016. ISBN 9781509007745. URL https://ieeexplore.ieee.org/ielx7/7792522/7807761/07807890.pdf?tp={&}arnumber=7807890{&}isnumber=7807761.

[7] Maureen Aller and Jonathan Pennell. The Measurement, Instrumentation and Sensors Handbook. Technical report, 1999. URL http://www.kelm.ftn.uns.ac.rs/literatura/si/pdf/MeasurementInstrumentationSensors.pdf.

[8] Andrei Anisimov and Roger M. Groves. World Class Composite Solutions (WCCS) Delft University of Technology. (November):1–56, 2018.

[9] Aldo Canova, Fabrizio Dughiero, Floriana Fasolo, Michele Forzan, Fabio Freschi, Luca Giaccone, Maurizio Repetto, and Saet Sp. Identification of Equivalent Material Properties for 3-D Numerical Modeling of Induction Heating of Ferromagnetic Workpieces. *IEEE TRANSACTIONS ON MAGNETICS*, 45(3), 2009. doi: 10.1109/TMAG.2009.2012830. URL https://ieeexplore.ieee.org/ielx5/20/4787272/04787334.pdf?tp={&}arnumber=4787334{&}isnumber=4787272.

[10] Y. Pleshivtseva E. Rapoport. *Optimal Control of Induction Heating Processes*. Taylor & Francis Group, first edition, 2007. ISBN 0-8493-3754-2.

[11] Quinten Rensen Fokker. Predictive Modelling of the out-of-Autoclave Induction Heated Process. Technical report, Fokker Aerostructures Hoogeveen, Hoogeveen, 2017.

[12] Ming-Shyan Huang and Yao-Lin Huang. Effect of multi-layered induction coils on efficiency and uniformity of surface heating. *International Journal of Heat and Mass Transfer*, 53:2414–2423, 2010. doi: 10.1016/j.ijheatmasstransfer.2010.01.042. URL https://ac.els-cdn.com/S0017931010000542/1-s2.0-S0017931010000542-main.pdf?{_}tid=f2235f0e-b119-42ec-a890-9ca40cb1ed40{&}acdnat=1539787483{_}03604343ab0e7ffb16e07b4dbbff85b6.

[13] Adeel Ikram, Nabeel Arif, and Hyun Chung. Design of an induction system for induction assisted alternating current gas metal arc welding. *Journal of Materials Processing Technology*, 231:162–170, 2016. doi: 10.1016/j.jmatprotec.2015.12.015. URL http://dx.doi.org/10.1016/j.jmatprotec.2015.12.015.

[14] Lenka Jakubovičová, Andrej Gašparec, Peter Kopas, and Milan Sága. Optimization of the Induction Heating Process in Order to Achieve Uniform Surface Temperature. 2016. doi: 10.1016/j.proeng.2016.01.185. URL www.sciencedirect.com.

[15] Todd A Jankowski, Norma H Pawley, Lindsey M Gonzales, Craig A Ross, and James D Jurney. Approximate analytical solution for induction heating of solid cylinders. *Applied Mathematical Modelling*, 40:2770–2782, 2015. doi: 10.1016/j.apm.2015.10.006. URL http://dx.doi.org/10.1016/j.apm.2015.10.006.

[16] Matej Kranjc, Anze Zupanic, Damijan Miklavcic, and Tomaz Jarm. Numerical analysis and thermographic investigation of induction heating. *International Journal of Heat and Mass Transfer*, 2010. ISSN 00179310. doi: 10.1016/j.ijheatmasstransfer.2010.04.030.

[17] O. Lucía, Pascal Maussion, E Dede, and J.M. Burdío. Induction heating technology and its applications: Past Developments, current Technology, and future challenges. *IEEE Transactions on Industrial Electronics*, 61(05):2509–2520, 2014. ISSN 02780046. doi: 10.1109/TIE.2013.2281162.

[18] Sergio Lupi, Michele Forzan, and Aleksandr Aliferov. *Induction and Direct Resistance Heating Theory and Numerical Modeling*. Springer, London, 2015. URL https://link.springer.com/content/pdf/10.1007{%}2F978-3-319-03479-9.pdf.

[19] Steve Meister and Dietmar Drummer. Investigation on the achievable flow length in injection moulding of polymeric materials with dynamic mould tempering. *The Scientific World Journal*, 2013(July), 2013. ISSN 1537744X. doi: 10.1155/2013/845916.

[20] Shih-Chih Nian, Sheng-Wei Tsai, Ming-Shyan Huang, Rong-Cheng Huang, and Chih-Hau Chen. Key parameters and optimal design of a single-layered induction coil for external rapid mold surface heat. *International Communications in Heat and Mass Transfer*, 57:109–117, 2014. doi: 10.1016/j.icheatmasstransfer.2014.07.019. URL http://dx.doi.org/10.1016/j.icheatmasstransfer.2014.07.019.

[21] Valery Rudnev and George Totten. ASM Handbook: Volume 4C - Induction Heating and Heat Treatment. 4:28–35, 2014.

[22] Valery Rudnev, Don Loveless, and Raymond L. Cook. *Handbook of Induction heating*. New York, 2003. ISBN 9781138748743. URL http://www.asminternational.org/{%}0Aweb/hts/home/-/journal{_}content/56/10192/75024G/PUBLICATION.

[23] Valery Rudnev, Don Loveless, Raymond L. Cook, and Micah Black. Handbook of Induction Heating. *Marcel Dekker, New York*, page 796, 2003. URL http://www.asminternational.org/web/hts/home/-/journal{_}content/56/10192/75024G/PUBLICATION.

[24] Mohammad Hamed Samimi, Arash Mahari, Mohammad Ali Farahnakian, and Hossein Mohseni. The Rogowski coil principles and applications: A review. *IEEE Sensors Journal*, 15(2):651–658, 2015. ISSN 1530437X. doi: 10.1109/JSEN.2014.2362940.

[25] N. Saunders, Z. Guo, X. Li, A. P. Miodownik, and J. Ph Schillé. Using JMatPro to model materials properties and behavior. *Jom*, 55(12):60–65, 2003. ISSN 10474838. doi: 10.1007/s11837-003-0013-2.

[26] Shiou Yueh Shih, Shih Chih Nian, and Ming Shyan Huang. Comparison between single- and multiple-zone induction heating of largely curved mold surfaces. *International Communications in Heat and Mass Transfer*, 75:24–35, 2016. ISSN 07351933. doi: 10.1016/j.icheatmasstransfer.2016.03.020. URL http://dx.doi.org/10.1016/j.icheatmasstransfer.2016.03.020.

[27] Dassault Systemes. Simulia Abaqus 2016 documentation, 2016. URL http://130.149.89.49:2080/v2016/index.html.

[28] Mohammad Hossein Tavakoli, Hossein Karbaschi, and Feridoun Samavat. Influence of workpiece height on the induction heating process. *Mathematical and Computer Modelling*, 54(1-2):50–58, 2011. ISSN 08957177. doi: 10.1016/j.mcm.2011.01.033. URL http://dx.doi.org/10.1016/j.mcm.2011.01.033.

[29] Tektronix. Multimeter/Data Acquisition/ Switch Systems. 44(0), 2010.

[30] Frank van Duin. Literature review report. *literature study*, (oktober):1–61, 2019.

[31] K Verwer. Modelling of Induction Heating for Offshore Pipeline Field Joints. Technical report, TU Delft, 2016.

[32] M Wielandt. Technology Development Plan for Out-of-Autoclave Press Co- consolidation of Thermoplastic Composites for small / mid-size parts for Aerospace. Technical report, Fokker GKN Aerospace, 2017.

[33] M Wielandt. Technology development plan for out-of-autoclave press consolidation of thermplastic composites for small / mid-size parts for the aerospace- CUD/PEKK spar with local reinforcents. Technical report, Fokker GKN Aerospace, 2018.

[34] Madina Yermekova and Sergei A Galunin. *Numerical Simulation and Automatic Optimization of the Disk Induction Heating System*. 2017. ISBN 9781509048656. URL https://ieeexplore.ieee.org/ielx7/7899013/7910472/07910744.pdf?tp={&}arnumber=7910744{&}isnumber=7910472.

[35] S Zinn and S L Semiatin. Coil design and fabrication: basic design and modifications. *Heat Treating*, (June), 1988.